VENTILATION PHENOTYPES OF SEVERE ASTHMA

^{129}XE MAGNETIC RESONANCE IMAGING VENTILATION PHENOTYPES OF SEVERE ASTHMA

By ASHUTOSH THAKAR, BSC (HONS)

A Thesis Submitted to the School of Graduate Studies in Partial Fulfilment
of the Requirements for the Degree Master of Sciences

Descriptive Note

McMaster University MASTER OF SCIENCE (2023) Hamilton, Ontario (Medical Sciences)

TITLE: ^{129}Xe Magnetic Resonance Imaging Ventilation Phenotypes of Severe Asthma

AUTHOR: Ashutosh Thakar, Honours B.Sc (McMaster University)

SUPERVISOR: Dr. Sarah Svenningsen, PhD

NUMBER OF PAGES: XVI, 92

Lay Abstract

Severe asthma is an airways disease that is characterized by inflamed, twitchy and obstructed airways. There is remarkable clinical heterogeneity between asthma patients due to the various mechanisms of disease. Abnormal ventilation is the functional consequence of abnormal airway pathology in asthma, which can be directly visualized by hyperpolarized ^{129}Xe magnetic resonance imaging (MRI). Each ventilation pattern is unique and there is significant inter-patient variability. Thus, the goal of the thesis was to extract quantitative information from the ^{129}Xe MRI ventilation patterns of patients with severe asthma, identify novel ventilation phenotypes, and determine their clinical relevance. An unsupervised machine learning approach using quantitative ventilation MRI features identified three unique, clinically relevant ventilation phenotypes of severe asthma with distinct clinical, physiological, and biological characteristics. The discordance in ventilation between phenotypes, and their characteristics, suggest different mechanisms that may be driving severe asthma.

Abstract

INTRODUCTION: Abnormal ventilation is the functional consequence of airway obstruction. In patients with severe asthma, ventilation patterns visualized by magnetic resonance imaging (MRI) exhibit significant inter-patient heterogeneity. Therefore, our objectives were to identify MRI ventilation phenotypes of severe asthma using an unsupervised clustering approach and examine their associated demographic, clinical, physiologic, and inflammatory characteristics.

METHODS: This retrospective analysis included 58 adults with severe asthma who underwent hyperpolarized ^{129}Xe ventilation MRI. Nineteen quantitative variables were extracted from ventilation MRI (including ventilation defect percent (VDP), ventilation defect size, and ventilation texture features) and transformed to principal components for hierarchical clustering. Differences in demographics, clinical characteristics, spirometry, inflammatory biomarkers, and computed tomography (CT) measurements between phenotypes were evaluated using one-way ANOVA or Kruskal-Wallis tests.

RESULTS: Three ventilation phenotypes of severe asthma were identified. They were significantly different with respect to their age, prevalence of obesity, spirometry, sputum neutrophil percent, sputum cytokines (interleukin-4, interleukin-6, interleukin-15, B-cell activating factor), total lung capacity, CT air-trapping, and CT mucus score (all $p<0.05$). They were not different with respect to their asthma control or medication requirement, and ~75% of each phenotype reported uncontrolled asthma (ACQ-5≥1.5). *Phenotype 1* had normal ventilation (VDP=1.7±0.9%) and predominantly consisted of young, obese females (88% female, 41±11 years old, 63% obese). They had normal-to-moderately reduced FEV_1 ($80\pm15\%_{pred}$), normal post-bronchodilator FEV_1/FVC, and reduced total lung capacity ($85\%_{pred}$ [57-108]). 25% had intraluminal inflammation (all eosinophilic) and their sputum interleukin-4 levels were elevated.

Phenotype 2 had markedly abnormal ventilation (VDP=6.2±3.8%) and was older than Phenotype 1, but also predominantly consisted of obese females (63% female, 54±13 years old, 59% obese). They had mildly-to-severely reduced FEV_1 (61±17%$_{pred}$) and partially reversible obstructive spirometry (72%, post-bronchodilator FEV_1/FVC<0.70). 50% had intraluminal inflammation (28% eosinophilic/13% neutrophilic/9% mixed-granulocytic) and their sputum interleukin-6 levels were elevated. *Phenotype 3* had severely abnormal ventilation (VDP=24.8±10.2%) and was also older than Phenotype 1 but was gender-balanced and not obese (50% female, 56±12 years old, 11% obese). They had moderately-to-very severely reduced FEV_1 (41±12%$_{pred}$) and partially reversible obstructive spirometry (89%, post-bronchodilator FEV_1/FVC<0.70). 72% had intraluminal inflammation (39% eosinophilic/17% neutrophilic/17% mixed-granulocytic) and their sputum interleukin-15 and B-cell activating factor levels were elevated. They had the highest burden of gas-trapping and mucus on CT.

CONCLUSION: Three distinct MRI ventilation phenotypes of severe asthma were identified through unbiased analysis, all of which reported uncontrolled asthma. The discordance in ventilation between phenotypes, and their characteristics, suggest different mechanisms that may be driving severe asthma.

Acknowledgements

In midst of a global pandemic, and with the future put on a tentative hold, the guidance from my undergraduate mentors, Dr. John Dawson and Dr. Neil Maclusky at the University of Guelph led me to pursue a research-based MSc at McMaster University. This decision has significantly transformed my professional and personal life.

First and foremost, to my supervisor and mentor Dr. Sarah Svenningsen, your unending patience, and invaluable expertise have been the driving force behind the successful completion of my MSc. You have always been supportive of my ideas and provided reassurance with your exceptional mentorship. For instance, during the 2021-22 Omicron surge when facilities were closed, your advice of leveraging acquired MRI scans with artificial intelligence and machine learning approaches ultimately led to this thesis. As one of your first trainees, I have witnessed firsthand the hurdles of setting up a new lab, and it is inspirational to see your resilience, and calm demeanour at the face of adversity. Your dedication to my growth as a researcher and your willingness to invest in my professional milestones have inspired me to reach new heights in my academic pursuits. I am indebted to you for your constant encouragement and for instilling in me a deep passion for scientific curiosity and discovery. As I endeavour to new goals, I know you will always be a guiding hand, and I will always value your experienced insight.

I express my heartfelt gratitude to the members of my advisory committee: Dr. Ehsan Haider and Dr. Parameswaran Nair. Their insightful feedback, constructive criticism, and willingness to engage in meaningful discussions have greatly enriched the quality of my research. As an aspiring translational scientist, Dr. Nair sets a high standard for research excellence, and his aptitude for translating research to real-world settings is truly inspirational.

Both Dr. Nair and Dr. Svenningsen had an open-door policy to encourage discussions about research. As knowledgeable mentors, they illuminated a path for me to follow but gave me the autonomy to discover my own interests.

To Dr. Manali Mukherjee, I extend my appreciation for being one of my trusted advisors during my time in graduate school. Your constant words of support, life guidance, and insightful explanations of the molecular aspects of my research have been invaluable to me.

I am immensely grateful for the tremendous help from all of Dr. Nair's clinical/research staff including Chynna Huang, Katherine Radford, Lindsey Dyment, and Melanie Kjarsgaard. All of you created a safe and enjoyable environment for trainees to ask questions and were a sounding board for all our research issues. This thesis and other projects would not have been efficiently completed without your resourceful contribution.

To the clinicians, especially Dr. Hana Serajeddini, Dr. Terence Ho and Dr. Carmen Venegas, thank you for your support, guidance, and patience for answering my endless list of questions. Despite having a busy schedule, all of you took the time to give advice with personal anecdotes and supported my professional aspirations. I am grateful for your continuous encouragement to achieving my goals.

I extend my sincere gratitude to all the members of our research lab: Nisarg Radadia, Nandhitha Ragunayakam, and Yonni Friedlander. We shared long hours in the lab talking about our projects, life goals, and shared laughs about the day's events. I will miss exploring the Hamilton food scene with you all and talking about popular culture and our favourite memes. To all the trainees I met along the way, especially Kayla Zhang, Kate Miyasaki, Rameen Jamil, Zil Patel, Nadia Suray Tan, Dr. Kiho Son, Tran Zhou, Tim Ju, and Cathy Cao, I am grateful for the friendships forged during this time, and I will cherish the memories we have created together.

To my beloved parents, your admiration, support, and encouragement have been the framework upon which I built my academic and personal aspirations. Your sacrifices and belief gave me the strength to persevere through the challenges and strive for excellence. You always were available for the countless hours of listening to my research, provided valuable life lessons, and have always been my pillars of strength.

To my brother, Om, thank you for your refreshing take and input about my research. Whenever I needed a break, you were always there to chat. You were my confidante during both the triumphs and tribulations of graduate school.

Finally, I appreciate the Canadian Institutes of Health Research for recognizing my scholarly potential by awarding the Canadian Graduate Scholarship to support my MSc.

Table of Contents

List of Figures

List of Tables

List of Abbreviations and Symbols

ACQ	Asthma Control Questionnaire
ADEPT	Airways Disease Endotyping for Personalized Therapeutics
ANOVA	Analysis of Variance
AQLQ	Asthma Quality of Life Questionnaire
ATS	American Thoracic Society
BAFF	B-cell Activating Factor
BD	Bronchodilator
BMI	Body Mass Index
CT	Computed Tomography
COPD	Chronic Obstructive Pulmonary Disease
CoV	Coefficient of Variation
FeNO	Fractional Exhaled Nitric Oxide
FEV_1	Forced Expiratory Volume in One Second
FOV	Field-Of-View
FRC	Functional Residual Capacity
FVC	Forced Vital Capacity
GINA	Global Initiative for Asthma
GLNU	Gray-Level Non-Uniformity
HGRE	High Gray-Level Emphasis
HU	Hounsfield Units
ICS	Inhaled Corticosteroid
IL	Interleukin
IFN-γ	Interferon-Gamma
LA	Lumen Area
LAA_{-856}	Low Attenuation Area of the lung less than -856 HU
LAA_{-950}	Low Attenuation Area of the lung less than -950 HU
LGRE	Low Gray-Level Emphasis
LRE	Long-Run Emphasis
LRHGE	Long-Run, High Gray-Level Emphasis
LRLGE	Long-Run, Low Gray-Level Emphasis
MRI	Magnetic Resonance Imaging
NETs	Neutrophil Extracellular Traps
NLRP3	Nucleotide-Binding Oligomerization Domain–Like Receptor Family, Pyrin Domain–Containing 3
N_2	Nitrogen
OCS	Oral Corticosteroids
PC20	Provocative Concentration Required to Decrease FEV_1 by 20%
PET	Positron Emission Tomography
RLNU	Run-Level Non-Uniformity
ROI	Region-Of-Interest
RP	Run Percentage
RV	Residual Volume
SARP	Severe Asthma Research Program
SD	Standard Deviation

SEOP	Spin-Exchange Optical Pumping
SNR	Signal to Noise Ratio
SPECT	Single Photon Emission Computed Tomography
SRE	Short-Run Emphasis
SRHGE	Short-Run, High Gray-Level Emphasis
SRLGE	Short-Run, Low Gray-Level Emphasis
T2	Type-2
TAC	Total Airway Count
TE	Echo Time
TLC	Total Lung Capacity
TNF-α	Tumour Necrosis Factor-Alpha
TR	Repetition Time
U-BIOPRED	Unbiased Biomarkers for the Prediction of Respiratory Disease Outcomes
VDP	Ventilation Defect Percent
WA%	Wall Area Percent
WT	Wall Thickness
^{1}H	Proton
^{3}He	Helium-3
^{13}NN	Nitrogen-13-Labeled-Nitrogen
^{18}F-FDG	Fluorine-18-Fluorodeoxyglucose
^{19}Ne	Neon-19
^{81m}Kr	Krypton-81m
^{99m}Tc	Technetium-99m
^{129}Xe	Xenon-129

Declaration of Academic Achievement

I declare that this MSc thesis dissertation has been entirely composed by myself and based on original research. This thesis has been reviewed and edited by myself and my supervisor, Dr. Sarah Svenningsen. All reported findings are an accurate representation of patients with severe asthma whom completed a study visit at the Firestone Institute for Respiratory Health.

This thesis is an original research project entitled "^{129}Xe Magnetic Resonance Imaging Ventilation Phenotypes of Severe Asthma" and will be reformatted into a research article to be submitted for scientific publication. This thesis was co-authored by Ashutosh Thakar, Nandhitha Ragunayakam, Yonni Friedlander, Carmen Venegas, Melanie Kjarsgaard, Chynna Huang, Katherine Radford, Kayla Zhang, Norm Konyer, Ehsan Haider, Manali Mukherjee, Anna Dvorkin-Gheva, Parameswaran Nair, and Sarah Svenningsen. Ashutosh Thakar and Sarah Svenningsen conceptualized the study. Ashutosh Thakar, Melanie Kjarsgaard, and Chynna Huang were responsible for data curation. Norm Konyer supported with the acquisition of ^{129}Xe ventilation MRI scans. Yonni Friedlander assisted with the ^{129}Xe ventilation MRI feature extraction. Anna Dvorkin-Gheva validated the methodology related to the unsupervised machine learning and statistical analysis. Nandhitha Ragunayakam and Carmen Venegas completed the quantitative computed tomography analysis. Katherine Radford, Kayla Zhang, and Manali Mukherjee quantified the cytokine and cytometry measurements. Carmen Venegas, Ehsan Haider, Manali Mukherjee, Parameswaran Nair, and Sarah Svenningsen provided their clinical/physiological interpretation of the data.

Chapter 1: Introduction

Severe asthma is driven by multifaceted mechanisms that lead to functional abnormalities and poor clinical outcomes. This chapter establishes the potential for functional lung imaging to better characterize the heterogeneity of severe asthma.

1.1 Overview and Motivation

Asthma is a common chronic lung disease that is estimated to affect 400 million individuals worldwide by 2025 and is a leading cause for hospitalizations.[5] As communities adopt western lifestyles, increased urbanization and greater asthma awareness and diagnosis, the prevalence of asthma continues to rise.[6] In Canada, in the past three decades, the prevalence of asthma has increased by 67%, and currently affects over 10% of the population, which is about 3.8 million individuals.[7] The primary goal of asthma management is to optimize control of symptoms and limit the risk of exacerbations. Despite adherence to maximal therapy as recommended by Global Initiative for Asthma (GINA) guidelines,[8] and advancements in biologic therapies,[9] about 5-10% of the asthma population continues to be poorly controlled and disproportionally contribute to healthcare utilization.[10] This subset of patients have severe asthma and require greater intensive care with high-dose corticosteroids and perhaps monoclonal therapy for relief and control of their symptoms. In the next 20 years, the burden of sub-optimal asthma control is projected to cost the Canadian economy over $200 billion.[11]

The clinical heterogeneity of severe asthma is a consequence of various etiological mechanisms that drive airway hyperresponsiveness and inflammation. The heterogeneous presentation of individuals with severe asthma highlights the complexity of care and the dire need to understand the underlying mechanisms of disease. The current objective measures for prevention, diagnosis, and management of lung diseases are obtained from lung volumes derived from pulmonary function tests. While these tests are easy to implement and the measurements are reproducible, they only provide a global measurement of airflow obstruction with no regional information about the underlying pathophysiology in patients.[12] As a result, pulmonary imaging approaches such as computed tomography (CT) and magnetic resonance imaging (MRI) have been developed to identify and provide regional measurements of lung structure and function. Understanding the heterogeneity of severe asthma is crucial for effective disease management and personalized treatment strategies. Incorporating pulmonary functional imaging to characterize patients with severe asthma may assist with reducing the gap to achieving optimal care.

In this chapter, the background knowledge relevant to this thesis is provided to support and motivate the original research presented in Chapters 2 to 5. The relationship between pulmonary structure and function is described (1.2), followed by the pathophysiology of asthma (1.3), and the clinical assessments (1.4) and the lung imaging modalities (1.5) to measure asthma. Previously identified asthma phenotypes from unsupervised clustering studies are discussed (1.6). Finally, the specific hypotheses and objectives for this thesis are presented (1.7).

1.2 Respiratory Structure and Function

The intricate design and coordinated functioning of the respiratory system is vital for regulating the transfer of oxygen into systemic circulation and removal of carbon dioxide and other metabolic by-products. The structure of the lung is comprised of the airways, parenchyma, and vasculature. The flow of air within the lung structures is known as ventilation, and it is vital for efficient gas-exchange and maintaining homeostasis.[13] However, in asthma, the impediment to airflow leads to a variable degree of ventilation impairment, and an increase in respiratory symptoms. In this section, the fundamental architecture of the lung will be discussed and subsequently, the effect of asthma on the structural integrity of the lungs.

1.2.1 Airways

The respiratory system is a highly integrated network that is subdivided into the conducting and the respiratory zones. The upper airways connect the lungs to the external environment, bringing the inspired air from the nasal or oral cavity which converges in the pharynx and travels to the trachea and bifurcates into the bronchi, which branch into smaller passageways that carry the air into the respiratory zone for gas-exchange to occur.

The air passages are covered with cells that secrete mucus and have cilia, working to eliminate inhaled particles. While bigger particles are typically filtered out in the nasal passages, smaller ones can enter the airways and get trapped by the mucus secreted by goblet cells. The cilia on the columnar epithelium then rhythmically beat, propelling the mucus upwards. The bronchial tree dichotomously divides from the trachea to the primary bronchi to the five lobar bronchi that supply ventilation to the 19 bronchopulmonary segments of the lung. As the cumulative cross-sectional area of the airway exponentially increases, there is a reduction in the airway resistance promoting laminar airflow. The conducting zone provides a passageway to the distal lung and holds approximately 150 mL of air, known as anatomic dead space, that does not participate in gas-exchange.

As outlined in **Figure 1-1**, the larger segmental bronchi, extending up to generation 7, are composed of cartilaginous rings to prevent airway collapse which transition to more smooth muscle as it becomes narrower into terminal bronchioles (generation 16). These bronchioles are tethered to the surrounding parenchyma that exerts an outwards force on the airway wall and contributes to the patency of the airways. Afterwards the bronchioles transition into the respiratory zone, which is comprised of the remaining 7 generations that directly lead into the alveoli, the functional units of the lungs.

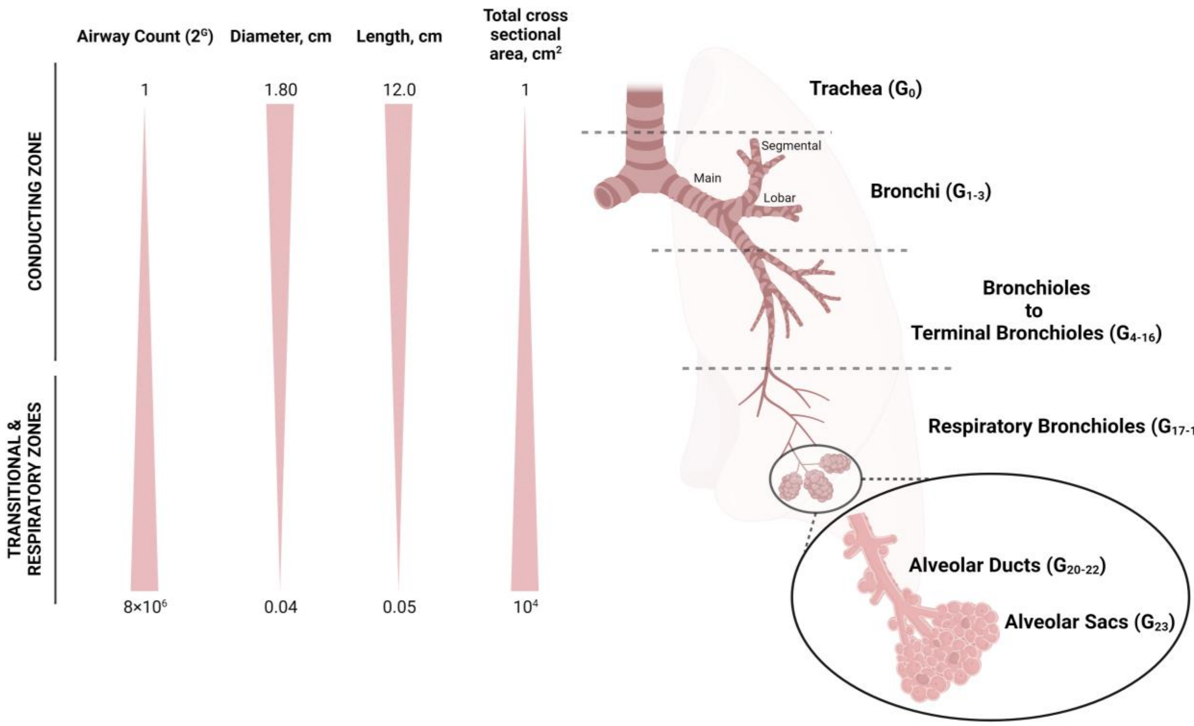

Figure 1-1 Dichotomous airway branching of 23 generations and approximate airway morphometric measurements
Adapted from Weibel, Science (1962)[1]; Bouhuys, The Physiology of Breathing (1977)[2]
(Created with BioRender.com).

1.2.2 Lung Parenchyma

The lung parenchyma has about 2.5-3 litres of lung volume within the respiratory bronchioles, alveolar ducts, and alveolar sacs.[14] In healthy adult human lungs, the average number of alveoli is approximately 500 million (range: 274-790 million depending on anthropometric characteristics of the individual),[15] with an average spherical diameter of 200-300 μm.[14] The blood-gas barrier forms a dense network around the alveoli to allow passive diffusion of oxygen and carbon dioxide. According to Fick's law the rate of diffusion is proportional to the surface area and inversely proportional to the alveolar thickness. Thus, the large surface area (50-100 m^2)[14] and thin walls (0.2-0.3 μm)[16] of the alveoli provides an effective interface for diffusion of gas across the one cell barrier.

1.3 Pathophysiology of Asthma

Since 2,600 B.C.E., respiratory symptoms related to asthma have been documented in ancient scriptures. “Asthma” was derived from the Greek word, “aazein” – short drawn breathing, hard breathing, or death rattle. Despite Hippocrates’ humoral view, he observed stress[17] and outdoor occupations[18] as triggers to asthma. One of the earliest accurate descriptions of asthma was described by Aretaeus, who noted the importance of vital air, recognized exercise-induced asthma and attributed breathlessness to thick phlegm.[19] The modern view of asthma has evolved with the advancement of methods to measure its pathophysiology.

Asthma is an airways disease that is characterized by variable airflow limitation that leads to respiratory symptoms including cough, wheeze, chest tightness, and shortness of breath. The pathology of asthma is a complex interplay of various factors related to bronchial hyperresponsiveness, inflammation, and airflow obstruction. As shown in **Figure 1-2**, the asthmatic airway undergoes structural remodeling in both large and small airways, regardless of disease severity. The main features of airway remodelling include smooth muscle hypertrophy and hyperplasia, goblet cell and submucosal gland hyperplasia, subepithelial fibrosis, and angiogenesis.[20] Altered airway wall structures are a response to either improper lung development or persistent chronic inflammation. The cardinal feature of asthma is airway hyperresponsiveness which is driven by intermittent bronchoconstriction via smooth muscle cells. The exaggerated response to an external stimulus (e.g., allergen exposure) provokes the smooth muscles to contract and narrow the airway to prevent airflow to the distal lung. The heightened bronchial reactivity is augmented by release of inflammatory mediators, and growth factors on the airway smooth muscle.[21] The infiltration of immune cells, and inflammatory mediators sustain the chronic inflammation processes in asthma. The cellular mechanisms of airway inflammation involve eosinophils, mast cells, basophils, lymphocytes, neutrophils, dendritic cells, macrophages, and epithelial cells.[22]

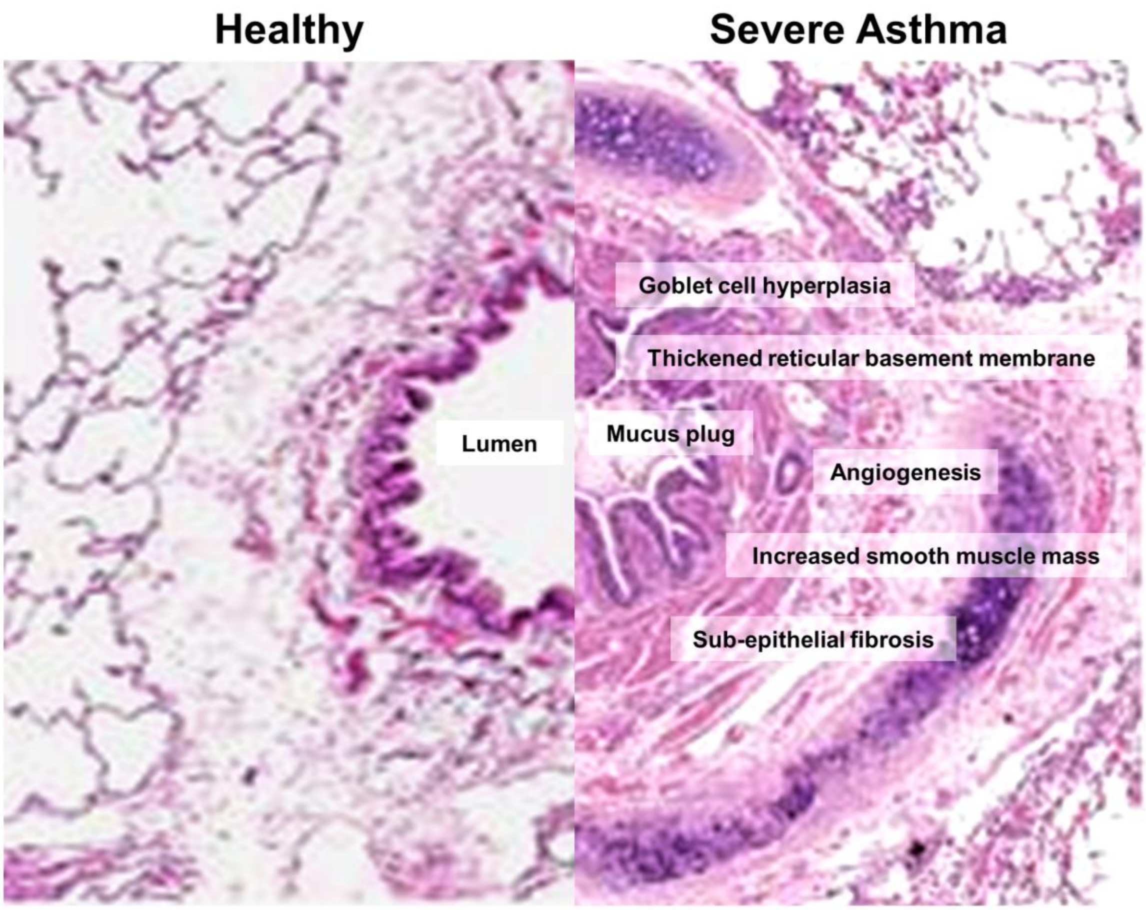

Figure 1-2 Large airway and parenchymal histopathology of a healthy individual and a patient with severe asthma

Lung tissue was formalin-fixed paraffin-embedded and stained with Hematoxylin and Eosin stains. Compared to a healthy airway, chronic inflammation in asthmatic airways leads to airway remodeling and contributes to increasing disease severity. Luminal narrowing and airflow obstruction is the result of increased deposition of muscle mass, goblet cell hyperplasia, mucoid impaction, loss of epithelial integrity, airways fibrosis, and angiogenesis.
Adapted from Hsieh, Assadinia and Hackket, Frontier Physiology (2023)[3]*; Mauad and Ferreira, Pulmão RJ* (2012)[4].

The endotype of "T-helper cell type 2 (Th2)-high" asthma is associated with eosinophilia, mast cell activation, and mucus hypersecretion mediated through cytokines, including interleukin (IL)-4, IL-5 and IL-13, as well as other inflammatory mediators (e.g., nitric oxide).[23] Furthermore, immunoglobin E (IgE) antibodies primed to environmental allergens facilitates the allergic response and subsequent degranulation from mast cells and basophils.[24] The discovery of non-classical immune cells such as innate lymphoid cells-type 2 influenced the change in nomenclature from Th2 to type-2 (T2) to be more inclusive of other cells that release the aforementioned cytokines.[25] "T2-low" asthma is identified in the absence of T2 inflammation and is observed in patients with neutrophilic or paucigranulocytic inflammation.[26]

The various pathological mechanisms of asthma contribute to the structural abnormalities, oedema, cellular debris, and mucus plugging observed in the airways. Collectively, these structural, and inflammatory changes reduce the patency of airways, restrict airflow, and make breathing difficult.

1.4 Clinical Assessments of Asthma

There is a toolkit of assessments to measure the components of airways disease in asthma and their impact on lung health. This section provides an overview of the various clinical assessments relevant to the diagnosis and management of asthma including lung physiology, inflammatory mechanisms, and the burden on the patient's quality of life and wellness.

1.4.1 Asthma Severity

The classifications of severity are categorized as mild-to-severe asthma based on the degree of treatment required to control symptoms and prevent exacerbations.[27] Adjustments to therapies are holistically completed to ensure personalized asthma management including compliance to medications, adequate inhaler technique, and accounting for masqueraders of asthma symptoms. There are three broad groups of therapies available for patients with asthma 1) bronchodilators to dilate and open airways, 2) corticosteroids for anti-inflammatory control and 3) monoclonal antibody biologics to suppress specific targets in the T2 pathway. The Global Initiative for Asthma (GINA) provides a stepwise approach to guide asthma care.[28] Recent modifications recommend adults with mild asthma a daily controller inhaler of low dose inhaled corticosteroid (ICS).[29] As the severity increases due to lack of control with prescribed treatment, GINA recommends an incremental increase in the dose of ICS with long acting β2 agonist. All patients are provided with a reliver inhaler of short acting β2 agonist for rapid relief of asthma symptoms. Individuals are diagnosed with severe asthma by having poor symptom control, and frequent exacerbations despite adherence to maximal optimized inhaled therapy and management of comorbid conditions or patient's health worsens when high intensity treatment is tapered off.[30] Patients with severe asthma require further phenotyping of factors contributing to their disease by examining their T2-signature, and precisely targeting the molecular pathway with add-on biologic therapies including anti-IgE (omalizumab),[31] anti-IL5 (benralizumab, mepolizumab and reslizumab),[32] anti-IL4Rα (dupilumab),[33] and anti-thymic stromal lymphopoietin (tezepelumab).[34] Additional non-monoclonal antibody add-on therapies include tiotropium, leukotriene modifier/leukotriene receptor antagonist, macrolide, or a maintenance systemic dose of oral corticosteroids.

1.4.2 Spirometry

Spirometry is a forced single-breath maneuver that measures the volume of air that an individual can expire with maximal effort.[35] It is often used as a screening test of general lung health in patients reporting respiratory symptoms.[35] The parameters derived from spirometry measure the volume of exhaled air over a function of time. The classification of lung function is based on forced expiratory volume in one second (FEV_1) and forced vital capacity (FVC). To improve interpretation of the results, the absolute volume in litres is corrected for anthropometric differences by comparing to a healthy population similar in sex, age, and height.[36] The severity of airflow limitation is based on the normalized FEV_1, and can be used to assess the degree of bronchoconstriction or bronchodilation. Moreover, spirometric patterns can be used to classify ventilatory impairments as obstructive, restrictive, or mixed.[37]

1.4.3 Airway Inflammation and Methods of Assessment

T2 immunity protects the host from helminth parasitic infections, and the overexpression of this inflammatory pathway is associated with allergic driven diseases including asthma, chronic rhinosinusitis with nasal polyposis, atopic dermatitis, and eosinophilic gastrointestinal disorders, among others.[38] In asthma, the pathologic molecular drivers of T2 inflammation are alarmin cytokines: IL-25, IL-33, thymic stromal lymphopoietin and effector cytokines: IL-4, IL-5, IL-13.[39] The exposure of environmental stimuli (e.g., noxious particles, allergens, and pathogens) disrupts the airway epithelium to release alarmins triggering a downstream cascade of effector cytokines secreted by type 2 helper lymphocytes and innate lymphoid cells resulting in IgE-specific antibodies to inhaled allergens, influx of effector cells (eosinophils, basophils, and mast cells), and remodelling of the airway epithelium.[25]

As Lord Kelvin once said "If you cannot measure it, you cannot improve it",[40] therefore it's important to use validated assessments to accurately endotype patients according to their underlying inflammatory pathway. Quantitative sputum cytometry is a direct measurement of intraluminal inflammation and is the most clinically validated non-invasive method to determine the dominant airway inflammatory endotype.[41] The use of hypertonic saline improves sputum production and expectorated sputum can be used to measure the relative airway count of neutrophils, eosinophils, basophils, macrophages, and lymphocytes. In addition, free eosinophilic granules and smoker's inclusion macrophages can also be observed and stratified by prevalence.[42] In clinical practice absolute blood eosinophil counts are used to measure T2 inflammation due to its accessibility and associations with asthma severity,[43] asthma control and exacerbations.[44] Greater counts of eosinophils in the blood have predicted response to corticosteroid[45] and biologic[46] treatment. However, sputum eosinophil counts have greater sensitivity to poorly controlled asthma than blood eosinophils.[47] Sputum guided management in patients with severe asthma have demonstrated greater reduction in exacerbations than traditional guidelines based on symptoms and airflow limitations.[48] Albeit modest correlations were previously reported between systemic and localized measures of eosinophils in asthma,[49] the relationship becomes weaker as the severity of asthma increases.[50] The discordance between blood and sputum eosinophils may be attributed to ILC-2 induced *in situ* eosinophilopoiesis.[51] Other surrogate biomarkers of T2 inflammation include serum IgE[52] and fractional exhaled nitric oxide (FeNO)[53] to provide complementary information about the underlying processes contributing to asthma pathology. In clinical practice, a patient's T2-signature is based on validated cut-offs from abovementioned inflammatory assessments.

1.4.4 Airway Responsiveness

A comprehensive review of symptoms and spirometry with a reversibility test is recommended to confirm a diagnosis of asthma.[28] A positive bronchodilator response is based on baseline recovery of at least 200 mL and 12% of FEV_1 or FVC after bronchodilator administration (commonly 400μg of salbutamol).[54] However bronchoprovocation is a recommended investigative assessment in symptomatic individuals suspected of asthma[21] to measure airway hyperresponsiveness (AHR) defined as an exaggerated response of the airways to a stimuli resulting in airflow obstruction. Airway smooth muscle is the primary tissue that mediates acute airway narrowing and can be stimulated by direct (acts on the smooth muscle receptors) and indirect (acts through an intermediate pathway) bronchoconstrictors.[55]

Direct stimulation (e.g., methacholine or histamine) on the smooth muscle receptors evokes a contractional response. In clinical practice, AHR is prominently measured with methacholine, a cholinergic agonist that stimulates the muscarinic receptors of the airway smooth muscle to induce bronchoconstriction.[56] The standardized procedure of incremental increases of stimuli aims to measure a provocative concentration that results in a 20% reduction in FEV_1 (PC_{20}). The definition of the degree of AHR by methacholine is defined as: PC_{20} more than 16 mg/mL, normal; 4 to 16 mg/mL, borderline; 1 to 4 mg/mL, mild AHR; 0.25 to 1 mg/mL, moderate AHR; and less than 0.25 mg/mL, marked AHR. Direct bronchial provocation tests are performed to rule out asthma's contribution to presenting respiratory symptoms.[21]

Indirect bronchial stimuli (e.g., hyperventilation, cold/dry air, exercise, hypertonic saline, mannitol, or adenosine) evokes airflow limitation by acting on the intermediate pathway (i.e., inflammatory cells and neuronal cells) to induce secondary bronchoconstriction.[57] In patients with asthma, bronchial responsiveness from the indirect challenge is associated with airway inflammation, and can be used to differentiate and confirm the diagnosis of current asthma.[58]

Individuals with controlled airway inflammation and significant airway hyperresponsiveness may benefit from bronchial thermoplasty to reduce the smooth muscle dysfunction in their airways. This specialized procedure delivers localized thermal energy to airway wall with the goal of ablating smooth muscles and reducing hyperactive airways. In previous studies, bronchial thermoplasty has demonstrated clinically meaningful reductions in airway hyperresponsiveness,[59] improvement in quality of life,[60] greater asthma control,[61] and reduction in exacerbations.[62] Bronchial thermoplasty is a viable procedure that has long term effects in a specific cohort of patients with asthma.[63]

1.4.5 Validated Asthma Questionnaires

The severity of asthma is associated with reported symptoms, healthcare utilization and disease burden on the patient.[64] There is marked variability in the occurrence of symptoms and requires monitoring with standardized and validated assessments of asthma control and asthma-related quality of life. The most used questionnaires are the Asthma Control Questionnaire (ACQ)[65] and Asthma Quality of Life Questionnaire (AQLQ).[66] The ACQ is a method to evaluate patient reported asthma control by assessing respiratory symptoms (5 self-administered questions), short-acting β2-agonist use (1 self-administered question), and airway calibre (FEV_1 measurement).[65] It is scaled on a 7-point Likert scale ranging from 0 to 6, with a higher score indicating worse asthma control. An ACQ of less than 0.75 indicates well-controlled asthma, while ACQ greater than 1.5 indicates poorly controlled asthma.[67] The AQLQ is used to understand the physical and emotional impact of asthma. It has 32 questions that evaluate four primary categories: symptoms, activity limitation, emotional function, and environmental exposure. It is scaled on a 7-point Likert scale ranging from 1 to 7, with a lower score indicating severe impairment.[66] The minimal clinically important difference is 0.5 for both questionnaires.[68,69] The primary goals of asthma management are to reduce or eliminate manifestations of asthma by achieving optimal control and minimization of future exacerbation risk.[70] Accordingly, these questionnaires are important clinical assessments commonly used as clinical trial endpoints.[71]

1.5 Imaging of Lung Structure and Function

Chest radiography (x-ray or CT) in asthma supports clinicians with identifying alternative diagnosis or evaluating complications that may be contributing to the severity of the disease.[72] Advancements in non-invasive lung imaging modalities shown in **Table 1** can quantify severe asthma's underlying pathologic features and evaluate the efficacy of therapeutic strategies.

Table 1 Comparison of different lung imaging modalities

	CT	HP ^{129}Xe MRI	SPECT	PET
Spatial Resolution	High	High	Low	Low
Breath Maneuver	Breath hold	Breath hold	Free breathing	Free breathing
Scan Length	Seconds	Seconds	Minutes	Minutes
Purpose	Structure	Function	Function	Function
Ionizing Radiation	Yes	No	Yes	Yes
Applications	- Lung Density - Lung Volume - Airway - Vasculature	- Ventilation - Alveolar-airspace size - Gas-exchange	- Ventilation - Perfusion	- Ventilation - Perfusion

Definition of abbreviations: CT=computed tomography; HP=hyperpolarized; MRI=magnetic resonance imaging; SPECT= single-photon emission computed tomography; PET = positron emission tomography

1.5.1 Structural Lung Imaging

Chest computed tomography (CT) is currently the gold-standard imaging modality to evaluate and assess thoracic abnormalities and guide clinical decisions.[73] The absorption or attenuation coefficient of x-rays are used for CT reconstruction into greyscale images, and the linear transformation of attenuation coefficient generates a relative quantitative measurement of radiodensity called Hounsfield units (HU). The Hounsfield scale arbitrarily defines water as 0 HU, air as -1000 HU and the denser tissues such as bone are 1000 HU.[74] While CT imaging has superior spatial resolution (e.g., 0.625 mm in all three dimensional planes) than other imaging modalities, the exposure to ionizing radiation creates a disadvantage.

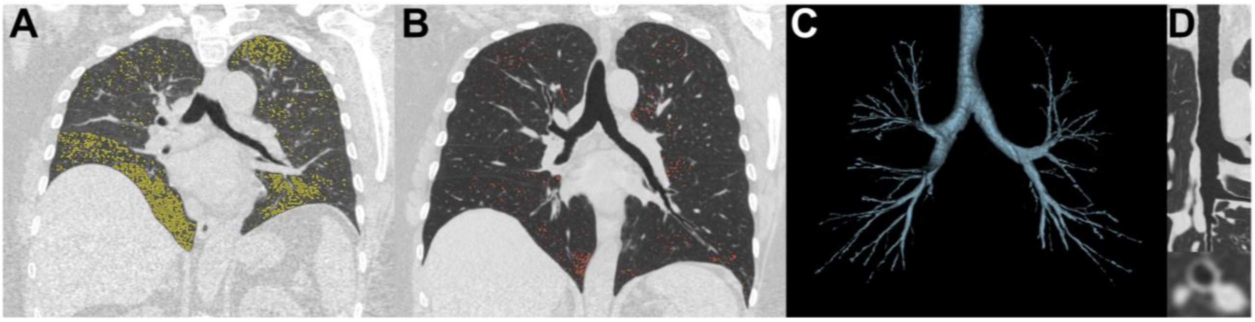

Figure 1-3 Quantitative CT parenchymal and structural airway endpoints

A) Gas trapping can be quantified by quantifying the percentage of low attenuation areas less than a threshold of -856 Hounsfield units on expiratory CT.
B) Emphysema can be quantified by quantifying the percentage of low attenuation areas less than a threshold of -950 Hounsfield units on inspiratory CT.
C) Segmented airway tree from inspiratory CT to assess large airway morphology.
D) Apical segmental airway of the right upper lobe

Radiologists currently contribute to the management of asthma by qualitatively assessing chest CTs for structural airway abnormalities, bronchial wall thickening, and gas-trapping on expiratory CT. Advances in post-processing software for CT has enabled detailed quantitative assessment of the airway tree, pulmonary vessels, and lung parenchyma.[75] As shown in **Figure 1-3**, quantitative imaging endpoints of lung structure and function complement traditional visual assessments, by providing an enhanced understanding of the pathophysiology of lung diseases.[75] The airways can be segmented by semi-automated or fully automated approaches by relying on tubular morphology and attenuation differences between the lumen, airway wall and the parenchyma. The airway tree is restricted from growing smaller airways (diameter ≤ 2mm) due to resolution limitations and partial volume effects that result in extra-luminal leaks from the region-based growing algorithm.[76] The larger airway morphology by CT assessment has shown to be accurate to anatomical and histopathological measurements, and can be a surrogate tool to assess airway remodeling.[77,78] As shown in **Figure 1-4,** structural airway abnormalities in asthma can be observed and quantified on CT including bronchial wall thickness (WT), bronchial dilation, and luminal narrowing.

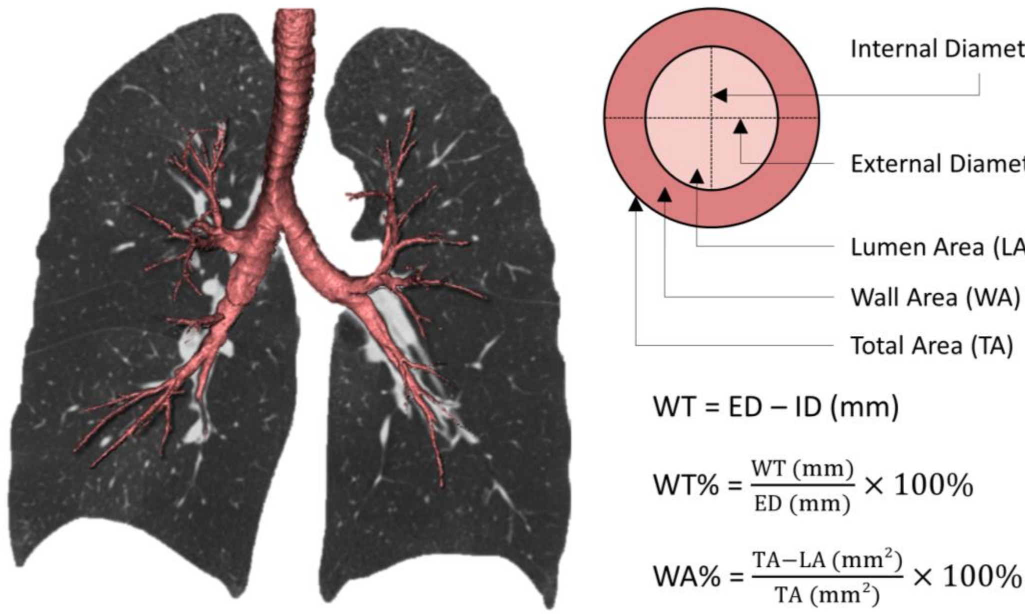

Figure 1-4 CT airway morphometric quantification

Various airway measurements can be quantified from the segmented large airways on inspiratory CT.

For the first time in 1998, quantitative CT (QCT) measurements of segmental and subsegmental airways in asthma patients unsurprisingly demonstrated greater airway wall thickening than healthy individuals, and was observed in more severe patients than those with milder asthma.[79] Subsequent studies examining QCT measurements of increased airway thickness have demonstrated associations with airway remodeling,[80] airflow obstruction,[81] asthma severity,[82] airway hyperresponsiveness,[83] and therapeutic response.[84,85] Asthmatic lungs with thickened airway walls, narrowed lumen and/or intraluminal occlusion can terminate the airway branching on CT and result in missing terminal airways. CT visible total airway count (TAC) was modestly correlated with lung function, airway lumen area and wall area fraction.[86] Based on GINA guidelines, TAC has been shown to be significantly lower in patients with severe asthma.[86]

Another important mechanism to asthma severity is mucus accumulation and plugging of the airway lumen.[87] Mucus plugs occluding the airways are recognized as a contributory factor to impaired mucociliary clearance and airflow obstruction.[88] In 2018, Dunican *et al.*[89] created the first radiographic CT mucus score to quantify the burden of mucus in the airways. Across various cross-sectional cohort studies,[89-91] the prevalence of mucus plugging assessed by CT was observed in approximately 60% of patients with asthma. Interestingly, in a longitudinal cohort study of the Severe Asthma Research Program (SARP)-3, airway mucus plugging was discovered to be a persistent asthma phenotype in a subset of patients with severe asthma.[92]

While it is difficult to directly visualize the small airways *in-vivo* due to limitations in resolution and exposure to high ionizing radiation, air trapping on expiratory CT is an indirect marker of small airways disease. The regional differences in small airways disease can be measured by low lung attenuation on expiratory CT. Airway closure prevents air from being exhaled and becomes trapped in the distal lung.[93] The magnitude of air trapping is quantified as the proportion of the lung less than -856 HU ($\%LAA_{-856}$). Since the attenuation value of a normally inflated lung is about -856 HU, the attenuation of a healthy lung should be greater than the -856 HU threshold.[94] Functional small airways disease is associated with decline in lung function and exacerbations in asthma.[95]

1.5.2 Functional Lung Imaging

The functional consequence of the above-mentioned airway structure abnormalities in asthma can be evaluated by functional lung imaging. Nuclear medicine and magnetic resonance imaging methods provide spatial localization of lung pathophysiology in asthma. Asthma is an airways disease and therefore, the primary focus of this section will be on functional lung imaging modalities that measure ventilation. The capability of imaging to assess perfusion and gas-exchange is acknowledged, but not discussed.

Ventilation Scintigraphy and Single Photon Emission Computed Tomography (SPECT)

Ventilation scintigraphy and SPECT imaging approaches use radioisotopes to assess ventilation by detecting the emission of gamma rays in the lungs. The radioactive decay by the injected or inhaled radionuclides are detected by gamma cameras to convert the emitted energy into an electrical signal to produce an image. Scintigraphy is a two-dimensional projection of the radioactivity within the body and regions of greater radioisotope deposition are seen as hot spots in the image. The radiotracer gases commonly used to measure ventilation are ^{133}Xe and krypton-81m (^{81m}Kr) and the radionuclide technetium-99m (^{99m}Tc) is used to label ^{99m}Tc-diethylene-triamine pentaacetate (DTPA) aerosol and Technegas (^{99m}Tc-labelled carbon).[96] Ventilation scintigraphy was the first method to regionally identify uneven inhaled ^{133}Xe gas distribution in asthmatic lungs.[97,98] The inhalation of Technegas has a similar deposition pattern as ^{133}Xe and is the preferred agent because of its temporal stability of adhering to the airway wall for more than 20 minutes.[99] In patients with asthma there was increased ventilation heterogeneity observed with scintigraphy after direct bronchoprovocation with methacholine[100] and histamine.[101]

While scintigraphy produces planar images, ventilation single photon emission computed tomography (V-SPECT) offers three-dimensional topographical analysis of ventilation distribution by inhaling ^{133}Xe, ^{81m}Kr or Technegas. In asthma, there is increased abnormal ventilation measured with V-SPECT than in healthy individuals,[102] the severity of ventilation heterogeneity at baseline in asthma was associated with methacholine-induced airway changes,[103] and low ventilation regions are related to multiple breath nitrogen washout index of peripheral ventilation heterogeneity.[104] V-SPECT has also been used to investigate the regional deposition of inhaled aerosol labeled ^{99m}Tc to evaluate treatment efficacy.[105,106] A few limitations of scintigraphy/V-SPECT includes the exposure to radionuclide-dependent radiation, poor spatial resolution, and long acquisition times.

Positron Emission Tomography

Positron emission tomography (PET) is similar to SPECT by providing three-dimensional information of radioactivity, however PET uses emission of positrons from radioisotopes to reconstruct an image. Inhaled tracers of nitrogen-13–labeled nitrogen (^{13}NN),[107] neon-19 (^{19}Ne)[108] and gallium-68 labeled carbon particles (Galligas)[109] provide regional information about pulmonary ventilation. ^{13}NN injected into systemic circulation is completely diffused into the alveolar airspace due to low solubility in tissues. Thus, low ventilated regions due to gas-trapping would have greater retention of tracer. Conversely, inhalation route of ^{13}NN reaches the well-ventilated regions of the lungs.[110] In mild to moderate asthma patients, PET images of pulmonary ^{13}NN tracer kinetics revealed greater abnormal ventilation during acute methacholine-induced bronchoconstriction in the large and small airways.[111] A subsequent study from the same research group demonstrated redistribution of perfusion away from non-ventilated regions in asthmatic lungs.[112] In clinical practice, PET is often accompanied with fluorine-18-fluorodeoxyglucose (^{18}F-FDG) tracer, a glucose analogue that is taken up by metabolically active cells such as malignant cells. The uptake of ^{18}F-FDG in airway inflammatory cells during an allergen challenge has sparked interest in the utility of ^{18}F-FDG-PET as a pulmonary biomarker of cellular inflammation in asthma.[113]

Magnetic Resonance Imaging

Magnetic resonance imaging (MRI) is a non-ionizing radiation modality that generates images by aligning the spin of specific nuclei in biological tissue to an external magnetic field. As the excited nuclei relax to their original spin, they emit a radiofrequency energy that is detected and reconstructed into an image. Anatomical ^{1}H MRI is inadequate to assess lung function because of the low ^{1}H density of the lungs (~0.1 g/cm^3) and the numerous air-tissue interfaces leads to magnetic field inhomogeneities resulting in the loss of ^{1}H signal.[114] Therefore, pulmonary ^{1}H MRI appears as a dark thoracic cavity with limited physiological information. As shown in **Figure 1-5**, hyperpolarized gas MRI enables the visualization of pulmonary function by imaging inhaled ^{3}He or ^{129}Xe gas in the lungs. Noble gases are inert and require hyperpolarization to increase the signal by 10^4-10^5 fold in order to be captured by the MRI.[115] Hyperpolarization is commonly achieved by a technique called spin-exchange optical pumping (SEOP).[116] In brief, SEOP is a two-step process whereby a circularly polarized laser is directed at an alkali metal, usually rubidium, to transfer angular momentum to the metal's electrons. Subsequently, the spin polarization is transferred from the valence electrons to the nuclei of the ^{3}He or ^{129}Xe gas-atoms through collisions.[117] Using hyperpolarized ^{3}He or ^{129}Xe as an inhaled contrast agent in lung MRI provides functional information with high temporal and spatial resolution in healthy subjects and patients with various lung diseases including asthma,[118] cystic fibrosis,[119] idiopathic pulmonary fibrosis,[120] and chronic obstructive pulmonary disease (COPD).[121] Due to the limited availability and cost of ^{3}He, hyperpolarized ^{129}Xe is currently the commonly used gaseous agent to image, and interestingly, it was used to acquire the first reported ventilation images from MRI.[122,123] With the recent advances in polarization equipment, high polarization values (10-40%)[124,125] can be reached in ^{129}Xe, thus reducing the signal-to-noise ratio (SNR) gap between the aforementioned noble gases.[126] Using hyperpolarized noble gas as inhaled contrast agents for lung imaging produces high-resolution images that can quantify ventilation and parenchymal microstructure. Furthermore, ^{129}Xe is modestly solubilized in biological tissues and can be used to probe gas exchange.[116] It is important to mention that the distribution of airflow can be visualized with other functional lung MRI techniques including inhaled fluorinated gas,[127] oxygen-enhanced techniques,[128] and free-breathing ^{1}H approaches.[129]

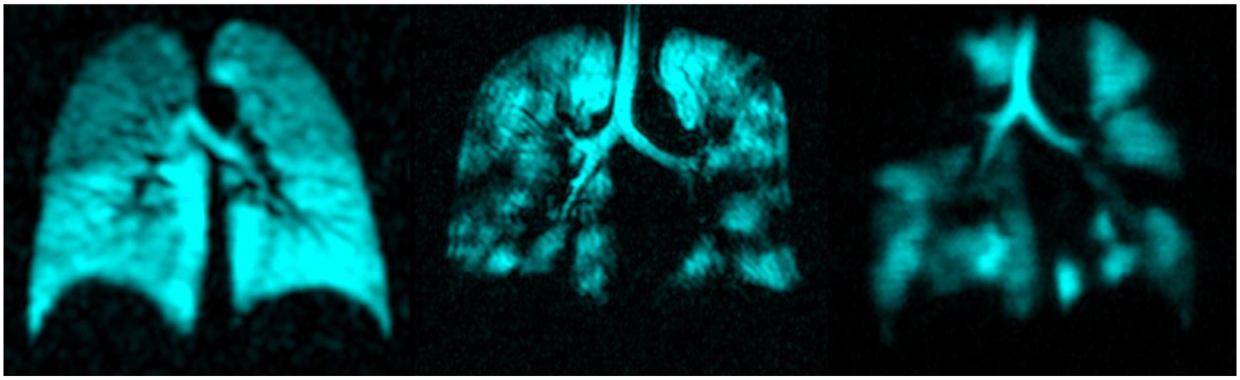

Figure 1-5 Hyperpolarized ^{129}Xe ventilation MRI of a healthy individual and patients with severe asthma

The centre coronal ^{129}Xe MRI slice shows homogeneous ventilation of a healthy individual and abnormal ventilation for two patients with severe asthma.

The most common application of hyperpolarized noble gas MRI is the acquisition of static ventilation images. To acquire three-dimensional whole-lung images, the patient is positioned supine in the scanner and hold their breath for about 10-12 seconds after inhaling up to one litre of gas from functional residual capacity (FRC). An individual with no history of lung pathology will have homogeneous distribution of the gas throughout the lung, while a lung with airways disease will have regions of signal void or ventilation defects. In asthma, low ventilation can arise from airways that are partially or completely occluded by mucus plugging,[130] airway remodeling,[118] and/or intraluminal cellular inflammation.[131] The earliest quantification of abnormal ventilation was visually scored,[132,133] however was limited by intra- and inter-observer variability. Thus, semi-automated[134,135] and automated[136,137] segmentation methods were developed to generate objective measures of ventilation. Quantitative imaging biomarkers of ventilation include ventilated volume, ventilated defect volume and the widely reported ventilation defect percent (VDP), which is defined as the ventilation defect volume normalized to the thoracic cavity volume. In patients with asthma, MRI VDP is predictive of exacerbation frequency,[138] associated with clinical biomarkers of disease pathophysiology,[131] spatially correlated with air trapping[139] and mucus plugging,[130] and is responsive to therapy.[131,138,140-148] As expected, methacholine induced bronchoconstriction in asthma patients and healthy volunteers resulted in increased MRI VDP and administration of salbutamol resolved the abnormal ventilation.[149] There is concealed information within the ventilated regions that can be extracted with texture features. Previous studies have shown good evidence that MRI ventilation texture features can differentiate between patients with asthma and healthy volunteers,[150] are sensitive to eosinophilic inflammation,[151] can assess bronchodilator response,[140] and can predict biologic response in severe asthma.[152] The use of ^{129}Xe MRI is limited in clinical and investigative settings, at the moment clinical use of ^{129}Xe ventilation MRI is approved in the United Kingdom, and most recently in the United States of America. In the past 30 years, the research in this field has demonstrated the usefulness of ventilation ^{129}Xe MRI to provide quantitative regional insight about lung physiology.[153]

1.6 Unsupervised Clustering in Asthma

Asthma is now considered to be an umbrella term that encompasses a heterogeneous population of patients with unique characteristics and distinct underlying mechanisms. The clinical heterogeneity of asthma makes it challenging to optimally mange patients who respond poorly to first-line inhaled therapies.[154] To address the urgent need for precision medicine in asthma, unsupervised machine learning approaches have been previously employed to group patients with similar features/characteristics (phenotypes) to tailor treatment and guide research.

In 2008, Haldar *et al.*[155] were the first to apply unsupervised machine learning to identify clinical asthma phenotypes. The authors independently examined a primary care asthma population and secondary-care refractory asthma care population by completing a k-means cluster analysis on clinical parameters. Focusing on the refractory asthma population they identified 4 clinical phenotypes: Cluster 1 had early-onset atopic asthma with evidence of airway dysfunction, symptoms, and eosinophilic airway inflammation; Cluster 2 was an obese, female predominant subgroup with asthma symptoms and absence of airway inflammation; Cluster 3 had greater early-onset asthma with uncontrolled symptoms and minimal inflammation; Cluster 4 had late-onset disease with greater proportion of males and eosinophilic inflammation predominance. They observed discordance with symptoms and airway inflammation within the clusters, and this led to a prospective sub-analysis that titrated ICS therapy according to either symptoms or airway eosinophil count. Those managed with sputum cell counts had a 10-fold reduction in exacerbation frequency in the inflammation predominant cluster and decrease in ICS dosage in the early symptoms predominant cluster.[156] Thereafter, the SARP, Airways disease Endotyping for Personalized Therapeutics (ADEPT), and Unbiased Biomarkers for the Prediction of Respiratory Disease Outcomes (U-BIOPRED) project conducted one of the first multicentre machine-learning driven studies to unbiasedly identify clinical phenotypes of mild-to-severe asthma derived from demographic, lung function, and questionnaire variables.[157-159] Interestingly, severe asthma participants defined by GINA[29] were found across all five SARP clusters, and four U-BIOPRED clusters. Collectively, there was substantial overlap between asthma clusters identified from the Leicester cohort,[156] SARP,[157] and U-BIOPRED[158] unsupervised clustering studies. The clusters ranged from well-controlled, atopic asthma with normal lung function to late-onset asthma with poor control and obstructed lung function. Despite different geographical cohorts, all produced phenotypes that discriminated based on age of asthma onset, obesity, inflammation, airflow limitation, and biological sex. Furthermore, clinically driven asthma phenotypes were validated on independent asthma cohorts and demonstrated stability of characteristics from previously identified clusters.[160] Subsequent clustering approaches with various "-omics" techniques including radiomics has provided novel insights into the pathophysiology of asthma.[161]

Radiomics is an emerging field that quantifies high-throughput imaging data into quantitative variables.[162] Thoracic imaging provides regional information of lung structure-function and has shown to recognize disease severity and progression at an earlier onset than spirometry in various lung diseases including cystic fibrosis,[163] COPD,[164] and asthma.[132] A follow-up study reviewed a subset of previously clustered individuals in the SARP cohort by examining their CT characteristics and determined airway morphometry had limited discernability, while lung deformation and functional small airways disease distinguished well between previously defined clinical SARP phenotypes.[165] However, to my knowledge, as tabulated in **Table 2,** there only have been four studies that solely performed image-based clustering of patients with asthma. Each of these studies utilized CT derived airway and/or parenchymal measurements to differentiate asthma patients.[166]

Table 2 Radiomic unsupervised clustering in asthma

Study	Severity	Modality & Parameters	Approach	Cluster Characteristics
Gupta *et al.*[167] *(2014)*	Non-severe (n=17) and severe (n=48)	*11 QCT* 1) RB1 WA/BSA 2) RB1 WA/BSA 3) RB1 total area 4) RB1 LV 5) RB1 WV 6) RB1WV% 7) VI -856 8) MLD E/I 9) Δ voxels 10) Fractal LAC 11) D_{sv} airway	PCA, Hierarchical and K-means	**Cluster 1:** severe air-trapping, bronchial wall thickening and bronchial lumen dilation **Cluster 2:** moderate air-trapping **Cluster 3:** severe air-trapping and bronchial lumen narrowing
Choi *et al.* [166] (2017)	Non-severe (n=106) and severe (n=142)	*57 QCT* 32) Local - θ, Cr, WT, WT*, Dh, D_h* 20) Lobar -%LAA_{-856}, ADI, ΔV_{air}, Jacobian 5) Global -ADI, Jacobian, U/[M+L] | V	PCA and K-means	**Cluster 1:** younger, early onset, non-severe, reversible lung function, easy to control symptoms **Cluster 2:** non-severe and severe patients, persistently altered lung function, marginal to no inflammation, difficult to control symptoms **Cluster 3:** obese, female dominant, severe asthma, reversible lung function, blood lymphopenia, difficult to control symptoms **Cluster 4:** older, late-onset, male dominant, severe asthma, persistently altered lung function, neutrophilic inflammation, difficult to control symptoms
Kim *et al.*[168] (2022)	Non-severe (n=28) and severe (n=33)	*4 QCT* 1) WT* 2) D_h* 3) fSAD% 4) Emph%	PCA and K-means	**Cluster 1:** older females with late-onset asthma, no previous smoking history, normal lung function, and lowest total serum IgE **Cluster 2:** younger females with early asthma onset, and 27% were on OCS therapy **Cluster 3:** mostly severe asthma with about a even split in biological sex, high total serum IgE and reduced lung function **Cluster 4:** males with severe asthma, a previous smoking history with the highest pack-years, lowest PC_{20} methacholine at diagnosis and severely reduced lung function
Eddy *et al.*[169] (2022)	Non-severe (n=26) and severe (n=19)	*3 QCT* 1) TAC 2) LA 3) WA% *1 ^{129}Xe MRI* 4) VDP	Hierarchical and K-means	**Cluster 1:** moderately abnormal ventilation and airway thickening but only mildly abnormal total airway count and luminal narrowing. No evidence of gas-trapping or airflow limitation. **Cluster 2:** female dominant, moderately abnormal ventilation and total airway count, severe airway wall thickening, mild luminal narrowing, with moderate airflow limitation, gas-trapping, and airway resistance **Cluster 3:** moderately abnormal ventilation and airway wall thickening, significantly reduced total airway count and luminal narrowing along with moderate airflow limitations and mild to negligible gas trapping. **Cluster 4:** male dominant, severely abnormal ventilation with significant gas trapping and airflow obstruction. Reduced total airway count, moderately thickened airways with significant luminal narrowing.

Notably, Choi *et al.*[166] performed a multiscale CT cluster analysis of asthma patients by examining 57 postprocessed variables related to segmental, lobar, and whole lung density and geometry, respectively. The derived four clusters were identified based on imaging features of luminal area, wall thickness, air-trapping, and lung deformation. The majority of patients with severe asthma were in clusters 3 and 4. Cluster 3 was described as an obese, female, dominant cohort with reversible lung function and blood lymphopenia, and cluster 4 was a late-onset, older, male dominant cohort with fixed airflow obstruction, increased gas-trapping, and airway neutrophilia.[166] Overall, CT imaging based clustering of structural parameters produced cluster memberships of clinical interest, however quantitative CT variables are unable to directly measure the functional consequences of the asthmatic lung structure. As discussed previously, ^{129}Xe ventilation MRI can visualize and quantify ventilation abnormalities from airway obstruction, a characteristic feature of severe asthma.[118] Eddy *et al.*[169] most recently demonstrated the use of quantitative CT and functional MRI to generate asthma clusters, but only used ventilation defect percent (VDP), the most commonly reported quantitative measurement of abnormal ventilation derived from hyperpolarized ^{129}Xe MRI. Incorporating MRI VDP into their unsupervised pipeline allowed them to distinguish cluster 4, a small severely abnormal ventilated group with greater obstruction and gas-trapping from Cluster 3 which had similar CT morphometric characteristics. ^{129}Xe ventilation MRI provides functional insight of the whole lung (i.e., large, and small airways), and this strength of the imaging platform compelled us to investigate the research question: Are there unique, clinically relevant ventilation phenotypes of severe asthma?

1.7 Thesis Hypotheses and Objectives

As shown in **Figure 1-6**, ventilation patterns in patients with severe asthma are unique, and there is significant inter-patient heterogeneity. The clinical relevance of this heterogeneity and inter-patient variability is not known. Inhaled hyperpolarized ^{129}Xe MRI may be exploited to extract inherent physiological information residing within the ventilation patterns.

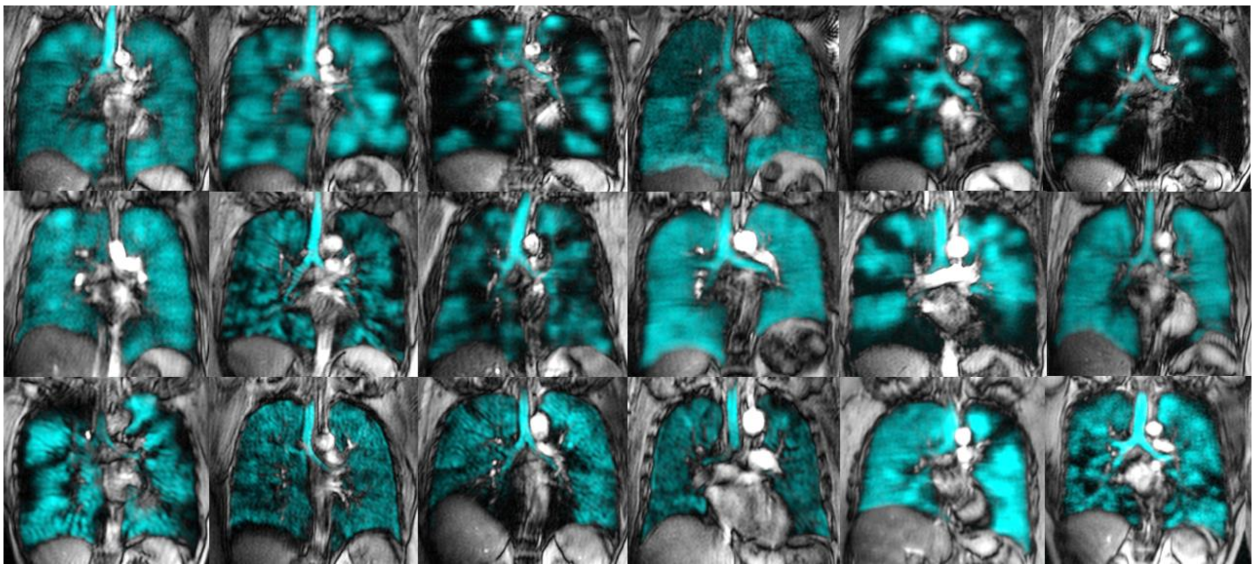

Figure 1-6 Representative pre-bronchodilator ^{129}Xe ventilation MRI centre coronal slice of patients with severe asthma

^{129}Xe MRI of the ventilation distribution (cyan) co-registered to the ^{1}H MRI of the thorax (in greyscale) for the centre coronal slice of eighteen patients with severe asthma.

Various radiomic approaches have explored the heterogeneity of severe asthma to profile disease phenotypes and guide treatment decisions. To our knowledge, none have solely used functional lung MRI biomarkers. We hypothesized that novel ^{129}Xe MRI-based ventilation phenotypes of severe asthma will be unbiasedly identified with unique clinical, physiological, and biological characteristics. Therefore, the objectives of this thesis were to **(1)** extract ^{129}Xe MRI features of ventilation, **(2)** identify ^{129}Xe MRI-based ventilation phenotypes of severe asthma using unsupervised clustering, and **(3)** to examine their clinical, physiological, and biological characteristics.

Chapter 2: Methods

2.1 Study Design and Participants

This was a single-centre retrospective analysis of 61 adults (>18 years of age) with severe asthma. All participants were recruited from the Firestone Institute for Respiratory Health, were well-characterized, and had severe asthma in accordance to the 2023 GINA guidelines.[28] They had no changes in respiratory medications in the previous 4 weeks, and had demonstrated post-bronchodilator reversibility (≥12% and 200 mL FEV_1 improvement) or PC_{20} <4mg/mL in the previous 12 months. They underwent ^{129}Xe ventilation MRI, and spirometry pre- and post-bronchodilator, fractional exhaled nitric oxide (FeNO), blood draw, sputum induction, and completed the Asthma Control Questionnaire (ACQ-5)[65] and Asthma Quality of Life Questionnaire (AQLQ) [66] during a clinic visit or under an ethics-board-approved research protocol (Hamilton Integrated Research Ethics Board #7585, #11471 and #12763; recruitment criteria for each protocol summarized in **Table 3**). Short-acting β-agonists were withheld for ≥6 hours, long-acting β-agonists for ≥48 hours and long-acting muscarinic antagonists for ≥72 hours prior. For post-bronchodilator measurements, four 100 µg doses of *Novo-Salbutamol® HFA* (Teva Novopharm Ltd.; Toronto, Canada) were delivered through a metered dose inhaler using a spacer.

Table 3 Recruitment criteria

Study name	n	Inclusion criteria	Exclusion criteria
Exploring the Utility of Hyperpolarized ^{129}Xe Magnetic Resonance Imaging in Healthy Volunteers and Patients with Lung Disease (NCT03455686)	31	- Male or female aged 18-85 with current or previously diagnosed lung disease or respiratory virus including but not limited to: asthma, emphysema, COPD, bronchiectasis, sarcoidosis, pulmonary fibrosis, alpha 1-anti-trypsin deficiency, eosinophilic granulomatosis with polyangiitis, bronchopulmonary dysplasia, and COVID-19 - Subject understands the study procedure and is willing to participate in the study as indicated by the signature on the informed consent - Subject is judged to be in otherwise stable health on the basis of medical history - Able to read and/or understand English	- Age < 18 years or >85 years - Pregnancy prior to or during study - In the opinion of the investigator, subject is mentally or legally incapacitated preventing informed consent from being obtained, or cannot read or understand the written material - Patient is unable to perform spirometry or plethysmography maneuvers - Patient is not MRI compatible
Dupilumab on Airway Hyper-responsiveness and Ventilation Heterogeneity in Patients with Asthma (NCT03884842)	26	- Able and willing to provide written informed consent - Able and willing to comply with study protocol - Males and females ≥ 18 years of age - Asthma diagnosed by a respiratory physician ≥ 12 months prior to study enrolment based on the GINA 2014 guidelines - ACQ>1 during the screening period - Airway hyperresponsiveness (methacholine $PC_{20} \leq 4$ mg/mL or ≥ 15% decreased in FEV_1 during saline inhalation for sputum induction or ≥ 25% improvement in FEV_1 after bronchodilator) during the screening period - FeNO >25 ppb and either ≥ 3% sputum eosinophils (preferred) or blood eosinophils ≥ 300/μL during the screening period - ICS dose ≥ 500 mcg of fluticasone equivalent/day. Patients on prednisone would not be excluded as long as they meet the rest of the inclusion criteria	- Acute or chronic parasitic, bacterial, fungal, or viral infections that required, or currently requires, hospitalization or antimicrobial treatment during the last four weeks - Acute asthma exacerbation event treated with increased doses of oral or any dose of intramuscular or intravenous corticosteroids within six weeks prior to screening - Other relevant pulmonary diseases (e.g., chronic obstructive pulmonary disease, idiopathic pulmonary fibrosis, cystic fibrosis, pulmonary arterial hypertension, tuberculosis) requiring treatment within 12 months prior to screening - Alcohol or substance abuse within 12 months prior to screening - Current smoker defined as having smoked at least one cigarette (or pipe, cigar, or marijuana) per day for ≥ 30 days within the three months prior to the screening - Ex-smokers with ≥ 10 pack-year smoking history - Treatment with anti-IG-E, anti-IL-4, anti-IL-5, or anti-IL-13 targeted therapy current or within three months prior to screening. - ACQ > 3.0 - Patient is not MRI compatible
Tezepelumab on Airway Structure and Function in Patients with Uncontrolled Moderate-to-severe Asthma (NCT05280418)	4	- Able and willing to provide written informed consent - Able and willing to comply with study protocol - Males and females ≥ 18 years of age - Asthma diagnosed by a respiratory physician ≥ 12 months prior to study enrolment based on the GINA 2021 guidelines - ACQ≥1.5 at screening - Airway hyperresponsiveness (methacholine $PC_{20} \leq 4$ mg/mL or ≥ 15% decreased in FEV_1 during saline inhalation for sputum induction or ≥ 15% improvement in FEV_1 after bronchodilator) during the screening period - Criteria met for moderate or severe asthma defined by GINA 2021 guidelines, i.e., treatment with low, medium, or high dose ICS (<250 mcg, 251-500 mcg, >500 mcg of fluticasone equivalent/day, respectively) plus another controller. Patients on prednisone would not be excluded as long as they meet the rest of the inclusion criteria - FeNO >25 ppb or ≥ 3% sputum eosinophils (preferred) or blood eosinophils ≥ 300/μL during the screening period - History of ≥ 1 exacerbation in the previous year	- Participation in any clinical trial of an investigational agent or procedure within six months prior to screening or during the study - History of anaphylaxis to any previous biologic therapy received - Receipt of live attenuated vaccine within 30 days, receipt of COVID vaccine within 28 days, known or suspected COVID infection at the time of enrolment - Acute or chronic parasitic, bacterial, fungal, or viral infections that required, or currently requires, hospitalization or antimicrobial treatment during the last four weeks - Acute asthma exacerbation event treated with increased doses of oral or any dose of intramuscular or intravenous corticosteroids within six weeks prior to screening - Other relevant pulmonary diseases (e.g., chronic obstructive pulmonary disease, idiopathic pulmonary fibrosis, cystic fibrosis, pulmonary arterial hypertension, tuberculosis) requiring treatment within 12 months prior to screening - Alcohol or substance abuse within 12 months prior to screening - Current smoker defined as having smoked at least one cigarette (or pipe, cigar, or marijuana) per day for ≥ 30 days within the three months prior to the screening - Ex-smokers with ≥ 10 pack-year smoking history - Pregnancy - Treatment with anti-IG-E, anti-IL-4, anti-IL-5, or anti-IL-13 targeted therapy current or within three months prior to screening. - Patient is not MRI compatible

As shown in **Figure 2-1,** we conceptualized an unsupervised machine learning workflow to generate data-driven ventilation phenotypes of severe asthma from ^{129}Xe ventilation MRI features. The methodology used to unbiasedly identify the ventilation clusters or phenotypes is extensively detailed below. Briefly, we acquired 61 pre-salbutamol ^{129}Xe ventilation MRI scans of patients with severe asthma. Then nineteen features related to signal intensity, ventilation defect size and ventilation texture were extracted from each MRI dataset. Afterwards, the unlabelled or unclassified data of only quantitative ventilation MRI variables were partitioned by various unsupervised machine learning models to generate stable clusters, which we termed "ventilation phenotypes." Finally, to understand the clinical relevance of each ventilation phenotype, a description of each phenotype was generated by comparing the clinical, physiological, and biological characteristics between phenotypes.

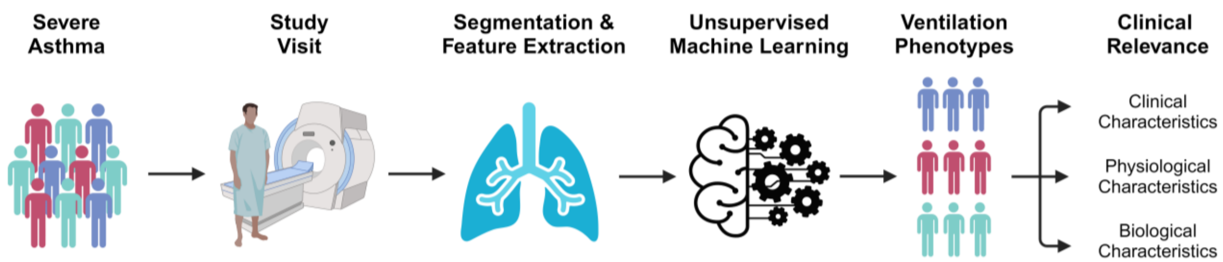

Figure 2-1 Proposed study design to generate MRI ventilation phenotypes of severe asthma

A heterogeneous group of patients with severe asthma (n=61) were recruited to undergo same day ^{129}Xe ventilation MRI, pulmonary function testing, fractional exhaled nitric oxide, sputum induction, blood collection and a subset of patients (n=43) also completed a non-contrast chest CT. Pre-bronchodilator ^{129}Xe MRI scans were segmented, and nineteen features were extracted for each patient. Principal component analysis was performed to reduce the dimensionality of the highly correlated dataset and ideal clustering conditions were determined to generate ventilation phenotypes. The clinical relevance of each phenotype was determined by extensively characterizing their clinical, physiological, and biological characteristics. (Created with BioRender.com).

2.2 MRI Acquisition, Segmentation, and Feature Extraction

2.2.1 MRI Acquisition

Participants underwent proton (^1H) and hyperpolarized ^{129}Xe ventilation MRI using a 3 Tesla Discovery™ 750MR system (GE Healthcare, Milwaukee, USA) and previously described methods.[170] A custom-built, unshielded quadrature-asymmetric bird-cage coil, tuned to the resonant frequency of ^{129}Xe was used to enable hyperpolarized ^{129}Xe MRI. Spin exchange optimal pumping polarizer systems (Polarean 9800 or 9820, Polarean, Durham, NC, USA) were used to polarize isotopic ^{129}Xe gas (86% enriched). Participants were coached and instructed to inhale a 1 L gas mixture (^1H MRI: 1 L N_2 gas, and ^{129}Xe MRI: ~600 ml ^{129}Xe / ~400 ml N_2 gas) from a Tedlar® bag (Jensen Inert Products, Coral Springs, USA) at their functional residual capacity (FRC) and image acquisition was performed under breath-hold conditions at FRC+1L. The inhalation of 100% polarized, 100% isotopically enriched ^{129}Xe during the acquisitions was a median dose equivalent volume[171] of 56 mL (25-159). Hyperpolarized ^{129}Xe static ventilation MRI was acquired using a three-dimensional fast gradient recalled echo sequence (acquisition time=10 s, field of view = 40x40x24cm^3, matrix size=128x128x16, voxel size=3.125x3.125x15 mm^3). A matching ^1H MRI was acquired prior to the ^{129}Xe static ventilation MRI to delineate the thoracic cavity. After inhaling 1L of N_2 gas from FRC, an anatomical ^1H MRI was acquired using a whole-body radiofrequency coil and a fast-spoiled gradient echo sequence (FOV=40x40 cm, matrix size=128x128x16, voxel size=3.125x3.125x15 mm^3).

2.2.2 MRI Segmentation

Anatomical ^1H and ^{129}Xe ventilation MRI were used to generate a binary mask of unventilated and ventilated lung from registration and semi-automated segmentation performed in MATLAB R2022a (The MathWorks Inc., Natick, MA, USA).[134] Briefly, a hierarchical K-means method was employed to classify the pixel signal intensity values of ^{129}Xe static ventilation images into five clusters which included a ventilation defect cluster (C1), hypo-intense cluster (C2), normal cluster (C3) and hyper-intense clusters (C4, C5). The boundaries of the thoracic cavity were delineated from ^{1}H MRI with a seeded region-growing algorithm and co-registered with the ^{129}Xe cluster map to generate the binary lung masks and quantify the ventilatory parameters.

2.2.3 MRI Feature Extraction

Nineteen whole-lung quantitative variables were derived from ^{129}Xe ventilation MRI as illustrated in **Figure 2-2** and are summarized in **Table 4**. Briefly, five variables corresponding to the normalized ventilation signal intensity, and two variables related to defect size were extracted from the ventilation defect lung mask. The coefficient of variation (CoV) of the signal intensity, and eleven second order texture features were extracted from the ventilated lung mask to provide further information about the spatial arrangement of ventilation patterns.

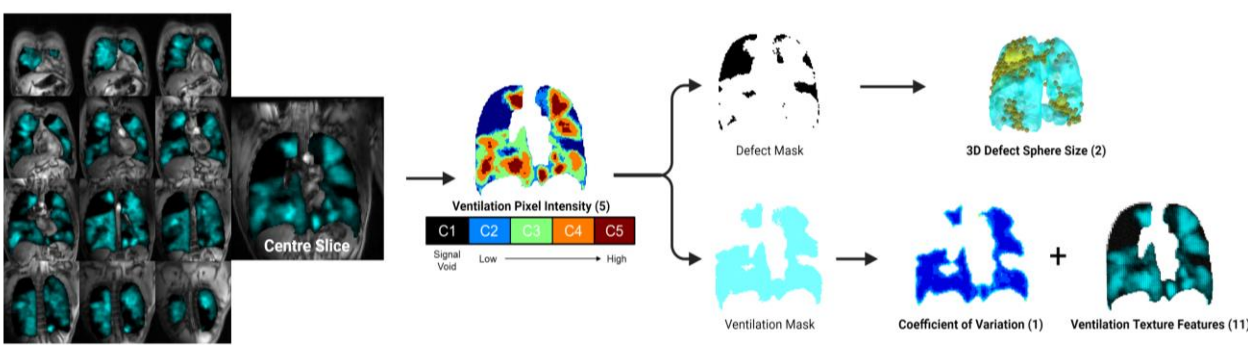

Figure 2-2 Schematic of ^{129}Xe ventilation MRI segmentation and feature extraction of nineteen whole-lung variables from a representative patient with severe asthma

All acquired ^{129}Xe MRI slices underwent semi-automated segmentation to classify the pixel intensity into five clusters of no signal (C1), and hypointense to hyperintense signal (C2-C5). The ventilation defect mask generated from the ^{129}Xe signal void cluster was used to quantify the maximum and median three-dimensional defect sphere size. The ventilation lung mask was generated from ^{129}Xe low to high ventilation clusters was used to quantify the coefficient of variation and eleven second-order texture features. (Created with BioRender.com).

The ^{129}Xe MRI VDP and other cluster percentages (i.e., C2 to C5) were determined by normalizing the cluster-specific volume to the thoracic cavity volume. Ventilation defect size was evaluated from the ventilation defect lung mask using a previously described sphere packing algorithm[172] and the median and maximum sphere sizes (i.e. ventilation defect size) were calculated from the ventilation defect mask. The CoV was calculated on a voxel-by-voxel basis using a 5x5 neighborhood and then averaged only over the ventilated lung mask as previously described.[141] Eleven second-order texture features from the gray-level run-length matrix (GLRLM) were generated from the ventilation lung mask using an open source MATLAB toolbox as previously described.[140] Texture features provide information about the spatial relationship of the ^{129}Xe signal and characterized the coarseness, smoothness, and regularity of the ventilation patterns. Texture features were extracted from the ventilation mask of varying run-lengths (a directional measurement of pixels with same signal intensity) and gray-levels (measures the relative magnitude of signal intensity). Texture features with joint descriptors of run-length (e.g., long, or short) and gray-levels (e.g., high, or low) were incorporated to capture combined information related to pixel distribution and varying intensities in the ventilated lung.

The image quality of the acquired ^{129}Xe ventilation MRI datasets were objectively measured with the signal-to-noise ratio (SNR) to account for non-physiological cofounders affecting ^{129}Xe ventilation features. SNR was determined by sampling four representative regions within the lung parenchyma, each with a 5x5 cm^2 region of interest (ROI). The average signal intensity in these ROIs was then divided by the average standard deviation of the signal in four 5x5 cm^2 ROIs selected outside of the thoracic cavity.[121] ^{129}Xe ventilation MRI datasets with a signal-to-noise ratio (SNR) of less than 15 were excluded due to noise contributing to the ventilatory features.

Table 4 ^{129}Xe MRI ventilation features

^{129}Xe MRI Features	Equation	Description
Ventilation Defect Percentage (VDP) and Cluster Volume Percentage	$= \frac{\text{Cluster Volume}}{\text{Thoracic Cavity Volume}} \times 100\%$	The volume of each cluster normalized to the total thoracic cavity volume. VDP is equal to the Cluster 1 volume percentage.
Coefficient of Variation (CoV)	$= \frac{\text{Ventilation Signal Standard Deviation}}{\text{Ventilation Signal Mean}}$	The variation in signal intensity within a neighborhood of pixels to quantify ventilation heterogeneity.
3D Ventilation Defect Size	Spherical Defect Packing Algorithm [172]	The median and maximum sphere volumes were generated based on segmented ventilation defect mask.
Gray-Level Nonuniformity (GLNU)	$= \frac{1}{n_r}\sum_{i=1}^{M}\left(\sum_{j=1}^{N} P(i,j)\right)^2$	Evaluates the variability of gray-level intensities in the image.
Run-Length Nonuniformity (RLNU)	$= \frac{1}{n_r}\sum_{j=1}^{N}\left(\sum_{i=1}^{M} P(i,j)\right)^2$	Evaluates the variability in the length of sequential pixels of the same gray-level.
Run Percentage (RP)	$= \frac{n_r}{n_p}$	Evaluates the homogeneity and distribution of runs of an image in a specific direction.
Low Gray-Level Run Emphasis (LGRE)	$= \frac{1}{n_r}\sum_{i=1}^{M}\sum_{j=1}^{N}\frac{P(i,j)}{i^2}$	Evaluates the distribution of relatively lower gray-level signal intensity values.
High Gray-Level Run Emphasis (HGRE)	$= \frac{1}{n_r}\sum_{i=1}^{M}\sum_{j=1}^{N} P(i,j) \times i^2$	Evaluates the distribution of relatively higher gray-level signal intensity values.
Short-Run Emphasis (SRE)	$= \frac{1}{n_r}\sum_{i=1}^{M}\sum_{j=1}^{N}\frac{p(i,j)}{j^2}$	Evaluates the distribution of relatively shorter run lengths and is correlated to finer textures.
Short-Run, Low Gray-Level Emphasis (SRLGE)	$= \frac{1}{n_r}\sum_{i=1}^{M}\sum_{j=1}^{N}\frac{p(i,j)}{i^2 \times j^2}$	Evaluates the distribution of relatively shorter run-lengths with lower gray-level signal intensity values.
Short-Run, High Gray-Level Emphasis (SRHGE),	$= \frac{1}{n_r}\sum_{i=1}^{M}\sum_{j=1}^{N}\frac{p(i,j) \times i^2}{j^2}$	Evaluates the distribution of relatively shorter run-lengths with higher gray-level signal intensity values.
Long-Run Emphasis (LRE)	$= \frac{1}{n_r}\sum_{i=1}^{M}\sum_{j=1}^{N}\frac{p(i,j)}{j^2} \times j^2$	Evaluates the distribution of relatively longer run lengths and is correlated to coarser textures.

Long-Run, Low Gray-Level Emphasis (LRLGE)	$=\frac{1}{n_r}\sum_{i=1}^{M}\sum_{j=1}^{N}\frac{p(i,j)\times j^2}{i^2}$	Evaluates the distribution of relatively longer run-lengths with lower gray-level signal intensity values.
Long-Run High Gray-Level Emphasis (LRHGE)	$=\frac{1}{n_r}\sum_{i=1}^{M}\sum_{j=1}^{N}p(i,j)\times i^2\times j^2$	Evaluates the distribution of relatively longer run-lengths with higher gray-level signal intensity values.

P(i,j)= original run-length matrix, n_r= total number of runs, n_p=total number of pixels, M=number of gray levels, N=maximum run length

2.3 Unsupervised Machine Learning Model

Pre-bronchodilator ^{129}Xe ventilation MRI datasets, each with nineteen postprocessed quantitative variables, were normalized using z-score standardization prior to implementation of machine learning models using R software (www.r-project.org). A Kaiser-Meyer-Olkin measure of sampling adequacy[173] was used to evaluate sufficient proportion of variance in the MRI features are caused by underlying factors. In addition, a Bartlett's test of sphericity[174] was performed to compare the correlation matrix of MRI features to an identity matrix (i.e., values along the diagonal are 1 and all of the other values are 0) in order to confirm suitability for data reduction. A principal component analysis (PCA) was performed to reduce the dimensionally of the highly correlated dataset and to obtain a set of linearly uncorrelated components.[175] Horn's parallel analysis determined the optimal number of principal components, and the clustering tendency was assessed with Hopkins statistic (>0.5) to confirm non-random grouping.[176,177] Hierarchical agglomerative, K-means and Gaussian mixture model unsupervised clustering algorithms were investigated with the *clValid*[178] and *NbClust*[179] R Stats package to validate the internal properties and determine the optimal number of the clusters, respectively.

2.4 Demographic, Clinical, Physiologic and Biologic Variables

2.4.1 Demographics and Asthma Characteristics

Age, biological sex, body mass index (BMI), smoking history, atopic status, and age of asthma-onset were recorded. All participants completed ACQ-5[65] and AQLQ[66] to assess asthma control and burden on quality of life, respectively. Dosage of inhaled and oral corticosteroids, biologic therapy, and previous history of bronchial thermoplasty were documented.

2.4.2 Spirometry

Spirometry was performed according to American Thoracic Society (ATS) technical guidelines[35,36] using an Elite Series plethysmograph (MGC Diagnostics Corporation, Saint Paul, USA) to measure FEV_1, FVC, and FEV_1/FVC.

2.4.3 Inflammation

Biomarkers of inflammation were assessed including sputum eosinophil percentage, sputum free eosinophil granules, sputum neutrophil percentage, blood eosinophil count, and FeNO. Intraluminal cellular inflammation was evaluated by quantitative cytometry of spontaneous or induced sputum. Sputum was induced, processed, and quantified according to standardized methods, as previously described.[42] Patients were retrospectively classified into the following airway inflammatory endotypes determined by sputum cell counts[180]: [1] eosinophilic (≥2.3% eosinophils and/or moderate or many eosinophil-free-granules), [2] neutrophilic (≥64% neutrophils and total cell count (TCC) $\geq 9.7\text{x}10^6$ cells/g without eosinophilia), [3] mixed-granulocytic (eosinophilic and neutrophilic), [4] trivial neutrophilic (≥64% neutrophils or total cell count (TCC) $\geq 9.7\text{x}10^6$ cells/g, but not both) and [5] paucigranulocytic (TCC$<9.7\text{x}10^6$ cells/g, <2.3% eosinophils, and <64% neutrophils). Patients who were unable to provide a sufficient sputum sample (<0.08g of sputum separated from saliva)[181] following three rounds of saline inhalation were considered paucigranulocytic. Cytokines and chemokines including IL-1β, IL-4, IL-5, IL-6, IL-12p70, IL-10. IL-13, IL-15, IL-17α, IL-18, B-cell activating factor (BAFF), interferon-gamma (INF-γ), and tumour necrosis factor-alpha (TNF-α) levels in sputa were measured using Ella™ automated ELISA system (Bio-Techne, Minneapolis, USA).

2.4.4 Chest CT

A subset of participants underwent a paired full inspiratory-expiratory, non-contrast chest CT scan with previously described parameters[182] using a 64-slice Lightspeed VCT system (GE

Healthcare, Milwaukee, USA). They were coached and instructed to inhale to total lung capacity and residual volume to ensure adequate inspiratory and expiratory lung volume for CT analysis. Quantitative CT evaluation was performed by a single observer using semi-automated airway segmentation on the Apollo 2.0 software package (VIDA Diagnostics Inc., Coralville, USA). CT airway measurements were quantified from the inspiratory chest CT and included airway lumen area (LA), wall area percent (WA%), wall thickness (WT) in absolute and normalized to the external airway diameter, and CT visible total airway count (TAC).[80,86] The burden of mucus plugging was quantified using the CT mucus score, assessed by a pulmonologist blinded to any clinical details.[89] A CT density mask was applied to quantify the extent of gas-trapping on expiratory chest CT as the percentage of low attenuation area of lung voxels below -856 HU and the extent of emphysema on inspiratory chest CT as the percentage of low attenuation area of lung voxels below -950 HU.[183]

2.5 Statistical Methods

Data were tested for normality using the Shapiro-Wilk normality test and when data were not normal, non-parametric tests were performed. One-way ANOVA or Kruskal-Wallis tests were performed to compare patient characteristics, pulmonary function, inflammatory biomarkers, MRI, and CT measurements between ventilation clusters/phenotypes. To correct for multiple comparisons, a Tukey's or Dunn's correction was applied, respectively. Chi-square or Fisher's exact tests were performed to compare proportions between clusters. Statistical analyses were performed using SPSS version 28.0 (IBM, Armonk, NY, USA) and GraphPad Prism version 9.00 (Graphpad Software Inc., La Jolla, CA, USA) and all results were considered statistically significant when the probability of making a Type I error was ≤ 5% ($p \leq 0.05$).

Chapter 3: Results

3.1 Study Participants

Sixty-one patients with a clinical diagnosis of severe asthma (37 females and 24 males; mean ± SD age, 53±13 years old) were recruited and underwent hyperpolarized ^{129}Xe ventilation MRI between July 2018 and April 2023. Three participants were excluded from our analysis due to low SNR (participant 08: 14.8; participant 13: 12.5; participant 26: 6.4) of ^{129}Xe ventilation MRI. ^{129}Xe ventilation MRI datasets from 58 participants were suitable for feature extraction and subsequent cluster analysis.

3.2 Unsupervised Clustering to Identify Ventilation Phenotypes of Severe Asthma

A single MRI dataset was composed of 19 imaging features related to the ventilation characteristics of each participant. Inspection of the correlation matrix revealed the presence of many MRI features of 0.3 or greater correlation strength. The Kaiser-Meyer-Olkin (KMO) test gave a value of 0.59, which exceeds minimum threshold of 0.5 for sufficient sampling adequacy[184] and is reasonably near the recommended value of 0.6 or greater.[173] Bartlett's test of sphericity was significant ($p<0.0001$) which confirmed the appropriateness of a principal component analysis to reduce highly dimensional quantitative MRI features to generate uncorrelated eigenvectors.[174] In **Figure 3-1**, the original eigenvalues were compared to a simulated random dataset, and Horn's parallel analysis[177] retained two principal components to accurately explain ~64% of the variance in the original dataset.

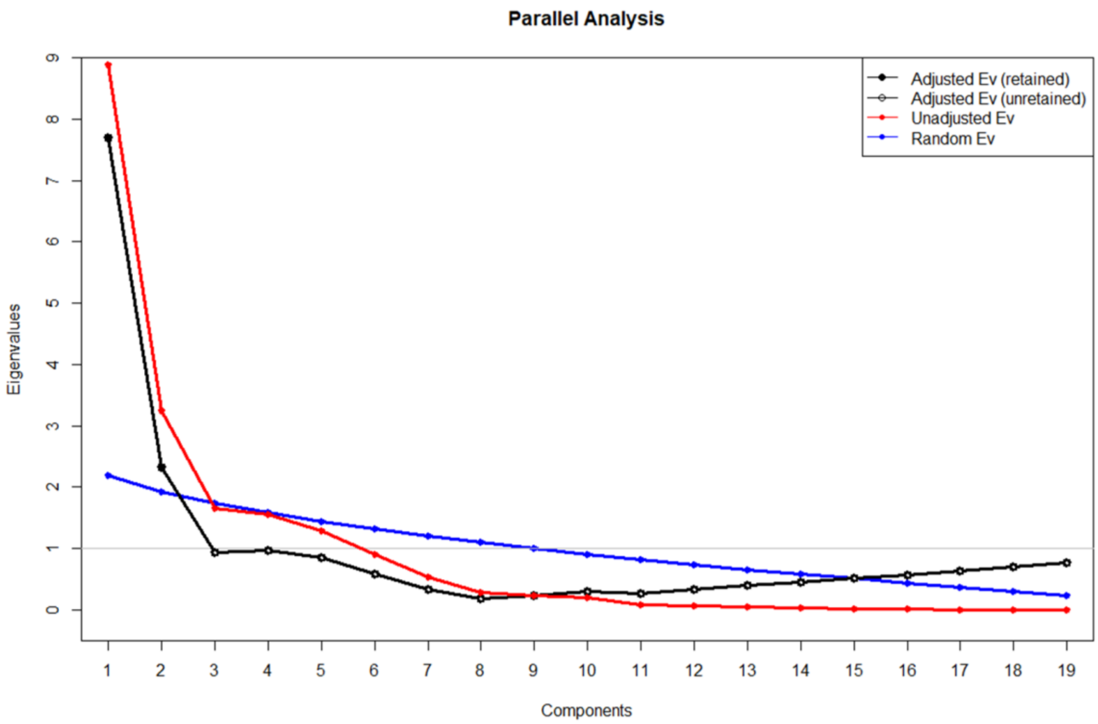

Figure 3-1 Plot of eigenvalues to principal components to determine optimal number of principal components.

The proportion of variance and standardized loadings for both principal components are reported in **Table 5**. The contribution of each imaging feature to the derived principal components can be interpreted from the correlation strength with the corresponding PCA loadings. Thus, the first principal component was primarily composed from VDP (0.88), C2 (0.68), C4 (-0.90), CoV (0.90), medium and maximum defect size (0.84), short-run emphasis (0.86), long-run emphasis (-0.84), short-run low-gray level emphasis (0.85), short-run high-gray level emphasis (0.84), long-run low gray-level emphasis (-0.83), and long-run high gray-level emphasis (-0.83); the second was mainly related to C3 (0.79), C5 (0.63), and run-level non-uniformity (-0.77). Hopkins statistic was greater than 0.5 (H=0.60), which confirmed non-random grouping and favoured towards the clustering tendency of the principal components.

Table 5 Principal component analysis and correlation of quantitative ^{129}Xe ventilation MRI measurements

	Principal Components	
	1	**2**
Principal Component Analysis		
Standard Deviation	2.98	1.80
Proportion of Variance, %	46.77	17.10
Cumulative Proportion, %	46.77	63.87
Correlation of Standardized Loadings		
VDP	0.88	0.18
Cluster 2	0.68	- 0.19
Cluster 3	- 0.13	0.79
Cluster 4	- 0.90	0.02
Cluster 5	- 0.48	0.63
CoV	0.90	0.00
Median Defect Size	0.84	0.14
Maximum Defect Size	0.84	0.16
SRE	0.86	0.29
LRE	- 0.84	0.44
GLNU	- 0.25	- 0.52
RLNU	0.13	- 0.77
RP	- 0.30	- 0.38
LGRE	0.21	0.27
HGRE	0.17	0.39
SRLGE	0.85	0.29
SRHGE	0.84	0.32
LRLGE	- 0.83	0.44
LRHGE	- 0.76	0.48

Definition of abbreviations: VDP = ventilation defect percent; CoV = coefficient of variation; SRE = short-run emphasis; LRE = long-run emphasis; GLNU = gray-level non-uniformity; RLNU = run-level non-uniformity; RP = run percentage; LGRE = low gray-level run emphasis; HGRE = high gray-level run emphasis; SRLGE = short-run, low gray-level emphasis; SRHGE = short-run, high gray-level emphasis; LRLGE = long-run, low gray-level emphasis; LRHGE = long-run high gray-level emphasis.

To identify the optimal clustering method, **Figure 3-2** shows the internal validation (i.e., evaluates the compactness, connectedness, and separation) of the three commonly used unsupervised approaches across two to four clusters. Based on the outputs, k-means or hierarchical clustering were the ideal approach to partition the unclassified quantitative MRI data. The various statistical tests for determining the optimal number of clusters using *NbClust* R package[179] had a majority consensus for a membership of 3 clusters. To ensure stability of clusters, the average Jaccard similarity index was determined on 1000 bootstrapped datasets and cluster analysis was performed on each dataset. If the index score of greater than 0.75 was achieved for all simulated clusters, than it had acceptable stability to procced with the analysis.[185] After collectively reviewing the internal validation results and Jaccard similarity index, the optimal method was hierarchical clustering to produce 3 distinct cluster memberships.

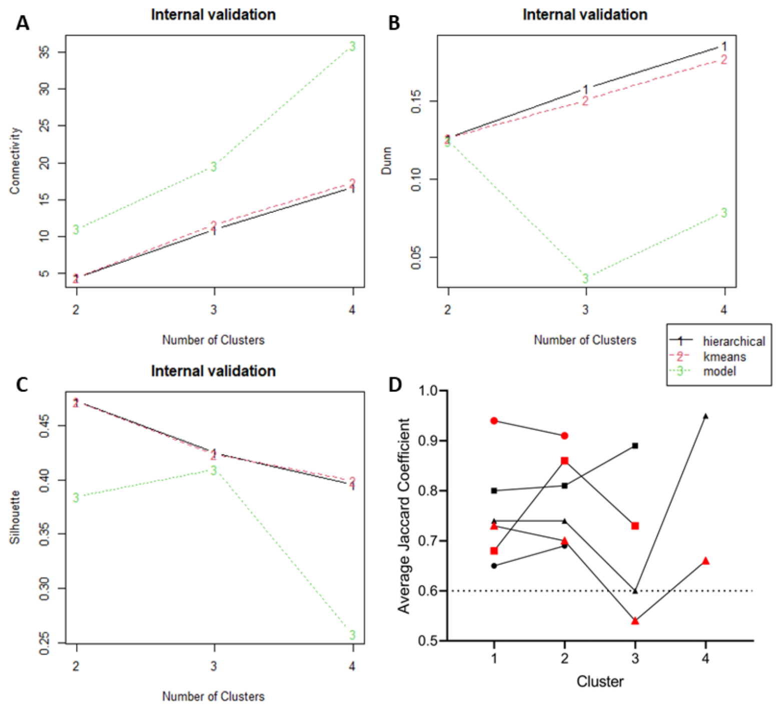

Figure 3-2 Internal properties and cluster stability validation of different clustering algorithms

Hierarchical clustering plotted as black; k-means plotted as red; Gaussian mixture model plotted as green.

A) Connectivity is the degree of connectedness of clusters and corresponds to the k-nearest neighbours being placed in the same cluster. The ideal cluster number should be close to zero. Hierarchical (Cluster 2=4.4, Cluster 3=11.0, and cluster 4=16.7); k-means (Cluster 2=4.4, Cluster 3=11.6, and cluster 4=17.3); Gaussian mixture model (Cluster 2=11.0, Cluster 3=19.6, and cluster 4=36.0)
B) Dunn's index evaluates the separation of clusters by taking the ratio of the between-cluster variance by the within-cluster variance. Higher the index, better the dispersion of clusters. Hierarchical (Cluster 2=0.13, Cluster 3=0.16, and cluster 4=0.19); k-means (Cluster 2=0.13, Cluster 3=0.15, and cluster 4=0.19); Gaussian mixture model (Cluster 2=0.12, Cluster 3=0.04, and cluster 4=0.08)
C) Silhouette score measures the distance between clusters. Observations that are well compacted and separated from neighbouring clusters have a higher score. Hierarchical (Cluster 2=0.47, Cluster 3=0.43, and cluster 4=0.40); k-means (Cluster 2=0.47, Cluster 3=0.42, and cluster 4=0.40); Gaussian mixture model (Cluster 2=0.38, Cluster 3=0.41, and cluster 4=0.26)
D) The membership stability of 2 to 4 clusters with hierarchical and k-means algorithms were assessed with Jaccard similarity coefficient on 1000 bootstrapped datasets. Hierarchical clustering with 3 clusters was determined to be the ideal approach. *Dotted line at 0.60 indicates the lower limit of cluster stability. Red symbols=k-means clustering, and black symbols=hierarchical clustering. Circle=2 clusters; square=3 clusters; triangle=4 clusters.*

3.3 MRI features of Ventilation Phenotypes of Severe Asthma

Figure 3-3 shows the hierarchical clustering heatmap of the original normalized nineteen ventilation MRI features and the composite principal component hierarchical clustering heatmap of the 58 patients with severe asthma. Three unique ventilation phenotypes of severe asthma were identified from the unsupervised clustering of ^{129}Xe ventilation MRI variables. Shown in **Figure 3-4** are four representative ^{129}Xe ventilation MRI coronal slices of patients with severe asthma for each ventilation phenotype. Cluster 1 had the smallest proportion of asthmatics (n=8, 14%) with a homogeneous distribution of ^{129}Xe gas with minimal ventilation defects, quite similar to a healthy individual[186] (VDP=1.7±0.9%). Cluster 2 had the highest proportion of asthmatics (n=32, 55%) with markedly abnormal ventilation (VDP=6.2±3.8%) and a mottled ventilation pattern throughout the lung. Cluster 3 (n=18, 31%) consisted of asthmatics with significantly abnormal ventilation (VDP=24.8±10.2%) due to the large defects and sparsely hyperintense regions from the accumulation of ^{129}Xe gas presumably in the limited unobstructed airways. **Table 6** shows nineteen MRI features that were incorporated into the machine learning algorithm and fifteen were significantly different between phenotypes. Notably, the signal-to-noise ratio was not different between clusters (p=0.32). A stepwise-forward discriminant analysis was performed to identify the major variables that contributed to the cluster memberships. Of the nineteen MRI variables VDP (Wilk λ=0.183), LRE (Wilk λ=0.214), and SRLGE (Wilk λ=0.157) were determined to be the dominant MRI parameters with the lowest Wilk λ values that significantly discriminated between ventilation patterns of each cluster.

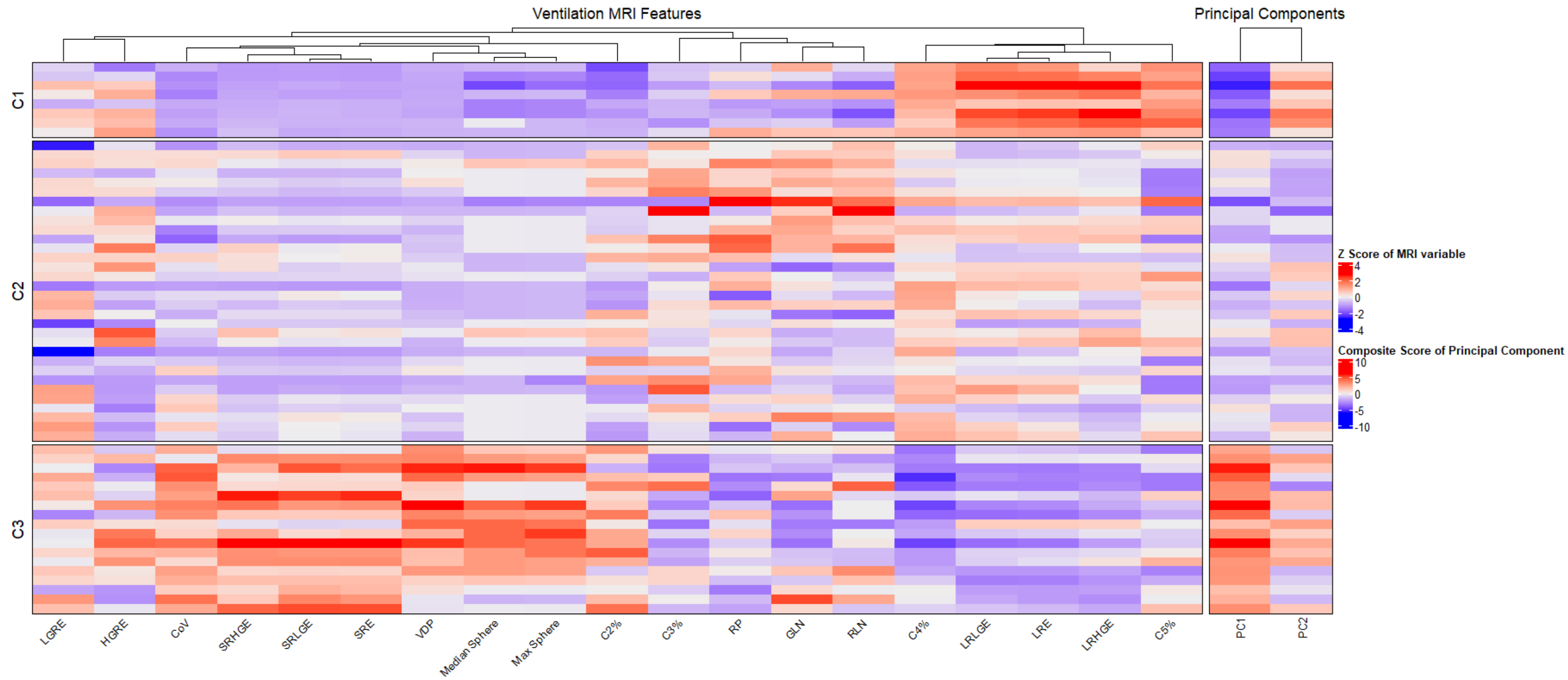

Figure 3-3 Distinct expression of ^{129}Xe MRI features within each ventilation phenotype

Heatmaps show the expression of nineteen normalized ^{129}Xe MRI features and composite score of principal components for 58 participants with severe asthma stratified by unsupervised cluster membership.

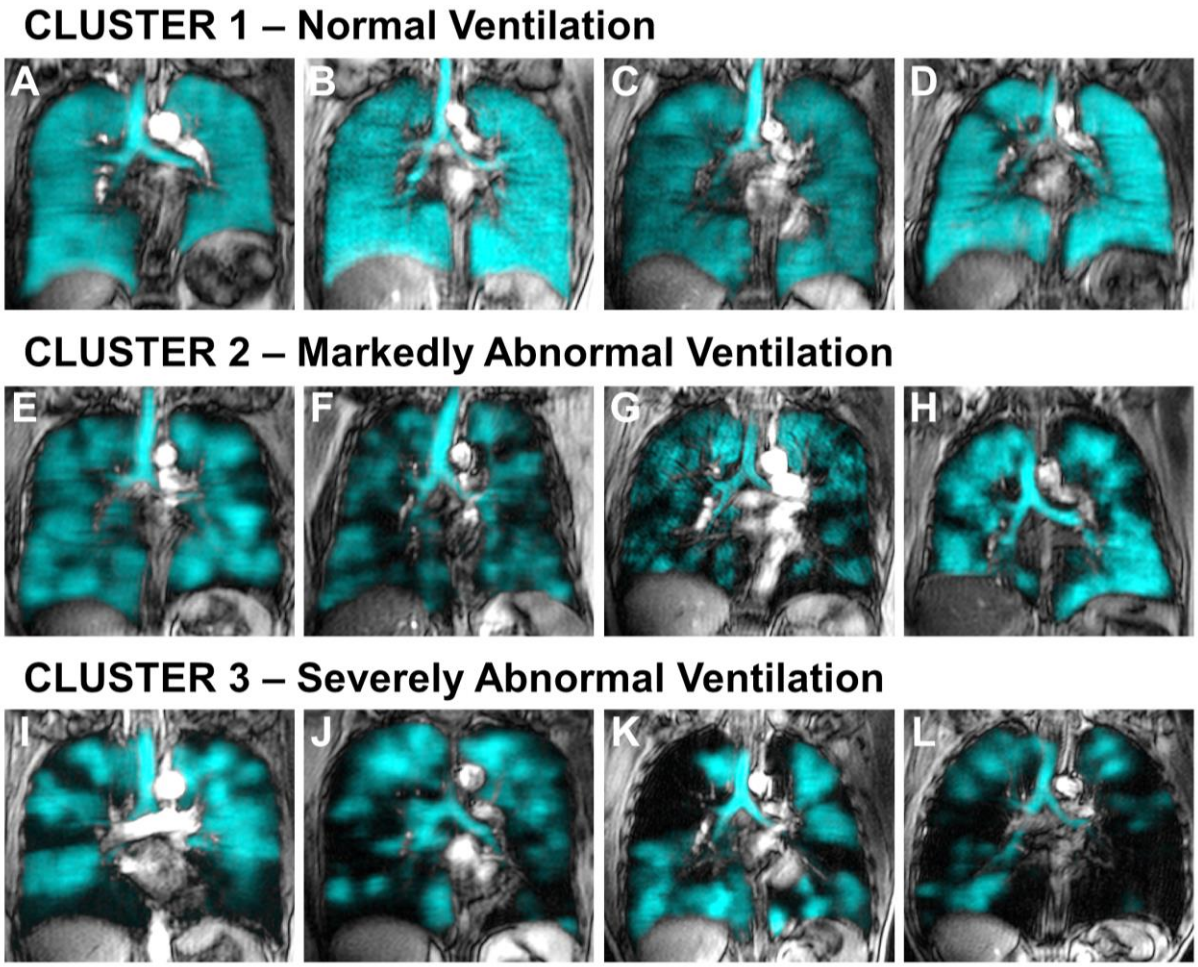

Figure 3-4 Representative pre-bronchodilator ^{129}Xe ventilation MRI coronal slices of patients with severe asthma by ventilation phenotype

Centre coronal slice ^{129}Xe MRI ventilation in cyan was co-registered to anatomical ^{1}H MRI in grayscale. **Patient A:** 60 years old male; ACQ-5=2.2; pre-BD FEV_1=65%$_{pred}$; pre-BD FEV_1/FVC=82%; pre-BD VDP = 1%. **Patient B:** 30 years old female; ACQ-5=1.0; pre-BD FEV_1=96%$_{pred}$; pre-BD FEV_1/FVC=76%; pre-BD VDP = 1.2%. **Patient C:** 36 years old female; ACQ-5=1.6; pre-BD FEV_1=91%$_{pred}$; pre-BD FEV_1/FVC=67%; pre-BD VDP = 2.8%. **Patient D:** 37 years old female; ACQ-5=2.2; pre-BD FEV_1=94%$_{pred}$; pre-BD FEV_1/FVC=82%; pre-BD VDP = 1%. **Patient E:** 49 years old female; ACQ-5=3.4; pre-BD FEV_1=42%$_{pred}$; pre-BD FEV_1/FVC=54%; pre-BD VDP = 6.5%. **Patient F:** 55 years old female; ACQ-5=3.8; pre-BD FEV_1=41%$_{pred}$; pre-BD FEV_1/FVC=60%; pre-BD VDP = 10.2%. **Patient G:** 55 years old female; ACQ-5=2.6; pre-BD FEV_1=81%$_{pred}$; pre-BD FEV_1/FVC=67%; pre-BD VDP = 11.3%. **Patient H:** 63 years old female; ACQ-5=4.2; pre-BD FEV_1=67%$_{pred}$; pre-BD FEV_1/FVC=57%; pre-BD VDP = 4.3%. **Patient I:** 53 years old female; ACQ-5=3.4; pre-BD FEV_1=38%$_{pred}$; pre-BD FEV_1/FVC=45%; pre-BD VDP = 29.2%. **Patient J:** 58 years old female; ACQ-5=1.8; pre-BD FEV_1=34%$_{pred}$; pre-BD FEV_1/FVC=41%; pre-BD VDP = 19.9%. **Patient K:** 40 years old male; ACQ-5=4.4; pre-BD FEV_1=38%$_{pred}$; pre-BD FEV_1/FVC=45%; pre-BD VDP = 21.7%. **Patient L:** 62 years old male; ACQ-5=1.4; pre-BD FEV_1=27%$_{pred}$; pre-BD FEV_1/FVC=38%; pre-BD VDP = 41.9%.

Table 6 ^{129}Xe MRI measures of ventilation signal intensity, ventilation heterogeneity, spherical defect size, and second-order texture features of severe asthma ventilation phenotypes

	Cluster 1	Cluster 2	Cluster 3	p-value* All	p-value* C1 vs. C2	p-value* C2 vs. C3	p-value* C3 vs. C1
n	8	32	18				
SNR	38±14	36±17	45±23	0.32	--	--	--
Ventilation Intensity							
VDP, %	1.7±0.9	6.2±3.8	24.8±10.2	**<0.001**	**0.03**	**<0.001**	**<0.001**
Cluster 2, %	10.6±1.3	14.0±2.2	16.3±2.2	**<0.001**	**<0.001**	**<0.001**	**<0.001**
Cluster 3, %	30.0±2.4	38.2±7.1	31.8±6.8	**<0.001**	**0.003**	**0.006**	>0.99
Cluster 4, %	36.4±1.9	31.9±3.8	20.3±5.4	**<0.001**	**0.02**	**<0.001**	**<0.001**
Cluster 5, %	21.6±3.3	10.2±6.9	8.4±5.7	**<0.001**	**0.001**	0.85	**<0.001**
Ventilation Heterogeneity							
CoV	0.24±0.02	0.30±0.05	0.42±0.05	**<0.001**	**0.01**	**<0.001**	**<0.001**
Spherical Ventilation Defect Size							
Median Defect Size, voxels	1.5 (0-3)	3 (1-4)	5 (2-7)	**<0.001**	0.07	**<0.001**	**<0.001**
Maximum Defect Size, voxels	2 (0-3)	5 (1-7)	9 (3-13)	**<0.001**	**0.03**	**<0.001**	**<0.001**
Second-Order Texture Features							
SRE	0.036±0.004	0.053±0.014	0.106±0.032	**<0.001**	0.11	**<0.001**	**<0.001**
LRE	73.6±8.33	52.7±6.34	41.5±7.47	**<0.001**	**<0.001**	**<0.001**	**<0.001**
GLNU	1034±143	1097±135	1009±159	0.11	--	--	--
RLNU	160±34	187±31	182±28	0.10	--	--	--
RP	0.081±0.012	0.090±0.017	0.075±0.011	**0.004**	0.25	**0.003**	0.66
LGRE	0.76±0.03	0.75±0.06	0.78±0.04	0.34	--	--	--
HGRE	2.63±0.36	2.48±0.37	2.59±0.40	0.40	--	--	--
SRLGE	0.030±0.003	0.042±0.011	0.083±0.025	**<0.001**	0.14	**<0.001**	**<0.001**
SRHGE	0.083±0.019	0.137±0.050	0.297±0.11	**<0.001**	0.16	**<0.001**	**<0.001**
LRLGE	55.8±5.7	41.4±4.9	33.6±5.4	**<0.001**	**<0.001**	**<0.001**	**<0.001**
LRHGE	224.3±49.8	134.2±25.9	97.2±28.4	**<0.001**	**0.005**	**0.002**	**<0.001**

Definition of abbreviations: SNR = signal-to-noise ratio; VDP = ventilation defect percent; CoV = coefficient of variation; SRE = short-run emphasis; LRE = long-run emphasis; GLNU = gray-level non-uniformity; RLNU = run-level non-uniformity; RP = run percentage; LGRE = low gray-level run emphasis; HGRE = high gray-level run emphasis; SRLGE = short-run, low gray-level emphasis; SRHGE = short-run, high gray-level emphasis; LRLGE = long-run, low gray-level emphasis; LRHGE = long-run high gray-level emphasis.
Values are mean ± standard deviation or median (minimum - maximum) except when indicated otherwise.
*Significance of difference between clusters determined using ANOVA with Tukey's correction, or Kruskal Wallis with Dunn's test.

3.4 Clinical Characterization of Ventilation Phenotypes of Severe Asthma

3.4.1 Demographics and Comorbidities

Ventilation phenotype demographics, smoking history, and comorbidities are summarized in **Table 7**. The ventilation phenotypes were significantly different with respect to age (p=0.02), BMI (p=0.02), and history of chest infections (p=0.008). Cluster 1 was predominately young females who were obese (88% female, 41±11 years old, 63% obese). Cluster 1 had the highest prevalence of common asthma masqueraders including gastroesophageal reflux (n=4, 50%), anxiety/depression (n=2, 25%) and vocal cord dysfunction (n=1, 13%). Cluster 2 was significantly older than Cluster 1, but also predominately obese females (63% females, 54±13 years old, 59% obese). Cluster 2 had a high prevalence of concomitant cardiovascular disease (n=12, 38%). Cluster 3 was also significantly older than Cluster 1, with an equal proportion of males and females, who were not obese (50% female, 56±12 years old, 11% obese). Cluster 3 had a higher proportion of participants with frequent respiratory tract infections (8 of 18, 44%), compared to Clusters 1 (0 of 8, 0%) and 2 (4 of 32, 13%). Most participants were never-smokers, and all phenotypes had a similar pack-year smoking history (p=0.65). The prevalence of atopy (p=0.95), chronic rhinosinusitis (p=0.80) and nasal polyps (p=0.88) were similar between the ventilation phenotypes.

Table 7 Demographics and comorbidities of severe asthma ventilation phenotypes

	Cluster 1	Cluster 2	Cluster 3	p-value*			
				All	C1 vs. C2	C2 vs. C3	C3 vs. C1
Demographics							
n	8	32	18				
Age, years	41±11	54±13	56±12	**0.02**	**0.04**	0.84	**0.02**
Female, n (%)	7 (88)	20 (63)	9 (50)	0.19	--	--	--
BMI, kg/m^2	31±8	32±6	27±4	**0.02**	0.96	**0.01**	0.18
Underweight/normal, n (%)	2 (25)	4 (13)	5 (28)	0.37	--	--	--
Overweight, n (%)	1 (13)	9 (28)	11 (61)	**0.02**	0.65	**0.04**	**0.04**
Obese, n (%)	5 (63)	19 (59)	2 (11)	**0.002**	>0.99	**0.001**	**0.01**
Smoking History							
n	8	32	18				
Never n (%)	5 (63)	19 (59)	13 (72)	0.66	--	--	--
Past n (%)	2 (25)	12 (38)	5 (28)	0.69	--	--	--
Current n (%)	1 (13)	1 (3)	0	0.56	--	--	--
Pack-years	0 (0-10)	0 (0-33)	0 (0-35)	0.65	--	--	--
Comorbidities & Life Factors							
n	8	32	18				
Premature birth, n (%)	0	3 (9)	0	0.28	--	--	--
Atopy, n (%)	5 (63)	20 (63)	12 (67)	0.95	--	--	--
Chronic rhinosinusitis, n (%)	3 (38)	16 (50)	8 (44)	0.80	--	--	--
Nasal polyps, n (%)	3 (38)	13 (41)	6 (33)	0.88	--	--	--
Gastroesophageal reflux, n (%)	4 (50)	10 (31)	5 (28)	0.52	--	--	--
Vocal cord dysfunction, n (%)	1 (13)	1 (3)	0	0.27	--	--	--
Anxiety/depression, n (%)	2 (25)	4 (13)	1 (6)	0.37	--	--	--
Cardiovascular disease, n (%)	0	12 (38)	3 (17)	0.05	--	--	--
Frequent infections, n (%)	0	4 (13)	8 (44)	**0.008**	0.57	**0.02**	**0.03**

Definition of abbreviations: BMI = body mass index
Values are mean ± standard deviation or median (minimum - maximum) except when indicated otherwise.
*Significance of difference between clusters determined using ANOVA with Tukey's correction, Kruskal Wallis with Dunn's test, or Chi-Square test.

3.4.2 Asthma Characteristics and Medications

Table 8 summarizes asthma onset, control, quality of life and asthma medications for each ventilation phenotype. The age of asthma onset was not statistically different between phenotypes (p=0.54). There was however a trend towards Cluster 2 having a higher proportion of participants with early-onset asthma (≤11 year of age, 16 of 31, 52%). Ventilation phenotypes were not different with respect to their self-reported asthma control (ACQ-5 p=0.23) or quality of life (AQLQ p=0.66). Notably, nearly 75% of participants in each phenotype had uncontrolled asthma, indicated by an ACQ-5 ≥ 1.5.[67] The prevalence of uncontrolled asthma was therefore high and not different between phenotypes (p=0.98). The phenotypes were not different with respect to current ICS dose (p=0.56) or OCS dose (p=0.86), and a similar proportion of participants were OCS dependent (C1: 2 of 8, 25%; C2: 9 of 32, 28%; C3: 6 of 18, 33%; p=0.89) and/or receiving a biologic (C1:3 of 8, 38%; C2: 9 of 32, 28%; C3: 5 of 18, 28%; p=0.86) for their asthma. Considering previous biologic use, nearly all participants in each phenotype had previously received biologic therapy for their asthma (88% of C1, 88% of C2, and 83% of C3, p=0.91), and had failed one or more biologics (83% of C1, 75% of C2, and 73% of C3, p=0.95). Cluster 1 had a significantly higher proportion of participants who previously underwent bronchial thermoplasty (38% of C1, 3% of C2, and 6% of C3, p=0.007).

Table 8 Asthma characteristics, medications, and healthcare utilization of severe asthma ventilation phenotypes

	Cluster 1	Cluster 2	Cluster 3	p-value*			
				All	C1 vs. C2	C2 vs. C3	C3 vs. C1
Asthma onset, control, and quality-of-life							
n	8	31	18				
Age of asthma onset, yrs	23±18	19±17	25±18	0.54	--	--	--
≤11 yrs of age, n (%)	3 (38)	16 (52)	5 (28)	--	--	--	--
12-18 yrs of age, n (%)	1 (13)	3 (10)	2 (11)	--	--	--	--
19-30 yrs of age, n (%)	1 (13)	2 (6)	7 (39)	--	--	--	--
31-40 yrs of age, n (%)	2 (25)	6 (19)	0	--	--	--	--
>40 yrs of age, n (%)	1 (13)	4 (13)	4 (22)	--	--	--	--
Asthma duration, yrs	18±13	35±17	30±20	0.08	--	--	--
n	8	32	18				
ACQ-5	1.8 (0.8-2.2)	2.7 (0-4.8)	2.6 (0.8-5.2)	0.23	--	--	--
≥ 1.5 n (%)	6 (75)	23 (72)	13 (72)	0.98	--	--	--
AQLQ	4.9 (2.9-6.4)	4.6 (2.0-6.9)	4.8 (2.7-6.3)	0.66	--	--	--
Symptoms	5.0 (2.7-6.4)	4.3 (1.3-6.9)	4.7 (3.4-6.5)	0.58	--	--	--
Activities	5.0 (3.7-6.1)	4.9 (1.9-6.9)	5.5 (3.4-6.5)	0.53	--	--	--
Emotions	4.5 (1.0-7.0)	3.6 (1.2-7.0)	3.4 (1.8-6.6)	0.91	--	--	--
Environment	5.6 (1.5-6.8)	4.9 (1.5-7.0)	5.8 (2.3-6.5)	0.88	--	--	--
Asthma Medications							
n	8	32	18				
ICS dose, µg/day	1000 (500-2000)	1000 (500-2000)	875 (250-2000)	0.56	--	--	--
OCS dependent, n (%)	2 (25)	9 (28)	6 (33)	0.89	--	--	--
OCS dose, mg/day	0 (0-25)	0 (0-20)	0 (0-25)	0.86			
n	8	32	18				
Bronchial thermoplasty, n (%)	3 (38)	1 (3)	1 (6)	**0.007**	**0.02**	>0.99	0.07
Current biologic, n (%)	3 (38)	9 (28) †	5 (28) ‡	0.86	--	--	--
Omalizumab, n (%)	2 (66)	0	0	--	--	--	--
Mepolizumab, n (%)	1 (33)	1 (11)	0	--	--	--	--
Reslizumab, n (%)	0	2 (22)	1 (20)	--	--	--	--
Benralizumab, n (%)	0	4 (44)	1 (20)	--	--	--	--
Dupilumab, n (%)	0	5 (56)	4 (80)	--	--	--	--
Ever biologic, n (%)	7 (88)	28 (88)	15 (83)	0.91	--	--	--
Ever failed biologic, n (%)	5 (83)	21 (75)	11 (73)	0.95	--	--	--

Definition of abbreviations: ACQ = asthma control questionnaire; AQLQ = asthma quality of life questionnaire; ICS = inhaled corticosteroids; OCS = oral corticosteroids.
Values are mean ± standard deviation or median (minimum - maximum) except when indicated otherwise.
*Significance of difference between clusters determined using ANOVA with Tukey's correction, Kruskal Wallis with Dunn's test, or Chi-Square test.
†n=3 on dual biologics (n=2 benralizumab and dupilumab; n=1 benralizumab and reslizumab); ‡n=1 on dual biologics (benralizumab and dupilumab)

3.5 Physiological Characterization of Ventilation Phenotypes of Severe Asthma

Table 9 summarizes spirometry, bronchodilator reversibility, and historical airway hyperresponsiveness for each ventilation phenotype. The ventilation phenotypes were significantly different with respect to $FEV_1\%_{pred}$, $FVC\%_{pred}$, and FEV_1/FVC measured pre- and post-bronchodilator (all $p<0.05$). Cluster 1 had normal or near-normal spirometry (pre/post-BD: $FEV_1=80\pm15\%_{pred}/87\pm16\%_{pred}$;$FVC=89\pm17\%_{pred}/FVC=91\pm17\%_{pred}$;$FEV_1/FVC=74\pm7\%/78\pm5\%$), Cluster 2 had obstructive spirometry (pre/post-BD: $FEV_1=61\pm17\%_{pred}/FEV_1=73\pm17\%_{pred}$; $FVC=79\pm15\%_{pred}$/ $FVC=87\pm14\%_{pred}$; $FEV_1/FVC=60\pm10\%$/ $FEV_1/FVC=66\pm10\%$), and Cluster 3 had severe airflow obstruction (pre/post-BD: $FEV_1=41\pm12\%_{pred}$/ $47\pm16\%_{pred}$; $FVC=67\pm11\%_{pred}$/ $77\pm13\%_{pred}$; $FEV_1/FVC=48\pm10\%$/ $51\pm12\%$). Cluster 1 had no participants with fixed airflow obstruction (post-bronchodilator $FEV_1/FVC<0.70$), but the prevalence of fixed airflow obstruction was high in Clusters 2 (n=23, 72%) and 3 (n=16, n=89%).

Bronchodilator reversibility, evaluated as the post-bronchodilator change in spirometry, was not significantly different between the ventilation phenotypes. However, Clusters 2 and 3 had numerically greater post-bronchodilator changes in FEV_1 and FVC compared to Cluster 1, with a trend towards significance in both measurements between clusters (Δ FEV_1 $p=0.09$; Δ FVC $p=0.06$). There was a significant difference in post-bronchodilator change in MRI VDP ($p<0.0001$) in Cluster 3 (VDP = -6% [-28- -2]) compared to Clusters 1 (VDP = 0% [-1-1]) and 2 (VDP = -1% [-10-2]).

A review of historical methacholine challenge tests revealed a similar proportion of participants in each cluster had ever documented severe airway hyperresponsiveness ($p=0.15$), defined as a $PC_{20}<1.0$ mg/mL.

Table 9 Physiological characteristics of severe asthma ventilation phenotypes

	Cluster 1	Cluster 2	Cluster 3	p-value*			
				All	**C1 vs. C2**	**C2 vs. C3**	**C3 vs. C1**
Spirometry, pre-bronchodilator							
n	8	32	18				
FEV_1, $\%_{pred}$	80±15	61±17	41±12	**<0.001**	0.06	**0.001**	**<0.001**
FVC, $\%_{pred}$	89±17	79±15	67±11	**0.002**	0.21	**0.02**	**0.002**
FEV_1/FVC, %	74±7	60±10	48±10	**<0.001**	**0.002**	**<0.001**	**<0.001**
Normal, n (%)	3 (38)	3 (9)	0	**0.01**	0.08	0.54	**0.02**
Non-obstructive, n (%)	2 (25)	2 (6)	1 (6)	0.21	--	--	--
Obstructive, n (%)	3 (38)	17 (53)	6 (33)	0.36	--	--	--
Mixed, n (%)	0	10 (31)	11 (61)	**0.008**	0.17	0.07	**0.007**
Spirometry, post-bronchodilator							
n	8	32	18				
FEV_1, $\%_{pred}$	87±16	73±17	47±16	**<0.001**	0.41	**0.002**	**<0.001**
FVC, $\%_{pred}$	91±17	87±14	77±13	**0.03**	0.67	0.06	0.05
FEV_1/FVC, %	78±5	66±10	51±12	**<0.001**	**0.006**	**<0.001**	**<0.001**
FEV_1/FVC < 70%, n (%)	0	23 (72)	16 (89)	**<0.001**	**0.0003**	0.29	**0.0001**
Normal, n (%)	6 (75)	15 (47)	1 (6)	**0.001**	0.24	**0.004**	**<0.001**
Non-obstructive, n (%)	2 (25)	0	0	**0.002**	**0.04**	>0.99	**0.09**
Obstructive, n (%)	0	13 (41)	11 (61)	**0.01**	**0.04**	0.24	**0.007**
Mixed, n (%)	0	4 (13)	6 (33)	0.07	--	--	--
Bronchodilator reversibility							
n	8	32	18				
Reversibility, n (%)	2 (25)	20 (63)	10 (56)	0.16	--	--	--
Δ FEV_1, %	8 (5-19)	20 (-7-68)	20 (-5-70)	0.09	--	--	--
Δ FVC, %	2 (0-6)	8 (-8-50)	15 (-5-37)	0.06	--	--	--
Δ VDP, %	0 (-1-1)	-1(-10-2)	-6 (-28- -2)	**<0.0001**	0.45	**<0.0001**	**<0.0001**
Airway Hyperresponsiveness							
n	8	17	5				
PC_{20}, mg/ml†	0.8±9.7	1.1±8.1	2.9±7.8	0.60	--	--	--
Ever PC_{20} <1.0 mg/mL	4 (50)	7 (41)	3 (60)	0.15	--	--	--

Definition of abbreviations: FEV_1= forced expiratory volume in one second; FVC = forced vital capacity; PC_{20} = methacholine concentration causing a 20% decreased in FEV_1.
Values are mean ± standard deviation or median (minimum - maximum) except when indicated otherwise.
*Significance of difference between clusters determined using ANOVA with Tukey's correction, Kruskal Wallis with Dunn's test, or Chi-Square test.
†Geometric mean and geometric standard deviation of most recent

3.6 Biological Characterization of Ventilation Phenotypes of Severe Asthma

As shown in **Table 10**, metrics of inflammation were reported for each ventilation phenotype. There were no significant differences in clinical biomarkers of type-2 inflammation, including blood eosinophil count (p=0.20), sputum eosinophil percent (p=0.28), and FeNO (p=0.15), between phenotypes. The ventilation phenotypes were significantly different with respect to sputum total cell count (p=0.03), sputum neutrophil percent (p=0.02), and sputum macrophage percent (p=0.009). Among the ventilation phenotypes, Cluster 3 had the highest total cell count (sputum TCC=6.5×10^6 cells/g [1.6-94.6]), relative neutrophil count (sputum neutrophils=70.6% [17.3-96.7]), and the lowest relative macrophage count (sputum macrophages=16.9% [0.5-61.3]). Considering sputum cellular endotype, Cluster 1 had significantly more paucigranulocytic sputum (n=6, 75%) compared to Cluster 3 (17%, p=0.008) and minimal airway eosinophilia (n=2, 25%), despite having the highest prevalence of elevated blood eosinophils (n=5, 63%). Cluster 2 had an approximately even proportion of individuals with paucigranulocytic sputum (n=14, 44%) and active airway inflammation (n=16, 50%), which were eosinophilic (n=9, 28%), neutrophilic (n=4, 13%) and mixed granulocytic (n=3, 9%). Cluster 3 had the highest proportion of participants with active airway inflammation (n=13, 72%), which were eosinophilic (n=7, 39%), neutrophilic (n=3, 17%) and mixed granulocytic (n=3, 17%). In addition, there was a significant proportion of individuals with an abnormal relative sputum neutrophil percent (sputum neutrophils $\geq$ 64%)[187] in Cluster 3 (n=12, 75%) compared to Clusters 1 (n=0, 0%; p=0.002) and 2 (n=10, 38%; p=0.02).

In a subset of participants with sufficient sample of sputum supernatant, cytokines associated with type 1/2 signatures (individual measurements n=41, 71%) and autoimmune immunological pathways (individual measurements n=27, 58%) were measured. All molecular measurements are summarized in **Table 10**, and those that were significantly different or had evident outliers between ventilation phenotypes are shown in **Figure 3-5**. The upper limit of normal (90^{th} percentile) of plotted sputum cytokines were derived from age-matched healthy controls. The ventilation phenotypes were significantly different with respect to sputum IL-4 (p=0.001), IL-6 (p=0.03), IL-15 (p=0.02), and BAFF (p=0.04). Cluster 1 had significantly higher sputum IL-4 than Clusters 2 (p=0.008) and 3 (p=0.0007) and all patients in Cluster 1 had sputum IL-4 levels greater than the upper limit of normal. Cluster 2 had higher IL-6 levels (87 pg/mL [5-764]) than Cluster 1 (p=0.02). Compared to Cluster 1, Cluster 3 had higher IL-15 (1.6 pg/mL [0.8-4.7], p=0.02) and BAFF (40 pg/mL [24-463], p=0.04).

Table 10 Biological characteristics of severe asthma ventilation phenotypes

	Cluster 1	Cluster 2	Cluster 3	p-value*			
				All	**C1 vs. C2**	**C2 vs. C3**	**C3 vs. C1**
Blood eos, 10^9 cells/L	0.3 (0-0.8)	0.1 (0-1.5) †	0.3 (0-3.3) ‡	0.20	--	--	--
≥0.3x10^9 cells/L, n (%)	5 (63)	13 (42)	8 (50)	0.56	--	--	--
FeNO, ppb	17 (5-51)	33 (8-140)	26 (5-227)	0.15	--	--	--
≥25ppb, n (%)	3 (38)	24 (75)	9 (50)	0.07	--	--	--
Sputum Cell Counts & Endotype							
n	4	26	16				
TCC, x10^6 cells/g	2.2(0.9-3.8)§	4.8 (0.6-227.4)ll	6.5 (1.6-94.6) ¶	**0.03**	0.24	0.34	**0.03**
≥9.7x10^6 cells/g, n (%)	0	9 (28)	7 (41)	0.22	--	--	--
Eosinophils, %	2.6 (0.3-9.3)	0.6 (0-26.3)	2.3 (0-22.7)	0.28	--	--	--
≥2.3%, n (%)	2 (50)	11 (42)	9 (56)	0.68	--	--	--
Neutrophils, %	35.4(16.3-54.7)	49.5(17.3-96.5)	70.6(17.3-96.7)	**0.02**	0.29	0.11	**0.03**
≥64%, n (%)	0	10 (38)	12 (75)	**0.003**	0.17	**0.02**	**0.002**
Macrophages, %	57.7 (30.7-80)	35.8 (0-77.5)	16.9 (0.5-61.3)	**0.009**	0.26	0.06	**0.02**
Lymphocytes, %	3.7 (1.5-5.3)	1.3 (0-7.3)	2.0 (0-5)	0.08	--	--	--
Bronchial epithelial, %	0.9 (0-2)	0.2 (0-5.7)	0.0 (0-2.5)	0.57	--	--	--
Sputum Cellular Endotype**							
n	8	32	18				
Paucigranulocytic, n (%)	6 (75)	14 (44)	3 (17)	**0.02**	0.24	0.07	**0.008**
Eosinophilic, n (%)	2 (25)	9 (28)	7 (39)	0.68	--	--	--
Neutrophilic, n (%)	0	4 (13)	3 (17)	0.48	--	--	--
Mixed-granulocytic, n (%)	0	3 (9)	3 (17)	0.42	--	--	--
Trivial Neutrophilic, n (%)	0	2 (6)	2 (11)	0.57	--	--	--
Sputum Cytokines							
n	6	22	13				
IL-4 pg/mL	1.1 (0.6-1.6)	0.3 (0.0-1.2)	0.1 (0.0-1.0)	**0.001**	**0.008**	0.69	**0.001**
IL-5 pg/mL	0.4 (0.0-0.5)	0.4 (0.0-11.9)	0.7 (0.0-8.9)	0.80	--	--	--
IL-13 pg/mL	0.4 (0.0-3.7)	1.7 (0.0-11.8)	0.1 (0.0-11.9)	0.74	--	--	--
IL-12p70 pg/mL	1.6 (0.1-2.4)	1.2 (0.0-2.5)	1.0 (0.2-6.4)	0.55	--	--	--
IL-17α pg/mL	4.7 (0.0-7.8)	2.4 (0-82.6)	1.2 (0-5.6)	0.27	--	--	--
IL-1β pg/mL	49 (25-166)	76 (15-2021)	156 (16-788)	0.09	--	--	--
IL-18 pg/mL	68.5 (16.4-447)	74.5 (0.8-287)	33.9 (6.9-278)	0.46	--	--	--
IL-10 pg/mL	0.9 (0.0-1.35)	0.9 (0.0-5.1)	0.7 (0.0-1.8)	0.50	--	--	--
n	4	14	9				
IL-15 pg/mL	0.6 (0.4-0.8)	0.9 (0.5-13.6)	1.6 (0.8-4.7)	**0.02**	0.22	0.45	**0.02**
INF-γ pg/mL	0.1 (0.1-0.2)	0.1 (0.0-0.4)	0.2 (0.0-0.2)	0.61	--	--	--
TNF-α pg/mL	2.2 (1.1-3.3)	1.9 (0.7-46.5)	2.9 (1.9-44.6)	0.41	--	--	--
IL-6 pg/mL	13 (4-18)	87 (5-764)	38 (15-1137)	**0.03**	**0.02**	>0.99	0.11
BAFF pg/mL	10 (4-16)	60 (5-328)	40 (24-463)	**0.04**	0.07	>0.99	**0.04**
IL-33 pg/mL	1.6 (0.7-5)	2.4 (0.9-8.9)	2.8 (0.5-8.7)	0.46	--	--	--

Definition of abbreviations: eos = eosinophils; FeNo = fractional concentration of exhaled nitric oxide; IL= interleukin; INF-γ = Interferon gamma; TNF-α = tumor necrosis factor alpha; BAFF = B-cell activating factor.

Values are mean ± standard deviation or median (minimum - maximum) except when indicated otherwise.

*Significance of difference between clusters determined using ANOVA with Tukey's correction, Kruskal Wallis with Dunn's test, or Chi-Square test. †n=31, ‡n=16, §n=5, ll n=27, ¶n=17.

**Paucigranulocytic: Total cell count (TCC)<9.7x10^6 cells/g, <2.3% eosinophils, and <64% neutrophils or produced insufficient sample after 3 rounds of sputum induction; Eosinophilic: ≥2.3% eosinophils and/or moderate or many eosinophil-free-granules; Neutrophilic: ≥64% neutrophils and TCC ≥9.7x10^6 cells/g without eosinophilia; Mixed-granulocytic: eosinophilic and neutrophilic; trivial neutrophilic: ≥64% neutrophils or TCC ≥9.7x10^6 cells/g (but not both).

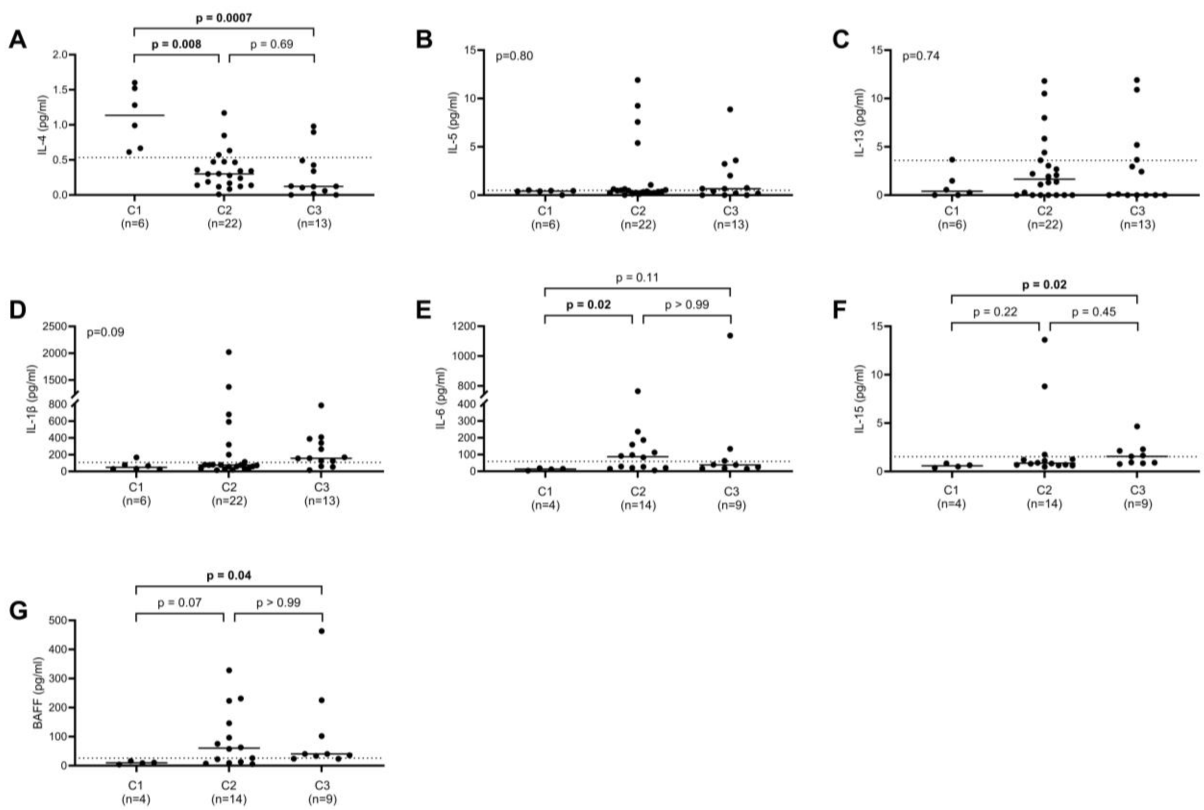

Figure 3-5 Molecular mediators that may be contributing to the pathological mechanisms in each ventilation phenotype of severe asthma.

Cytokines related to type-2 inflammation (A, B, C) and dysregulated immunological responses (D, E, F, G) were quantified in a subset of individuals to better understand the molecular mechanism within each ventilation phenotype. Dashed lines are the upper limit of normal (90th percentile) of age-matched healthy controls.

A) IL-4 was significantly higher in Cluster 1 patients with normal ventilation compared to abnormally ventilated individuals in Cluster 2 (p=0.008) and Cluster 3 (p=0.0007).
B) IL-5 was not significantly different between clusters; however, outliers were observed in patients with abnormal ventilation.
C) IL-13 was not significantly different between clusters; however, outliers were observed in patients with abnormal ventilation.
D) IL-1β was not significantly different between clusters; however, outliers were observed in patients with abnormal ventilation.
E) IL-6 was significantly higher in Cluster 2 patients with markedly abnormal ventilation compared to Cluster 1 (p=0.02).
F) IL-15 was significantly higher in Cluster 3 patients with severely abnormal ventilation compared to Cluster 1 (p=0.02). Outliers were observed in markedly abnormal ventilated patients in Cluster 2.
G) BAFF was significantly higher in Cluster 3 patients with severely abnormal ventilation compared to Cluster 1 (p=0.04). Outliers were observed in markedly abnormal ventilated patients in Cluster 2.

3.7 Quantitative CT Measurements

CT derived airway measurements, mucus scores, lung volumes, and the lung attenuation are shown in **Table 11**. The airway LA, outer area, WA% and WT% were averaged by the five representative segmental airways (RB1, RB4, RB10, LB1, and LB10) and all nineteen bronchopulmonary segments, none of which demonstrated significant differences between the ventilation phenotypes (all p>0.05). Notably, the bronchial dimensions were significantly different for increased thickness of the airway walls between the ventilation phenotypes (p=0.04); however, the differences were not significant after normalizing the airway size by expressing wall thickness as a percentage of external airway diameter (p=0.86). In **Figure 3-6**, the LA, WT and WT% are plotted for each of the 19 bronchopulmonary segments. The morphology of the 19 segmental airways by ventilation phenotypes indicates trends toward Cluster 2 having larger LA and greater airway calibre relative to Clusters 1 and 3. In addition, a significant difference was observed in WT% of the RB1 airway being greater in Cluster 1 compared to Cluster 3 (p=0.03). The total airway count was not different between clusters (p=0.76).

The burden of mucus plugging assessed by the CT mucus score was different between clusters (p=0.007). The median CT mucus score was 0 (0-7) in Cluster 1, 6 (0-14) in Cluster 2, and 9 (0-14) in Cluster 3. Compared to Cluster 1, a higher proportion of patients in Clusters 2 (n=19, 90%) and 3 (n=16, 94%) (p=0.006) had one or more airways completely occluded by mucus.

The CT-derived RV (p=0.002), RV$\%_{pred}$ (p=0.001), and TLC$\%_{pred}$ (p=0.007) were significantly different between the ventilation phenotypes. Cluster 3 had a higher RV (RV=3.6L [2.5-5.1]; RV=205$\%_{pred}$ [141-292]) than Cluster 1 (RV=1.8L [1.5-2.5]; RV=123$\%_{pred}$ [75-164]) and Cluster 2 (RV=3.1L [1.6-4.6]; RV=163$\%_{pred}$ [122-238]). The CT-derived TLC$\%_{pred}$ was very low in

Cluster 1 (85%$_{pred}$ [57-108]), and this was significantly lower than Clusters 2 (98%$_{pred}$ [85-126], p=0.02) and 3 (100%$_{pred}$ [82-131], p=0.005).

Quantitative analysis of CT lung attenuation revealed that the clusters were different with respect to the magnitude of gas-trapping on expiratory CT (%LAA$_{-856}$ at RV, p=0.001) and emphysema on inspiratory CT (%LAA$_{-950}$ at TLC, p=0.05). Cluster 3 had significantly more gas-trapping (%LAA$_{-856}$=22% [3-51]) compared to Clusters 1 (%LAA$_{-856}$=1% [1-3], p=0.003) and 2 (%LAA$_{-856}$=13% [1-38], p=0.04). In addition, Cluster 3 had statistically more emphysema (%LAA$_{-950}$=2% [1-16]) compared to Cluster 1 (%LAA$_{-950}$=1% [1-2], p=0.046), although the magnitude of emphysema was not clinically meaningful.

Table 11 Quantitative CT measures of airway morphology, mucus plugging, lung volume, and gas-trapping of severe asthma ventilation phenotypes

	Cluster 1	Cluster 2	Cluster 3	p-value			
				All	**C1 vs. C2**	**C2 vs. C3**	**C3 vs. C1**
Airway Morphology							
n	5	21	17				
Lumen area mm^2							
5 segments	16±5	22±7	18±6	0.07	--	--	--
19 segments	19±4	23±6	20±6	0.23	--	--	--
Outer area mm^2							
5 segments	45±12	58±16	50±11	0.15	--	--	--
19 segments	50±9	60±13	53±11	0.12	--	--	--
Wall thickness mm							
5 segments	1.4±0.1	1.6±0.2	1.5±0.1	0.08	--	--	--
19 segments	1.5±0.1	1.6±0.2	1.5±0.1	**0.04**	0.11	0.08	0.82
Wall area %							
5 segments	64.2±3.0	63.2±2.5	64.0±4.3	0.69	--	--	--
19 segments	63.1±1.8	63.4±2.2	63.6±4.0	0.93	--	--	--
Wall thickness %							
5 segments	17.4±1.2	16.7±1.5	17.0±2.5	0.73	--	--	--
19 segments	17.2±2.0	17.0±1.0	17.3±2.1	0.86	--	--	--
Total airway count	170(151-204)	185(135-254)	194(117-289)	0.76	--	--	--
Mucus Score	0 (0-7)	6 (0-14)	9 (0-14)	**0.007**	0.23	0.14	**0.008**
Presence of mucus plugs	2 (40)	19 (90)	16 (94)	**0.006**	**0.03**	>0.99	**0.02**
≥4 mucus plugs[89]	1 (20)	13 (62)	15 (88)	**0.01**	0.15	0.14	**0.009**
Lung Volume							
n	5	21	17				
Residual Volume							
Litres	1.8 (1.5-2.5) †	3.1 (1.6-4.6)	3.6 (2.5-5.1)	**0.002**	0.09	**0.03**	**0.003**
%Predicted	123 (75-164) †	163 (122-238)	205 (141-292)	**0.001**	0.13	**0.01**	**0.003**
Total Lung Capacity							
Litres	4.3 (4.0-6.8)	6.1 (3.8-7.7)	5.8 (4.2-8.8)	0.08	--	--	--
%Predicted	85 (57-108)	98 (85-126)	100 (82-131)	**0.007**	**0.02**	0.59	**0.005**
Lung Attenuation							
n	5	21	15				
Gas-trapping							
%LAA$_{-856}$ HU at RV	1 (1-3) †	13 (1-38)	22 (3-51)	**0.001**	0.15	**0.04**	**0.003**
Emphysema							
%LAA$_{-950}$ HU at TLC	1 (1-2)	2 (1-10)	2 (1-16)	**0.05**	0.28	0.65	**0.046**

Definition of abbreviations: LAA= low attenuation area; HU = Hounsfield units; RV = residual volume; TLC = total lung capacity.
Values are mean ± standard deviation or median (minimum - maximum) except when indicated otherwise.
*Significance of difference between clusters determined using ANOVA with Tukey's correction, Kruskal Wallis with Dunn's test, or Chi-Square test. †n=3.

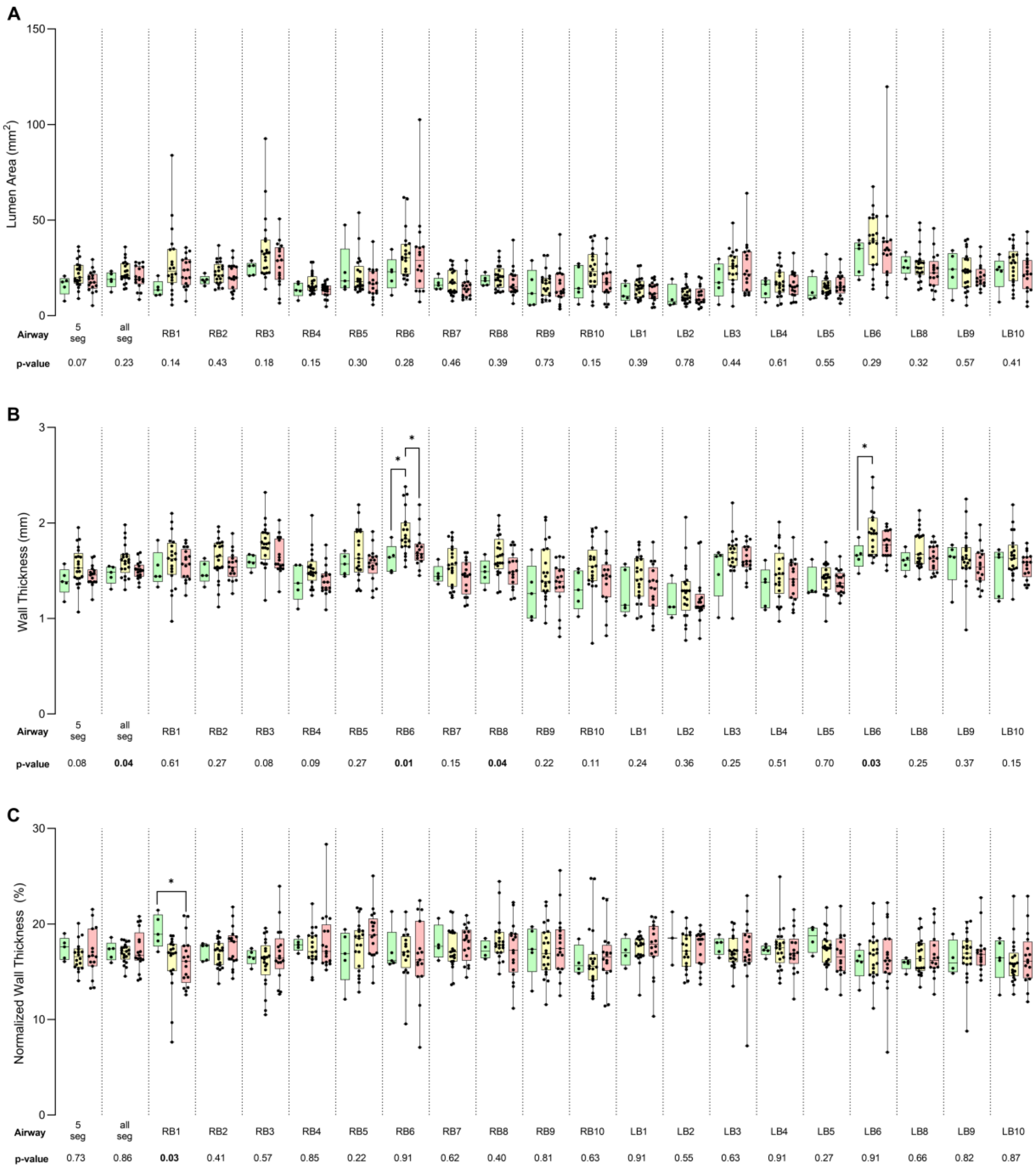

Figure 3-6 CT airway morphology measurements for each bronchopulmonary segment stratified by severe asthma ventilation phenotypes.

CT derived airway measurements of lumen area (A), wall thickness (B), and normalized wall thickness area (C) plotted by average of 5 representative segmental airways, all segmental airways and each of the 19 bronchopulmonary segments. Whiskers represent minimum and maximum values. *Green=Cluster 1; yellow=Cluster 2; red=Cluster 3. *p<0.05.*

Chapter 4: Discussion

An unsupervised machine learning model was employed to generate three clusters that were identified as three novel ventilation phenotypes of severe asthma. Utilizing nineteen ^{129}Xe ventilation MRI features of 58 patients with severe asthma, we observed significant differences in their demographic, clinical, physiological, and biological characteristics. Our approach differs from previous clustering models that employed clinical outcomes,[156,157] molecular expression,[188,189] or CT structural imaging biomarkers.[166,167] The majority of clustering studies in severe asthma have identified phenotypes that, in part, explain the heterogeneity. Taken together, the findings from the ventilation phenotypes summarized in **Figure 4-1** provide novel insights to the pathophysiology of severe asthma. To our knowledge, this is the only study to date that solely examined functional lung MRI biomarkers in an unsupervised cluster approach. Also, our analysis only examined patients with severe asthma to generate functional phenotypes using MRI. Since one of the integral components of asthma is airway hyperresponsiveness, pre-bronchodilator ventilation imaging features were examined to account for all three clinical features of asthma including the burden of airway smooth muscle dysfunction.

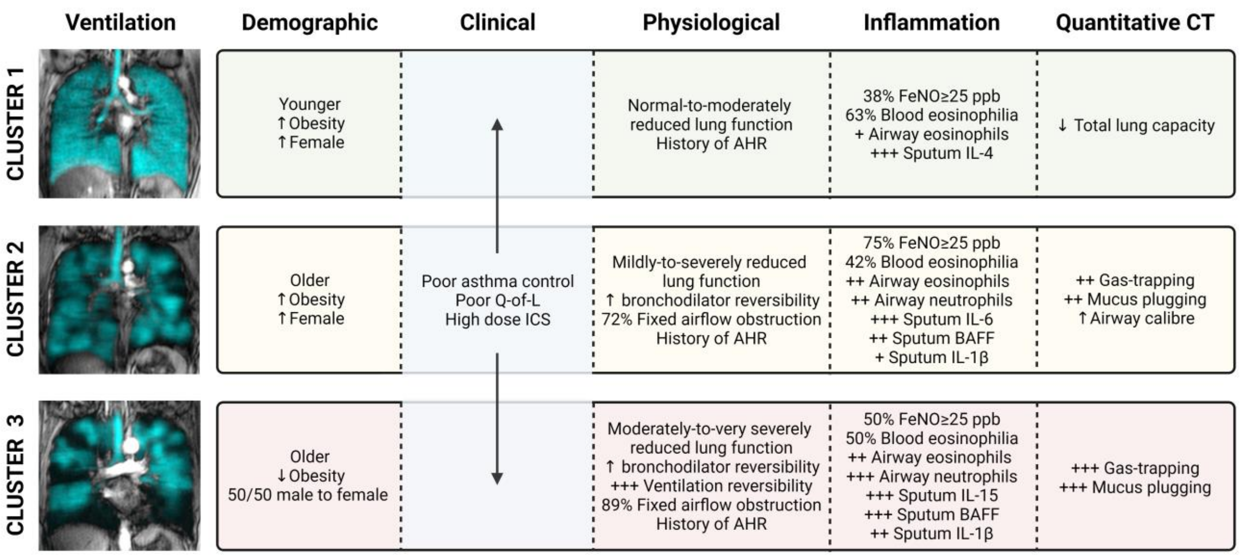

Figure 4-1 Summary of findings from unsupervised clustering analysis of hyperpolarized ^{129}Xe ventilation MRI in severe asthma

The significant and clinically relevant observations of severe asthma ventilation phenotypes reported according to demographic characteristics, clinical outcomes, physiological response, inflammatory mechanisms, and quantitative CT measurements. (Created with BioRender.com).

4.1 Normal Ventilation Cluster

Cluster 1 was comprised of young females, nearly all of whom were obese with normal-to-moderately reduced lung function measured by spirometry that had ventilation comparable to a healthy individual[186] and modest prevalence of inflammation (n=2, 25%) and bronchodilator reversibility (n=2, 25%). Consistent with previous studies,[89,91,130,139] this group had minimal burden of mucus plugging (CT mucus score=0 [0-7]). Interestingly, while these individuals had clinically significant historical airway hyperresponsiveness, they had minimal ventilation defects despite withholding medications that prevent hyperreactive airways. It is counter-intuitive to observe a cohort of patients with severe asthma with normal ventilation and lung function to have inadequate control of their symptoms despite being on high-dose ICS and previously trialed on biologics. CT derived lung volumes were significantly lower at total lung capacity, suggesting these patients may have anatomically smaller lungs or are unable to completely inspire to their maximum capacity. Moreover, a significant proportion (n=3, 38%) had underwent bronchial thermoplasty. Yet, these patients continue to have uncontrolled asthma. Initially we thought these patients may have normal ventilation due to a positive response to bronchial thermoplasty however their ventilation patterns were similar before and after the procedure.[148] These observations suggest cofounders may be contributing to the bronchial hyperresponsiveness in this cohort. Skloot *et al*[190] demonstrated that healthy participants restricted from taking a deep inspiration during the methacholine procedure had airway hyperresponsiveness comparable to patients with asthma. The cumulative effects of excessive chest and abdominal fat, and inability to fully expand the airways may augment the methacholine-induced airway hyperresponsiveness in these patients due to geometric effects.[21,190] While the average normalized wall thickness did not differ between clusters, there was a significantly greater normalized airway thickness in the RB1 airway in these patients. Post-mortem review of obese individuals with asthma demonstrated accumulation of adipose tissue in the outer airway wall led to greater airway thickness.[191] In addition to the thoracic compression, another reason for increased airway hyperresponsiveness in these patients may be increased airway resistance in select thickened “fatty airways” after bronchial challenge.[192] Interestingly, Eddy *et al*[86] demonstrated CT-derived TAC was reduced with abnormal ventilation and greater asthma severity. But in our analysis, TAC did not differ between phenotypes despite the varying spectrum of ventilation heterogeneity. This observation may be because Cluster 1 was unable to fully expand their airways to permit accurate CT segmentation, or perhaps bronchial thermoplasty in the select individuals led to scarring and narrowing of the airway lumen. Similar to this thesis, normal ventilation in asthma measured by MRI VDP was previously reported.[118] However, unlike our observations their patients had mild-to-moderate asthma with minimal respiratory symptoms and had borderline normal airway hyperresponsiveness measured by methacholine. MRI VDP is a robust marker of airflow obstruction, and Mummy *et al.*[138]

demonstrated the usefulness of it at predicting exacerbations in asthma. Interestingly, a small subset of patients in their cohort with normal or near-normal MRI VDP[186] had exacerbations too. Though not specified in their analysis, this suggests there are other contributors to breathlessness including chronic rhinosinusitis, nasal polyps, and gastroesophageal reflux. These asthma masqueraders were observed in our cohort of patients with normal ventilation and suggest a plausible explanation for "asthma-like symptoms".

The discordance between blood and sputum eosinophils is quite evident in this cluster of individuals with normal ventilation. More participants in this cluster had blood eosinophilia (n=5, 63%) than sputum eosinophilia (n=2, 25%). This observation supports the notion that localized rather than systemic markers of inflammation are more representative of the airway pathology in severe asthma.[50] All patients in Cluster 1 had IL-4 levels elevated in their sputum compared to the other phenotypes with significantly abnormal ventilation. The role of IL-4 is crucial in developing the allergic sensitization phase by directing T2 cell polarization and facilitating IgE synthesis.[193] However, other classical T2 cytokines and eosinophils were not significantly increased in the lumen, which suggests other cellular sources including basophils and mast cells may be contributing to the release of IL-4 into the intraluminal space, resulting to inadequate control, and airway hyperresponsiveness.[194] More work is needed to understand the exact mechanism of IL-4 in this cohort of patients with no functional lung impairments, but persistent symptoms (e.g., dyspnea). Collectively, our observations suggest currently reported symptoms are not directly related to airway obstruction but rather may be due to asthma masqueraders and/or deconditioning and altered lung mechanics related to obesity.

4.2 Markedly Abnormal Ventilation Cluster

Cluster 2 was predominantly older, obese females with mildly-to-severely reduced FEV_1 and partially reversible obstructive spirometry. They had markedly abnormal ventilation with a trend towards greater bronchodilator reversibility, and higher prevalence of early-onset asthma. This largest cluster of patients with severe asthma had substantial mucus plugging (mucus score = 6 [0-14]) and gas trapping (%LAA_{-950}=13% [1-38]). This phenotype had elevated sputum levels of IL-6, suggesting pro-inflammatory mechanisms.[195] Also, there were a substantial proportion of individuals with abnormal levels of airway neutrophils (n=10, 38%) and greater co-morbidity for cardiovascular disease including hypertension (n=12, 38%).

In agreement with our observations, previously reported obese individuals with severe asthma were shown to have elevated IL-6 inflammation, however it was observed in systemic circulation.[195,196] Specifically, in the SARP cohort, individuals with high plasma IL-6 had greater prevalence of females, obesity, hypertension, and blood neutrophils.[196] Adipose tissue and inflammatory macrophages induce low-grade systemic inflammation by secreting pro-inflammatory cytokines including IL-6, which may act upon adaptive immune responses.[197,198] Greater levels of sputum IL-6 were observed to be associated with FEV_1 decline[199,200] and poorly controlled asthma measured with ACQ-5.[199] Interestingly, despite being not significant, there were evident outliers of patients with abnormally elevated IL-5 and IL-13 levels in their sputum. Both cytokines are associated with T2 inflammation and shown to contribute to airway remodeling, mucus hypersecretion, and smooth muscle hyperresponsiveness.[201-203]

In addition, a substantial proportion of patients in this phenotype had elevated FeNO (n=24, 75%) based on the cut-off value of 25 ppb or greater. This may suggest the up regulation of airway inflammation.[204] Furthermore, morphometric airway measurements of IL-6 transgenic mice have demonstrated increased bronchiolar calibre[205] and this observation was replicated in this unbiased analysis for a subset of patients with severe asthma. This was an interesting finding accompanied with a trend towards increased lumen area in a subset of patients may suggest sub-clinical bronchiectasis or larger airways. Longitudinal analysis demonstrated IL-6 is a predictive biomarker of loss of lung function, and exacerbation in asthma.[206] Therefore, these individuals need to be attentively monitored for accelerated decline in lung health.

4.3 Severely Abnormal Ventilation Cluster

Cluster 3 were older individuals with moderately-to-very severely reduced FEV_1 and partially reversible obstructive spirometry. They had significant ventilation abnormalities, elevated levels of sputum neutrophils and the highest burden of mucus plugging. Consistent with previous literature, this cohort with significant gas trapping had a history of recurrent chest infections, higher count of airway neutrophils, fixed airflow obstruction,[207,208] and mucus plugging.[139,209] Of the patients with airway inflammation (n=13, 72%), a substantial portion of patients had eosinophilic inflammation (n=9 had ≥2.3% eosinophils, 56%), but localized and systemic eosinophil count were not significantly different between clusters. Interestingly, despite the dominant T2 inflammatory endotype, only a small subset of individuals (n=5, 28%) were prescribed biologic therapy at the time of study visit. Subsequently, many individuals were enrolled into a phase 3 randomized clinical trial of dupilumab (NCT03884842) or received biologic treatment through clinical care. This cohort had high total sputum cell count, and high relative airway count of neutrophils, but many did not meet the clinical criteria of airway infection due to total cell count being less than $9.7x10^6$ cells/g.[41] Soley examining the relative normal cut-off of airway leukocytes, there were a significant proportion of individuals with elevated airway neutrophils (n=12 had ≥64% neutrophils, 75%) and greater proportion of patients with mixed-granulocytic inflammation (n=7 had ≥64% neutrophils and ≥2.3% eosinophils, 44%). Being on high-dose ICS, in part, may prevent apoptosis of neutrophils and support their survival in the airways.[210] Previously, Choi *et al.*[166] unsupervised clustering analysis of 57 quantitative CT local, lobar, and global structural lung features identified a similar cohort of older patients with severe asthma that had significant air-trapping, predominance of fixed airflow obstruction, and high sputum neutrophil count.

Regardless of the criteria of airway inflammation, it does not provide any information about cellular activation, activity, and regulation. Therefore, it was necessary to analyze their sputum cytokines to better understand the molecular pathways that may be involved in this severe phenotype. A subset of individuals had a dominant non-T2 signature with increased levels of IL-15, IL1β and BAFF. These elevated cytokines in this cluster are implicated in severe, steroid-resistant,[211] neutrophilic inflammation,[212] and autoimmune processes in asthma.[213-216] This severe clinical phenotype aligned with previous findings from a sputum cell transcriptomics analysis in asthma. In this study, Kuo *et al.*[189] performed unsupervised hierarchical clustering on the expression of gene signatures from intraluminal inflammatory cells in eosinophilic and non-eosinophilic patients. They identified a molecular phenotype of asthma with neutrophilic driven mechanisms, and excessive nucleotide-binding oligomerization domain–like receptor family, pyrin domain–containing 3 (NLRP3) inflammasome activation. The gene expression of IL-1β and NLRP3 were previously demonstrated to be elevated in severe asthma and associated with severe airflow obstruction and increased sputum neutrophils.[211] The frequent bacterial chest infections observed in this cohort likely promotes the influx of neutrophils into the local lung milieu to eradicate and control the infection through phagocytosis and may release neutrophil extracellular traps (NETs). The increased extracellular DNA content and oxidative stress induced by NETs may contribute to impaired airway clearance and mucus plugging by increasing the mucus viscoelasticity and making the mucus plug more rigid and solid-like.[217] Important to note, mucus plugging in Clusters 2 and 3 were accompanied with abnormal ventilation, and fixed airflow obstruction. These observations provide further evidence of the role of mucus plugs as major contributors to airflow obstruction in asthma.[139] Similar to our findings, a bronchoscopy study by Wenzel *et. al*[218] reported significantly higher levels of airway neutrophils in patients with severe asthma who had poor lung function and were on high doses of oral and inhaled corticosteroids. In addition, the neutrophil count in endobronchial tissue biopsies were greater in patients with severe asthma compared to milder asthma and healthy participants, and there was a trend towards a greater neutrophil count in the eosinophilic, severe asthma subgroup.[219] Furthermore, in the SARP cohort, elevations in both sputum eosinophils and neutrophils were associated with greater lung function decline.[220] Combined with our observations of mixed-granulocytic inflammation, significant mucus plugging and functional impairment, we speculate airway neutrophils and eosinophils may be contributing, in part, to abnormal ventilation by releasing mediators[217,221] that make mucus stiffer, tenacious, and difficult to propel leading to intraluminal plugging. This needs to be further studied by characterizing the mucus composition in this severe clinical phenotype.

Additionally, the molecular expression of this ventilation phenotype is similar to previously reported findings of autoimmunity in severe asthma and may suggest a plausible mechanism for a subset of individuals with abnormal ventilation. The release of nuclear antigens from NETs has shown to trigger autoantibody formation promoting eosinophilic degranulation, and subsequent worsening in clinical indices of pulmonary health.[216,222]

It is important to acknowledge that previous work supports a positive relationship between abnormal ventilation and sputum eosinophil count.[131] However, our results did not demonstrate a significant difference in airway eosinophils between ventilation phenotypes. The median relative airway eosinophil count was less than 3% in all three ventilation phenotypes. This observation may be due to the suppression of eosinophils by high-dose glucocorticoids and anti-T2 monoclonal therapies.

4.4 Concordance of MRI Ventilation Phenotypes with Large Cohort Phenotyping Studies in Asthma

The findings from this unsupervised study design produced phenotypes with similar characteristics from larger asthma cohorts.[157,158] The normal ventilation phenotype (i.e., Cluster 1) is similar to SARP Cluster 3 and U-BIOPRED Phenotype 4 by consisting of an obese, female dominant cohort with inadequate control of their asthma despite normal lung function. The markedly abnormal ventilation phenotype (i.e., Cluster 2) is similar to SARP Cluster 2 by consisting of the largest group characterized by older females with greater bronchodilator reversibility and trend towards early-onset asthma. The severely abnormal ventilation phenotype (i.e., Cluster 3) related to SARP Clusters 4/5 and U-BIOPRED Phenotype 3 by consisting of the most severe airflow obstructed asthma participants with greater airway inflammation. The novelty of unsupervised machine learning of ventilation patterns is the clustering of patients was based solely on the direct functional consequence related to whole-lung asthma pathology. The ^{129}Xe MRI features were able to differentiate between Clusters 1 and 2, despite the severity of airflow limitation (i.e., FEV_1) not being significant. Furthermore, the reported asthma control, asthma quality of life, the dosage of medications and biologic use did not differ between clusters. These observations from the ventilation phenotypes emphasize the sensitivity of ^{129}Xe MRI to differentiate patients with similar subjectively reported disease burden.

4.5 Clinical Relevance

The outcomes from this unsupervised analysis produced findings consistent with various findings from other independent asthma studies[91,118,130,139,205,208] and supports the utility of ventilation ^{129}Xe MRI in understanding asthma pathophysiology. In a clinical setting, incorporating functional lung MRI may assist with gauging the extent of airway pathology, and the potential for efficacy of therapeutic interventions prior to commencement. For example, if normal ventilation (MRI features of Cluster 1) is observed after bronchorelaxant medications were withheld in a patient with absent or controlled airway inflammation suggests re-evaluation for other diagnoses that are masqueraders of asthma symptoms.[223] If significant abnormal ventilation is observed after a positive direct bronchoprovocation challenge, perhaps mechanical/structural reasons led to the methacholine induced bronchoconstriction. In contrast, individuals with abnormal ventilation (MRI features of Clusters 2 and 3) with significant airway inflammation and airway hyperresponsiveness may benefit from monitoring their ventilation after starting treatment to observe spatial and temporal changes in ventilation. As ^{129}Xe MRI begins to be integrated into clinical settings, it will be necessary to have a consensus to guide clinicians to know 1) when is it beneficial to use ^{129}Xe MRI in the context of severe asthma, and 2) how to accurately interpret the ventilation images and quantitative metrics.[224]

4.6 Limitations

We recognize and acknowledge that this thesis has several limitations including the generalizability of the findings due to a relatively small sample size, and recruitment from a single asthma care centre. However, we would like to note that this is the largest dataset of quantitative ^{129}Xe ventilation MRI features of patients with severe asthma. Furthermore, findings from this thesis were observed in various other unsupervised clustering studies from multidisciplinary asthma care centres.[157,158,166,167,189] To be more confident in the findings of this thesis, an external validation on an independent dataset is necessary to confirm the generalizability of our unsupervised model, and if there are sub-populations within identified ventilation phenotypes of severe asthma. While unique ventilation phenotypes of severe asthma were identified at our site, this was a cross-sectional analysis, and it remains to be seen of the predictive and prognostic value from a longitudinal assessment. In addition, longitudinal studies are required to better understand the clinical relevance of each ventilation phenotype. Furthermore, there are inherent limitations to the CT mucus score[89] used in our analysis including the difficultly to discern on CT that mucus is the primary contributor to intraluminal occlusion in the distal, smaller airways. Furthermore, we used the term "mucus plugs" to describe CT-visible intraluminal plugs, however it may be comprised of inflammatory cells, extracellular traps, Charcot-Leyden crystals, and plasma proteins.[87,225] Due to innate properties of performing a radiomic analysis, we are aware of the susceptibility of MRI features to skew from the true physiological value due to the background noise. To circumvent this issue, we set a high SNR threshold of greater than 15 and confirmed the clusters did not differ based on SNR. Furthermore additional texture features could have been used to characterize the ventilation patchiness by extracting the size-zone, co-occurrence, dependence, and neighbourhood gray-tone difference matrices.[226] However, these additional texture features from PyRadiomics,[226] an open source radiomic platform originally intended to address the needs in cancer research has not been extensively validated in the field of functional lung MRI and asthma.[227] Therefore, we opted to use MRI features that have been previously published and demonstrated relevant findings.[140,151,152] Future unsupervised machine learning studies may be able to further differentiate the ventilation patterns and perhaps identify sub-populations within the three ventilation phenotypes that we observed to be clinically relevant. Additionally, we recognize the whole-lung MRI features used in our analysis do not provide regional information about asthma pathology, and the unsupervised clustering pipeline may be improved in the future by incorporating lobar and segmental functional MRI biomarkers. Nevertheless, for the first time in severe asthma, we demonstrated the use of an unsupervised machine learning pipeline of composite functional lung MRI features to identify ventilation phenotypes of clinical relevance.

In summary, for the first time we have shown the use of unsupervised machine learning method to identify three distinct cohorts of severe asthma with varying degree of abnormal ventilation. The outcomes from this thesis suggest disease mechanisms within each cluster including age, obesity, airway remodeling, small airways disease, mucus plugging and airway inflammation. The discrete patterns of ventilation heterogeneity between phenotypes provides insight to the pathology of severe asthma and may be used to support precise and personalized asthma management.

Chapter 5: Conclusion and Future Directions

In the past 30 years, the advancements in understanding the underpinnings of severe asthma, and subsequent development of therapies has reduced the global mortality.[228] However, the high level of morbidity continues to be a significant issue and underscores the need to better understand and characterize severe asthma. There have been numerous unsupervised clustering studies with various assessment tools to identify phenotypes with the goal of improving asthma care. But the translation of the findings has been difficult to integrate into clinical practice. To identify novel phenotypes of severe asthma to ultimately support targeted care, we proposed the use of hyperpolarized ^{129}Xe ventilation MRI, an emerging clinical tool that has been extensively researched in relation to asthma pathology, progression, and severity.[118,130,132,138,139,150,229]

This study was executed in a top-down manner by examining the functional consequence of disease with ventilation MRI and then examining the underlying pathobiological mechanisms. An unbiased clustering of nineteen ventilation MRI features identified three novel clusters or ventilation phenotypes of severe asthma. The severity of abnormal ventilation of each phenotype had distinct characteristics that likely contribute to uncontrolled symptoms, and the need to use high intensity treatment. One of the primary objectives of unsupervised clustering of high-dimensional data is to assist with generating hypotheses. Based on our findings, various research questions have emerged that may be explored to further understand asthma pathophysiology including autoimmunity, functional small airways disease, mucus plugging and vascular pruning.

5.1 Prognostic and Predictive Value of ^{129}Xe MRI Ventilation Phenotypes of Severe Asthma

Research Questions:

- What is the prognostic and predictive value of these ^{129}Xe MRI ventilation phenotypes?
- What are the clinical, imaging, and molecular outcomes of each ventilation phenotype over a period of time?
- Do the ventilation phenotypes assist with precise and personalized treatment in severe asthma?

There were unique mechanisms of disease that were identified that may be clinically managed to relieve symptom burden and improve asthma control. The prognostic and predictive value of these ventilation phenotypes will be the imminent focus of future work. Majority of the patients in our analysis completed their ^{129}Xe MRI and other assessments at least a year ago. They were subsequently managed at a tertiary care centre for their respiratory symptoms and all their relevant clinical history was well-documented. This provides a great resource to investigate the association of the ventilation phenotypes with accelerated lung function decline, healthcare utilization (emergency room visit/hospitalization), optimal therapeutic response to anti-T2 biologics and improvement in asthma control and quality of life.

Of great interest, we anticipate obese individuals with normal ventilation and controlled airway inflammation in Cluster 1 to benefit from lifestyle changes, and/or if warranted semaglutide[230] to reduce their weight and improve their asthma control.

In individuals with marked abnormal ventilation in Cluster 2, it may be beneficial to understand the predominant endotype responsible for pathology in the airways and accordingly modify their treatment. Lack of targeted treatment in these individuals may make them prone to exacerbations and lung function decline.[206] For future studies, in this cohort, a subset of patients may benefit from IL-6 inhibition (e.g., tocilizumab) as a reasonable therapeutic target to alleviate inflammation and mucus plugging.[196]

In individuals with severely abnormal ventilation in Cluster 3 with aberrant airway inflammation and highly prevalent mucus plugging need high intense treatment with biologics that target both the eosinophils, and the mucus burden in the airways to resolve abnormal ventilation, perhaps treatment with dupilumab.[231] Another complementary treatment is antibiotics such as macrolides for airway bacterial infection,[232] which may likely reduce the neutrophilic inflammation and in part the mucus plugging in this cohort. However, studies that directly target T2 low cytokines such as IL-1β may be warranted for patients who fail to improve from the available therapeutic interventions.[233,234]

Identifying the prognostic and predictive value of MRI ventilation phenotypes will provide evidence for the usefulness of functional MRI in asthma management and decision making.

5.2 Autoimmunity and Abnormal MRI Ventilation in Severe Asthma

Research Questions:

- Could alternate autoimmune pathology contribute to sub-optimal response to biologic therapy in patients with abnormal ventilation?
- Do autoimmune mechanisms contribute to persistent mucus plugging, and abnormal ventilation?
- Which autoantibodies are highly prevalent in individuals with severe asthma and abnormal ventilation?

Severe asthma is not an autoimmune disease, however chronic cellular inflammation, and dysregulated immune responses in the lung microenvironment may induce an autoimmunity cascade that further exacerbate the decline in lung function, and overall health.[222] Select individuals with abnormal ventilation had elevated indirect airway markers of autoimmunity, however airway and circulating autoantibodies were not quantified. It is prudent to determine the array of autoantibody levels to identify possible therapeutic targets that may be contributing to disease burden. Furthermore, successful responders of biologic therapy may have an overall reduction in autoimmune markers in severe asthma,[222] but is this change in concordance with a reduction in mucus plugging, airway remodeling, and ultimately abnormal ventilation still needs to be investigated.

5.3 Airway Inflammatory Endotypes and MRI Ventilation in Asthma with Fixed Airflow Obstruction

Research Questions:

- What are the predominant contributors to airway obstruction in this severe phenotype?
- What is the underlying inflammatory endotype that contributes to parenchymal alternations and abnormal ventilation?
- How does fixed airflow obstruction and abnormal ventilation affect deposition patterns of first-line inhaled therapies?

To assist with the diagnose of asthma, bronchodilator reversibility criteria and variable airflow obstruction can be used to support the concept of bronchospasms or twitchy airways. In our analysis, we identified a substantial proportion of fixed airflow obstructed individuals with severe asthma in the markedly abnormal (n=23, 72%) and severely abnormal (n=16, 89%) ventilation phenotypes. Ventilation heterogeneity reflects the pathology in the small and large airways, and as presented in this study there was greater predominance of small airways disease in severely abnormal ventilated patients. In a subset of these individuals, there was a lack of resolution in ventilation abnormalities after bronchodilator administration, and this may signify a possible mechanism of inadequate response to first line inhaled therapies due to severe narrowing and closure of small airways preventing the passage of aerosolized drugs to distal sites of inflammation.[235] Many of the patients in our cohort are lifetime non-smokers and were not exposed to noxious particles to diagnosis them with COPD. It has been well documented that severe airflow obstruction in asthma is due to airway remodeling and parenchymal alterations driven by chronic localized inflammation.[236] However the intraluminal cellular inflammation, and pro-inflammatory molecular expression associated with fixed airflow obstruction still remains to be investigated.

Physiologic mechanistic studies are needed to better understand the underlying mechanisms associated with this severe clinical phenotype.

5.4 MRI Ventilation Abnormalities, Pulmonary Vasculature Pruning, and Small Airways Disease in Severe Asthma

Research Questions:

- How does airway pathology (i.e., remodeling, mucus plugging, and inflammation) affect pulmonary vasculature redistribution in asthma?
- What is the driving physiological mechanism for pulmonary vascular pruning in asthma?
- What is the spatial relationship between abnormal ventilation, gas-trapping and vascular pruning in asthma?

Asthma bronchial obstruction is visualized as ventilation defects on hyperpolarized gas MRI and reflects respiratory disability. Beyond the proximal airways, the significance of gas-trapping in severe asthma, and its effects on adverse physiological effects on ventilation is well-recognized. Interestingly, greater asthma severity is related to reduced CT-visible total airway count,[86] and loss of peripheral pulmonary vasculature.[237] There are currently two postulated mechanisms for vascular pruning in obstructive lung diseases: 1) hypoxic vasoconstriction redirects blood to ventilated areas and prunes the vessels in the unventilated regions; 2) local airspace hyperinflation increases alveolar pressure to mechanically force the pulmonary vessels to compress. Pulmonary vascular pruning has been linked to airway obstruction and airway inflammation.[237] Recently, McIntosh *et al.*[238] reported changes in pulmonary vasculature and ventilation after long-term use of benralizumab treatment in eosinophilic asthma. However, the regional relationship underlying the complex interplay between abnormal ventilation, small airways disease, and peripheral pulmonary vascular pruning still remains to be determined.

In conclusion, for this thesis we employed an unsupervised clustering algorithm of nineteen ventilation MRI features and identified three unique ventilation phenotypes of severe asthma. The composite MRI-radiomic signature provided clinical insight to the pathophysiology and provides suggestions of therapeutic options in severe asthma.

Chapter 6: References

1 Weibel, E. R. & Gomez, D. M. Architecture of the Human Lung. *Science* **137**, 577-585 (1962). https://doi.org:doi:10.1126/science.137.3530.577

2 Bouhuys, A. *The Physiology of Breathing: A Textbook for Medical Students*. (Grune & Stratton, 1977).

3 Hsieh, A., Assadinia, N. & Hackett, T.-L. Airway remodeling heterogeneity in asthma and its relationship to disease outcomes. *Frontiers in Physiology* **14** (2023). https://doi.org:10.3389/fphys.2023.1113100

4 Thais Mauad, D. S. F. Asthma as a Cause of Death. *Pulmão RJ* **21**, 18-24 (2012).

5 Masoli, M., Fabian, D., Holt, S. & Beasley, R. The global burden of asthma: executive summary of the GINA Dissemination Committee report. *Allergy* **59**, 469-478 (2004). https://doi.org:10.1111/j.1398-9995.2004.00526.x

6 Partridge, M. R. Examining the unmet need in adults with severe asthma. *European Respiratory Review* **16**, 67-72 (2007). https://doi.org:10.1183/09059180.00010402

7 Public Health Agency of Canada: REPORT FROM THE CANADIAN CHRONIC DISEASE SURVEILLANCE SYSTEM: ASTHMA AND CHRONIC OBSTRUCTIVE PULMONARY DISEASE (COPD) IN CANADA. (2018).

8 Mauer, Y. & Taliercio, R. M. Managing adult asthma: The 2019 GINA guidelines. *Cleveland Clinic Journal of Medicine* **87**, 569-575 (2020). https://doi.org:10.3949/ccjm.87a.19136

9 McGregor, M. C., Krings, J. G., Nair, P. & Castro, M. Role of Biologics in Asthma. *American Journal of Respiratory and Critical Care Medicine* **199**, 433-445 (2019). https://doi.org:10.1164/rccm.201810-1944CI

10 Czira, A. *et al.* A systematic literature review of burden of illness in adults with uncontrolled moderate/severe asthma. *Respir Med* **191**, 106670 (2022). https://doi.org:10.1016/j.rmed.2021.106670

11 Zafari, Z., Sadatsafavi, M., Chen, W. & FitzGerald, J. M. The projected economic and health burden of sub-optimal asthma control in Canada. *Respir Med* **138**, 7-12 (2018). https://doi.org:10.1016/j.rmed.2018.03.018

12 Rodriguez-Roisin, R., Rabe, K. F., Vestbo, J., Vogelmeier, C. & Agustí, A. Global Initiative for Chronic Obstructive Lung Disease (GOLD) 20th Anniversary: a brief history of time. *European Respiratory Journal* **50**, 1700671 (2017). https://doi.org:10.1183/13993003.00671-2017

13 Effros, R. M. Anatomy, development, and physiology of the lungs. *GI Motility* (2006).

14 West, J. B. & Luks, A. M. *West's Respiratory Physiology*. (Wolters Kluwer Health, 2020).

15 Ochs, M. *et al.* The number of alveoli in the human lung. *Am J Respir Crit Care Med* **169**, 120-124 (2004). https://doi.org:10.1164/rccm.200308-1107OC

16 Gil, J., Bachofen, H., Gehr, P. & Weibel, E. R. Alveolar volume-surface area relation in air- and saline-filled lungs fixed by vascular perfusion. *J Appl Physiol Respir Environ Exerc Physiol* **47**, 990-1001 (1979). https://doi.org:10.1152/jappl.1979.47.5.990

17 Adams, F. *The genuine works of Hippocrates*. Vol. 1 (W. Wood, 1886).

18 The Lancet Respiratory, M. Asthma on the job. *The Lancet Respiratory Medicine* **3**, 329 (2015). https://doi.org:10.1016/S2213-2600(15)00153-8

19 Karamanou, M. & Androutsos, G. Aretaeus of Cappadocia and the First Clinical Description of Asthma. *American Journal of Respiratory and Critical Care Medicine* **184**, 1420-1421 (2011). https://doi.org:10.1164/ajrccm.184.12.1420b
20 Bergeron, C., Tulic, M. K. & Hamid, Q. Airway remodelling in asthma: from benchside to clinical practice. *Can Respir J* **17**, e85-93 (2010). https://doi.org:10.1155/2010/318029
21 Nair, P. *et al.* Airway Hyperresponsiveness in Asthma: Measurement and Clinical Relevance. *J Allergy Clin Immunol Pract* **5**, 649-659.e642 (2017). https://doi.org:10.1016/j.jaip.2016.11.030
22 Hammad, H. & Lambrecht, B. N. The basic immunology of asthma. *Cell* **184**, 1469-1485 (2021). https://doi.org:10.1016/j.cell.2021.02.016
23 Maspero, J. *et al.* Type 2 inflammation in asthma and other airways diseases. *ERJ Open Research* **8**, 00576-02021 (2022). https://doi.org:10.1183/23120541.00576-2021
24 PLATTS-MILLS, T. A. E. The Role of Immunoglobulin E in Allergy and Asthma. *American Journal of Respiratory and Critical Care Medicine* **164**, S1-S5 (2001). https://doi.org:10.1164/ajrccm.164.supplement_1.2103024
25 Fahy, J. V. Type 2 inflammation in asthma — present in most, absent in many. *Nature Reviews Immunology* **15**, 57-65 (2015). https://doi.org:10.1038/nri3786
26 Kyriakopoulos, C., Gogali, A., Bartziokas, K. & Kostikas, K. Identification and treatment of T2-low asthma in the era of biologics. *ERJ Open Research* **7**, 00309-02020 (2021). https://doi.org:10.1183/23120541.00309-2020
27 Taylor, D. R. *et al.* A new perspective on concepts of asthma severity and control. *European Respiratory Journal* **32**, 545-554 (2008). https://doi.org:10.1183/09031936.00155307
28 Asthma, G. I. f. Global Strategy for Asthma Management and Prevention. (2023).
29 Reddel, H. K. *et al.* GINA 2019: a fundamental change in asthma management. *Treatment of asthma with short-acting bronchodilators alone is no longer recommended for adults and adolescents* **53**, 1901046 (2019). https://doi.org:10.1183/13993003.01046-2019
30 Chung, K. F. *et al.* International ERS/ATS guidelines on definition, evaluation and treatment of severe asthma. *European Respiratory Journal* **43**, 343-373 (2014). https://doi.org:10.1183/09031936.00202013
31 Thomson, N. C. & Chaudhuri, R. Omalizumab: Clinical Use for the Management of Asthma. *Clinical Medicine Insights: Circulatory, Respiratory and Pulmonary Medicine* **6**, CCRPM.S7793 (2012). https://doi.org:10.4137/ccrpm.s7793
32 Garcia, G. *et al.* Anti-interleukin-5 therapy in severe asthma. *European Respiratory Review* **22**, 251-257 (2013). https://doi.org:10.1183/09059180.00004013
33 Harb, H. & Chatila, T. A. Mechanisms of Dupilumab. *Clinical & Experimental Allergy* **50**, 5-14 (2020). https://doi.org:10.1111/cea.13491
34 Marone, G. *et al.* Tezepelumab: a novel biological therapy for the treatment of severe uncontrolled asthma. *Expert Opin Investig Drugs* **28**, 931-940 (2019). https://doi.org:10.1080/13543784.2019.1672657
35 Graham, B. L. *et al.* Standardization of Spirometry 2019 Update. An Official American Thoracic Society and European Respiratory Society Technical Statement. *American Journal of Respiratory and Critical Care Medicine* **200**, e70-e88 (2019). https://doi.org:10.1164/rccm.201908-1590ST

36 Bhakta, N. R. *et al.* Race and Ethnicity in Pulmonary Function Test Interpretation: An Official American Thoracic Society Statement. *American Journal of Respiratory and Critical Care Medicine* **207**, 978-995 (2023). https://doi.org:10.1164/rccm.202302-0310ST

37 Stanojevic, S. *et al.* ERS/ATS technical standard on interpretive strategies for routine lung function tests. *European Respiratory Journal* **60**, 2101499 (2022). https://doi.org:10.1183/13993003.01499-2021

38 Akdis, C. A. *et al.* Type 2 immunity in the skin and lungs. *Allergy* **75**, 1582-1605 (2020). https://doi.org:10.1111/all.14318

39 Kolkhir, P. *et al.* Type 2 chronic inflammatory diseases: targets, therapies and unmet needs. *Nature Reviews Drug Discovery* (2023). https://doi.org:10.1038/s41573-023-00750-1

40 Ratcliffe, S. (Oxford University Press, 2016).

41 Svenningsen, S. & Nair, P. Asthma Endotypes and an Overview of Targeted Therapy for Asthma. *Front Med (Lausanne)* **4**, 158 (2017). https://doi.org:10.3389/fmed.2017.00158

42 Pizzichini, E. *et al.* Indices of airway inflammation in induced sputum: reproducibility and validity of cell and fluid-phase measurements. *American Journal of Respiratory and Critical Care Medicine* **154**, 308-317 (1996). https://doi.org:10.1164/ajrccm.154.2.8756799

43 Bousquet, J. *et al.* Eosinophilic inflammation in asthma. *N Engl J Med* **323**, 1033-1039 (1990). https://doi.org:10.1056/nejm199010113231505

44 Tran, T. N., Khatry, D. B., Ke, X., Ward, C. K. & Gossage, D. High blood eosinophil count is associated with more frequent asthma attacks in asthma patients. *Ann Allergy Asthma Immunol* **113**, 19-24 (2014). https://doi.org:10.1016/j.anai.2014.04.011

45 Horn, B. R., Robin, E. D., Theodore, J. & Van Kessel, A. Total eosinophil counts in the management of bronchial asthma. *N Engl J Med* **292**, 1152-1155 (1975). https://doi.org:10.1056/nejm197505292922204

46 Pavord, I. D. *et al.* Mepolizumab for severe eosinophilic asthma (DREAM): a multicentre, double-blind, placebo-controlled trial. *Lancet* **380**, 651-659 (2012). https://doi.org:10.1016/s0140-6736(12)60988-x

47 Pizzichini, M. M. *et al.* Prednisone-dependent asthma: inflammatory indices in induced sputum. *Eur Respir J* **13**, 15-21 (1999). https://doi.org:10.1183/09031936.99.13101599

48 Jayaram, L. Determining asthma treatment by monitoring sputum cell counts: effect on exacerbations. *European Respiratory Journal* **27**, 483-494 (2006). https://doi.org:10.1183/09031936.06.00137704

49 Pignatti, P. *et al.* Do blood eosinophils strictly reflect airway inflammation in COPD? Comparison with asthmatic patients. *Respir Res* **20**, 145 (2019). https://doi.org:10.1186/s12931-019-1111-1

50 Mukherjee, M. & Nair, P. Blood or sputum eosinophils to guide asthma therapy? *The Lancet Respiratory Medicine* **3**, 824-825 (2015). https://doi.org:10.1016/s2213-2600(15)00419-1

51 Sehmi, R. *et al.* Role of local eosinophilopoietic processes in the development of airway eosinophilia in prednisone-dependent severe asthma. *Clin Exp Allergy* **46**, 793-802 (2016). https://doi.org:10.1111/cea.12695

52 Sandeep, T., Roopakala, M. S., Silvia, C. R., Chandrashekara, S. & Rao, M. Evaluation of serum immunoglobulin E levels in bronchial asthma. *Lung India* **27**, 138-140 (2010). https://doi.org:10.4103/0970-2113.68312
53 Marcos, M. C. & Cisneros Serrano, C. What is the added value of FeNO as T2 biomarker? *Front Allergy* **3**, 957106 (2022). https://doi.org:10.3389/falgy.2022.957106
54 Pellegrino, R. *et al.* Interpretative strategies for lung function tests. *European respiratory journal* **26**, 948-968 (2005).
55 Chapman, D. G. & Irvin, C. G. Mechanisms of airway hyper-responsiveness in asthma: the past, present and yet to come. *Clinical & Experimental Allergy* **45**, 706-719 (2015). https://doi.org:10.1111/cea.12506
56 Coates, A. L. *et al.* ERS technical standard on bronchial challenge testing: general considerations and performance of methacholine challenge tests. *European Respiratory Journal* **49**, 1601526 (2017). https://doi.org:10.1183/13993003.01526-2016
57 Cockcroft, D. W. How Best to Measure Airway Responsiveness. *American Journal of Respiratory and Critical Care Medicine* **163**, 1514-1515 (2001). https://doi.org:10.1164/ajrccm.163.7.2103055b
58 Joos, G. F. & O'Connor, B. Indirect airway challenges. *European Respiratory Journal* **21**, 1050-1068 (2003). https://doi.org:10.1183/09031936.03.00008403
59 Cox, G., Miller, J. D., McWilliams, A., FitzGerald, J. M. & Lam, S. Bronchial thermoplasty for asthma. *American journal of respiratory and critical care medicine* **173**, 965-969 (2006).
60 Castro, M. *et al.* Effectiveness and safety of bronchial thermoplasty in the treatment of severe asthma: a multicenter, randomized, double-blind, sham-controlled clinical trial. *Am J Respir Crit Care Med* **181**, 116-124 (2010). https://doi.org:10.1164/rccm.200903-0354OC
61 Cox, G. *et al.* Asthma Control during the Year after Bronchial Thermoplasty. *New England Journal of Medicine* **356**, 1327-1337 (2007). https://doi.org:10.1056/nejmoa064707
62 Akaba, T. *et al.* Reduced Asthma Exacerbations in Adult Patients Treated With Bronchial Thermoplasty. *The Journal of Allergy and Clinical Immunology: In Practice* (2023). https://doi.org:10.1016/j.jaip.2023.04.036
63 Chaudhuri, R. *et al.* Safety and effectiveness of bronchial thermoplasty after 10 years in patients with persistent asthma (BT10+): a follow-up of three randomised controlled trials. *The Lancet Respiratory Medicine* **9**, 457-466 (2021). https://doi.org:10.1016/s2213-2600(20)30408-2
64 Antonicelli, L. *et al.* Asthma severity and medical resource utilisation. *European Respiratory Journal* **23**, 723-729 (2004). https://doi.org:10.1183/09031936.04.00004904
65 Juniper, E. F., O'Byrne, P. M., Guyatt, G. H., Ferrie, P. J. & King, D. R. Development and validation of a questionnaire to measure asthma control. *Eur Respir J* **14**, 902-907 (1999). https://doi.org:10.1034/j.1399-3003.1999.14d29.x
66 Juniper, E. F. *et al.* Evaluation of impairment of health related quality of life in asthma: development of a questionnaire for use in clinical trials. *Thorax* **47**, 76-83 (1992). https://doi.org:10.1136/thx.47.2.76
67 Juniper, E. F., Bousquet, J., Abetz, L. & Bateman, E. D. Identifying 'well-controlled' and 'not well-controlled' asthma using the Asthma Control Questionnaire. *Respir Med* **100**, 616-621 (2006). https://doi.org:10.1016/j.rmed.2005.08.012

68 Juniper, E. F., Guyatt, G. H., Willan, A. & Griffith, L. E. Determining a minimal important change in a disease-specific Quality of Life Questionnaire. *J Clin Epidemiol* **47**, 81-87 (1994). https://doi.org:10.1016/0895-4356(94)90036-1

69 Juniper, E. F., Svensson, K., Mörk, A.-C. & Ståhl, E. Measurement properties and interpretation of three shortened versions of the asthma control questionnaire. *Respiratory Medicine* **99**, 553-558 (2005). https://doi.org:10.1016/j.rmed.2004.10.008

70 Reddel, H. K. *et al.* An Official American Thoracic Society/European Respiratory Society Statement: Asthma Control and Exacerbations. *American Journal of Respiratory and Critical Care Medicine* **180**, 59-99 (2009). https://doi.org:10.1164/rccm.200801-060ST

71 Barnes, P. J., Casale, T. B., Dahl, R., Pavord, I. D. & Wechsler, M. E. The Asthma Control Questionnaire as a clinical trial endpoint: past experience and recommendations for future use. *Allergy* **69**, 1119-1140 (2014). https://doi.org:10.1111/all.12415

72 Trivedi, A. *et al.* Using imaging as a biomarker for asthma. *J Allergy Clin Immunol* **139**, 1-10 (2017). https://doi.org:10.1016/j.jaci.2016.11.009

73 DeBoer, E. M., Spielberg, D. R. & Brody, A. S. Clinical potential for imaging in patients with asthma and other lung disorders. *Journal of Allergy and Clinical Immunology* **139**, 21-28 (2017). https://doi.org:10.1016/j.jaci.2016.11.004

74 DenOtter, T. D. & Schubert, J. in *StatPearls* (StatPearls Publishing Copyright © 2023, StatPearls Publishing LLC., 2023).

75 Hsia, C. C. W. *et al.* Quantitative Imaging Metrics for the Assessment of Pulmonary Pathophysiology: An Official American Thoracic Society and Fleischner Society Joint Workshop Report. *Ann Am Thorac Soc* **20**, 161-195 (2023). https://doi.org:10.1513/AnnalsATS.202211-915ST

76 Pu, J. *et al.* CT based computerized identification and analysis of human airways: a review. *Med Phys* **39**, 2603-2616 (2012). https://doi.org:10.1118/1.4703901

77 De Jong, P. A. Computed tomographic imaging of the airways: relationship to structure and function. *European Respiratory Journal* **26**, 140-152 (2005). https://doi.org:10.1183/09031936.05.00007105

78 Tschirren, J., McLennan, G., Palagyi, K., Hoffman, E. A. & Sonka, M. Matching and anatomical labeling of human airway tree. *IEEE Transactions on Medical Imaging* **24**, 1540-1547 (2005). https://doi.org:10.1109/tmi.2005.857653

79 Awadh, N., Muller, N. L., Park, C. S., Abboud, R. T. & Fitzgerald, J. M. Airway wall thickness in patients with near fatal asthma and control groups: assessment with high resolution computed tomographic scanning. *Thorax* **53**, 248-253 (1998). https://doi.org:10.1136/thx.53.4.248

80 Aysola, R. S. *et al.* Airway Remodeling Measured by Multidetector CT Is Increased in Severe Asthma and Correlates With Pathology. *Chest* **134**, 1183-1191 (2008). https://doi.org:10.1378/chest.07-2779

81 Gupta, S. *et al.* Quantitative analysis of high-resolution computed tomography scans in severe asthma subphenotypes. *Thorax* **65**, 775-781 (2010). https://doi.org:10.1136/thx.2010.136374

82 Little, S. A. *et al.* High resolution computed tomographic assessment of airway wall thickness in chronic asthma: reproducibility and relationship with lung function and severity. *Thorax* **57**, 247-253 (2002). https://doi.org:10.1136/thorax.57.3.247

83 Niimi, A. *et al.* Relationship of airway wall thickness to airway sensitivity and airway reactivity in asthma. *Am J Respir Crit Care Med* **168**, 983-988 (2003). https://doi.org:10.1164/rccm.200211-1268OC
84 Konietzke, P. *et al.* Quantitative CT detects changes in airway dimensions and air-trapping after bronchial thermoplasty for severe asthma. *Eur J Radiol* **107**, 33-38 (2018). https://doi.org:10.1016/j.ejrad.2018.08.007
85 Lee, Y. M. *et al.* High-resolution CT findings in patients with near-fatal asthma: comparison of patients with mild-to-severe asthma and normal control subjects and changes in airway abnormalities following steroid treatment. *Chest* **126**, 1840-1848 (2004). https://doi.org:10.1378/chest.126.6.1840
86 Eddy, R. L. *et al.* Is Computed Tomography Airway Count Related to Asthma Severity and Airway Structure and Function? *Am J Respir Crit Care Med* **201**, 923-933 (2020). https://doi.org:10.1164/rccm.201908-1552OC
87 Svenningsen, S. & Nair, P. Persistent Airway Plugs: A Call for Clinical Recognition and Novel Therapies. *Am J Respir Crit Care Med* **205**, 977-978 (2022). https://doi.org:10.1164/rccm.202201-0147ED
88 Chan, R., Duraikannu, C. & Lipworth, B. Clinical Associations of Mucus Plugging in Moderate to Severe Asthma. *The Journal of Allergy and Clinical Immunology: In Practice* **11**, 195-199.e192 (2023). https://doi.org:10.1016/j.jaip.2022.09.008
89 Dunican, E. M. *et al.* Mucus plugs in patients with asthma linked to eosinophilia and airflow obstruction. *Journal of Clinical Investigation* **128**, 997-1009 (2018). https://doi.org:10.1172/jci95693
90 Hearn, A. P. *et al.* The prevalence of mucus plugging in severe eosinophilic asthma and its relationship to clinical efficacy of anti–IL-5R treatment. *The Journal of Allergy and Clinical Immunology: In Practice* **10**, 1102-1103. e1101 (2022).
91 Svenningsen, S. *et al.* CT and Functional MRI to Evaluate Airway Mucus in Severe Asthma. *Chest* **155**, 1178-1189 (2019). https://doi.org:10.1016/j.chest.2019.02.403
92 Tang, M. *et al.* Mucus plugs persist in asthma, and changes in mucus plugs associate with changes in airflow over time. *American journal of respiratory and critical care medicine* **205**, 1036-1045 (2022).
93 Burgel, P. R. The role of small airways in obstructive airways diseases. *European Respiratory Review* **20**, 023-033 (2011). https://doi.org:10.1183/09059180.00010410
94 Lynch, D. A. & Al-Qaisi, M. A. Quantitative computed tomography in chronic obstructive pulmonary disease. *J Thorac Imaging* **28**, 284-290 (2013). https://doi.org:10.1097/RTI.0b013e318298733c
95 Krings, J. G. *et al.* Quantitative CT metrics are associated with longitudinal lung function decline and future asthma exacerbations: Results from SARP-3. *Journal of Allergy and Clinical Immunology* **148**, 752-762 (2021). https://doi.org:https://doi.org/10.1016/j.jaci.2021.01.029
96 Petersson, J., Sánchez-Crespo, A., Larsson, S. A. & Mure, M. Physiological imaging of the lung: single-photon-emission computed tomography (SPECT). *J Appl Physiol (1985)* **102**, 468-476 (2007). https://doi.org:10.1152/japplphysiol.00732.2006
97 Heckscher, T. *et al.* Regional lung function in patients with bronchial asthma. *J Clin Invest* **47**, 1063-1070 (1968). https://doi.org:10.1172/jci105796

98 Bentivoglio, L. G. *et al.* REGIONAL PULMONARY FUNCTION STUDIED WITH XENON IN PATIENTS WITH BRONCHIAL ASTHMA. *J Clin Invest* **42**, 1193-1200 (1963). https://doi.org:10.1172/jci104805
99 Amis, T. C., Crawford, A. B., Davison, A. & Engel, L. A. Distribution of inhaled 99mtechnetium labelled ultrafine carbon particle aerosol (Technegas) in human lungs. *Eur Respir J* **3**, 679-685 (1990).
100 Engel, L. A., Landau, L., Taussig, L., Martin, R. R. & Sybrecht, G. Influence of bronchomotor tone on regional ventilation distribution at residual volume. *J Appl Physiol* **40**, 411-416 (1976). https://doi.org:10.1152/jappl.1976.40.3.411
101 Clague, H., Ahmad, D., Chamberlain, M. J., Morgan, W. K. & Vinitski, S. Histamine bronchial challenge: effect on regional ventilation and aerosol deposition. *Thorax* **38**, 668-675 (1983). https://doi.org:10.1136/thx.38.9.668
102 King, G. G., Eberl, S., Salome, C. M., Young, I. H. & Woolcock, A. J. Differences in airway closure between normal and asthmatic subjects measured with single-photon emission computed tomography and technegas. *Am J Respir Crit Care Med* **158**, 1900-1906 (1998). https://doi.org:10.1164/ajrccm.158.6.9608027
103 Farrow, C. E. *et al.* Airway closure on imaging relates to airway hyperresponsiveness and peripheral airways disease in asthma. *Journal of Applied Physiology* **113**, 958-966 (2012). https://doi.org:10.1152/japplphysiol.01618.2011
104 Farrow, C. E. *et al.* Peripheral ventilation heterogeneity determines the extent of bronchoconstriction in asthma. *Journal of Applied Physiology* **123**, 1188-1194 (2017). https://doi.org:10.1152/japplphysiol.00640.2016
105 Leach, C. L. *et al.* Characterization of respiratory deposition of fluticasone-salmeterol hydrofluoroalkane-134a and hydrofluoroalkane-134a beclomethasone in asthmatic patients. *Ann Allergy Asthma Immunol* **108**, 195-200 (2012). https://doi.org:10.1016/j.anai.2012.01.010
106 Newman, S., Salmon, A., Nave, R. & Drollmann, A. High lung deposition of 99mTc-labeled ciclesonide administered via HFA-MDI to patients with asthma. *Respir Med* **100**, 375-384 (2006). https://doi.org:10.1016/j.rmed.2005.09.027
107 Rhodes, C. *et al.* Quantification of regional V/Q ratios in humans by use of PET. I. Theory. *Journal of Applied Physiology* **66**, 1896-1904 (1989).
108 Valind, S. O., Rhodes, C. G., Brudin, L. H. & Jones, T. Measurements of regional ventilation pulmonary gas volume: theory and error analysis with special reference to positron emission tomography. *VENTILATION AND VENTILATION/PERFUSION RATIOS Measurements of regional lung function based on* (1991).
109 Hofman, M. S. *et al.* 68Ga PET/CT ventilation–perfusion imaging for pulmonary embolism: a pilot study with comparison to conventional scintigraphy. *Journal of Nuclear Medicine* **52**, 1513-1519 (2011).
110 Musch, G. & Venegas, J. G. Positron emission tomography imaging of regional pulmonary perfusion and ventilation. *Proc Am Thorac Soc* **2**, 522-527, 508-529 (2005). https://doi.org:10.1513/pats.200508-088DS
111 Venegas, J. G. *et al.* Self-organized patchiness in asthma as a prelude to catastrophic shifts. *Nature* **434**, 777-782 (2005). https://doi.org:10.1038/nature03490
112 Harris, R. S. *et al.* Regional Pulmonary Perfusion, Inflation, and Ventilation Defects in Bronchoconstricted Patients with Asthma. *American Journal of Respiratory and Critical Care Medicine* **174**, 245-253 (2006). https://doi.org:10.1164/rccm.200510-1634oc

113 Harris, R. S. *et al.* 18F-FDG uptake rate is a biomarker of eosinophilic inflammation and airway response in asthma. *J Nucl Med* **52**, 1713-1720 (2011). https://doi.org:10.2967/jnumed.110.086355
114 Bergin, C. J., Glover, G. M. & Pauly, J. Magnetic resonance imaging of lung parenchyma. *J Thorac Imaging* **8**, 12-17 (1993).
115 Foo, C. T., Langton, D., Thompson, B. R. & Thien, F. Functional lung imaging using novel and emerging MRI techniques. *Front Med (Lausanne)* **10**, 1060940 (2023). https://doi.org:10.3389/fmed.2023.1060940
116 Kern, A. L. & Vogel-Claussen, J. Hyperpolarized gas MRI in pulmonology. *The British Journal of Radiology*, 20170647 (2018). https://doi.org:10.1259/bjr.20170647
117 Khan, A. S. *et al.* Enabling Clinical Technologies for Hyperpolarized (129) Xenon Magnetic Resonance Imaging and Spectroscopy. *Angew Chem Int Ed Engl* **60**, 22126-22147 (2021). https://doi.org:10.1002/anie.202015200
118 Svenningsen, S. *et al.* What are ventilation defects in asthma? *Thorax* **69**, 63-71 (2014). https://doi.org:10.1136/thoraxjnl-2013-203711
119 Rayment, J. H. *et al.* Hyperpolarised¹²⁹Xe magnetic resonance imaging to monitor treatment response in children with cystic fibrosis. *European Respiratory Journal* **53**, 1802188 (2019). https://doi.org:10.1183/13993003.02188-2018
120 Wang, J. M. *et al.* Using hyperpolarized ¹²⁹Xe MRI to quantify regional gas transfer in idiopathic pulmonary fibrosis. *Thorax* **73**, 21-28 (2018). https://doi.org:10.1136/thoraxjnl-2017-210070
121 Kirby, M. *et al.* Hyperpolarized 3He and 129Xe MR Imaging in Healthy Volunteers and Patients with Chronic Obstructive Pulmonary Disease. *Radiology* **265**, 600-610 (2012). https://doi.org:10.1148/radiol.12120485
122 Mugler, J. P., 3rd *et al.* MR imaging and spectroscopy using hyperpolarized 129Xe gas: preliminary human results. *Magn Reson Med* **37**, 809-815 (1997). https://doi.org:10.1002/mrm.1910370602
123 Albert, M. S. *et al.* Biological magnetic resonance imaging using laser-polarized 129Xe. *Nature* **370**, 199-201 (1994). https://doi.org:10.1038/370199a0
124 Ruset, I., Ketel, S. & Hersman, F. W. Optical pumping system design for large production of hyperpolarized Xe 129. *Physical review letters* **96**, 053002 (2006).
125 Roos, J. E., McAdams, H. P., Kaushik, S. S. & Driehuys, B. Hyperpolarized Gas MR Imaging. *Magnetic Resonance Imaging Clinics of North America* **23**, 217-229 (2015). https://doi.org:10.1016/j.mric.2015.01.003
126 Lilburn, D. M. L., Pavlovskaya, G. E. & Meersmann, T. Perspectives of hyperpolarized noble gas MRI beyond 3He. *Journal of Magnetic Resonance* **229**, 173-186 (2013). https://doi.org:https://doi.org/10.1016/j.jmr.2012.11.014
127 Couch, M. J. *et al.* Inert fluorinated gas MRI: a new pulmonary imaging modality. *NMR in Biomedicine* **27**, 1525-1534 (2014).
128 Edelman, R. R., Hatabu, H., Tadamura, E., Li, W. & Prasad, P. V. Noninvasive assessment of regional ventilation in the human lung using oxygen–enhanced magnetic resonance imaging. *Nature medicine* **2**, 1236-1239 (1996).
129 Capaldi, D. P. I. *et al.* Free-breathing Pulmonary MR Imaging to Quantify Regional Ventilation. *Radiology* **287**, 693-704 (2018). https://doi.org:10.1148/radiol.2018171993

130 Mummy, D. G. *et al.* Mucus Plugs in Asthma at CT Associated with Regional Ventilation Defects at (3)He MRI. *Radiology* **303**, 184-190 (2022). https://doi.org:10.1148/radiol.2021204616
131 Svenningsen, S. *et al.* Sputum Eosinophilia and Magnetic Resonance Imaging Ventilation Heterogeneity in Severe Asthma. *Am J Respir Crit Care Med* **197**, 876-884 (2018). https://doi.org:10.1164/rccm.201709-1948OC
132 de Lange, E. E. *et al.* Evaluation of asthma with hyperpolarized helium-3 MRI: correlation with clinical severity and spirometry. *Chest* **130**, 1055-1062 (2006). https://doi.org:10.1378/chest.130.4.1055
133 Donnelly, L. F. *et al.* Cystic fibrosis: combined hyperpolarized 3He-enhanced and conventional proton MR imaging in the lung--preliminary observations. *Radiology* **212**, 885-889 (1999). https://doi.org:10.1148/radiology.212.3.r99se20885
134 Kirby, M. *et al.* Hyperpolarized 3He Magnetic Resonance Functional Imaging Semiautomated Segmentation. *Academic Radiology* **19**, 141-152 (2012). https://doi.org:10.1016/j.acra.2011.10.007
135 He, M. *et al.* Extending semiautomatic ventilation defect analysis for hyperpolarized (129)Xe ventilation MRI. *Acad Radiol* **21**, 1530-1541 (2014). https://doi.org:10.1016/j.acra.2014.07.017
136 Tustison, N. J. *et al.* Ventilation-based segmentation of the lungs using hyperpolarized 3He MRI. *Journal of Magnetic Resonance Imaging* **34**, 831-841 (2011). https://doi.org:10.1002/jmri.22738
137 Astley, J. R. *et al.* Large-scale investigation of deep learning approaches for ventilated lung segmentation using multi-nuclear hyperpolarized gas MRI. *Scientific Reports* **12** (2022). https://doi.org:10.1038/s41598-022-14672-2
138 Mummy, D. G. *et al.* Ventilation defects on hyperpolarized helium-3 MRI in asthma are predictive of 2-year exacerbation frequency. *J Allergy Clin Immunol* **146**, 831-839.e836 (2020). https://doi.org:10.1016/j.jaci.2020.02.029
139 Carey, K. J. *et al.* Comparison of hyperpolarized 3He-MRI, CT based parametric response mapping, and mucus scores in asthmatics. *Frontiers in Physiology* **14** (2023). https://doi.org:10.3389/fphys.2023.1178339
140 Zha, N. *et al.* Second-order Texture Measurements of (3)He Ventilation MRI: Proof-of-concept Evaluation of Asthma Bronchodilator Response. *Acad Radiol* **23**, 176-185 (2016). https://doi.org:10.1016/j.acra.2015.10.010
141 Svenningsen, S. *et al.* Hyperpolarized 3He and 129Xe MRI: Differences in asthma before bronchodilation. *Journal of Magnetic Resonance Imaging* **38**, 1521-1530 (2013). https://doi.org:10.1002/jmri.24111
142 Marshall, H. *et al.* Peripheral and proximal lung ventilation in asthma: Short-term variation and response to bronchodilator inhalation. *J Allergy Clin Immunol* **147**, 2154-2161.e2156 (2021). https://doi.org:10.1016/j.jaci.2020.11.035
143 Kruger, S. J. *et al.* Hyperpolarized Helium-3 MRI of exercise-induced bronchoconstriction during challenge and therapy. *Journal of Magnetic Resonance Imaging* **39**, 1230-1237 (2014). https://doi.org:10.1002/jmri.24272
144 Svenningsen, S., Eddy, R. L., Kjarsgaard, M., Parraga, G. & Nair, P. Effects of Anti-T2 Biologic Treatment on Lung Ventilation Evaluated by MRI in Adults With Prednisone-Dependent Asthma. *Chest* **158**, 1350-1360 (2020). https://doi.org:10.1016/j.chest.2020.04.056

145 McIntosh, M. J. *et al.* Asthma Control, Airway Mucus, and 129Xe MRI Ventilation After a Single Benralizumab Dose. *Chest* **162**, 520-533 (2022). https://doi.org:10.1016/j.chest.2022.03.003
146 Thomen, R. P. *et al.* Regional ventilation changes in severe asthma after bronchial thermoplasty with (3)He MR imaging and CT. *Radiology* **274**, 250-259 (2015). https://doi.org:10.1148/radiol.14140080
147 Hall, C. S. *et al.* Single-Session Bronchial Thermoplasty Guided by 129Xe Magnetic Resonance Imaging. A Pilot Randomized Controlled Clinical Trial. *American Journal of Respiratory and Critical Care Medicine* **202**, 524-534 (2020). https://doi.org:10.1164/rccm.201905-1021OC
148 Svenningsen, S. *et al.* Bronchial thermoplasty guided by hyperpolarised gas magnetic resonance imaging in adults with severe asthma: a 1-year pilot randomised trial. *ERJ Open Res* **7** (2021). https://doi.org:10.1183/23120541.00268-2021
149 Costella, S. *et al.* Regional pulmonary response to a methacholine challenge using hyperpolarized³He magnetic resonance imaging. *Respirology* **17**, 1237-1246 (2012). https://doi.org:10.1111/j.1440-1843.2012.02250.x
150 Tustison, N. J. *et al.* Feature analysis of hyperpolarized helium-3 pulmonary MRI: A study of asthmatics versus nonasthmatics. *Magnetic Resonance in Medicine* **63**, 1448-1455 (2010). https://doi.org:10.1002/mrm.22390
151 Svenningsen, S. *et al.* MRI Ventilation Texture Features Discriminate Severe Asthmatics with and without Eosinophilic Airway Inflammation.
152 McIntosh, M. *et al.* Supervised shallow learning of 129 Xe MRI texture features to predict response to Anti-IL-5 biologic therapy in severe asthma.
153 Marshall, H. *et al.* In vivo methods and applications of xenon-129 magnetic resonance. *Progress in Nuclear Magnetic Resonance Spectroscopy* **122**, 42-62 (2021). https://doi.org:https://doi.org/10.1016/j.pnmrs.2020.11.002
154 Gauthier, M., Ray, A. & Wenzel, S. E. Evolving Concepts of Asthma. *American Journal of Respiratory and Critical Care Medicine* **192**, 660-668 (2015). https://doi.org:10.1164/rccm.201504-0763pp
155 Haldar, P. *et al.* Cluster Analysis and Clinical Asthma Phenotypes. *American Journal of Respiratory and Critical Care Medicine* **178**, 218-224 (2008). https://doi.org:10.1164/rccm.200711-1754oc
156 Haldar, P. *et al.* Cluster analysis and clinical asthma phenotypes. *Am J Respir Crit Care Med* **178**, 218-224 (2008). https://doi.org:10.1164/rccm.200711-1754OC
157 Moore, W. C. *et al.* Identification of Asthma Phenotypes Using Cluster Analysis in the Severe Asthma Research Program. *American Journal of Respiratory and Critical Care Medicine* **181**, 315-323 (2010). https://doi.org:10.1164/rccm.200906-0896oc
158 Lefaudeux, D. *et al.* U-BIOPRED clinical adult asthma clusters linked to a subset of sputum omics. *J Allergy Clin Immunol* **139**, 1797-1807 (2017). https://doi.org:10.1016/j.jaci.2016.08.048
159 Lefaudeux, D. *et al.* Clustering analysis of clinical variables in U-BIOPRED adult asthma cohort. *European Respiratory Journal* **44**, 225 (2014).
160 Loza, M. J. *et al.* Validated and longitudinally stable asthma phenotypes based on cluster analysis of the ADEPT study. *Respiratory Research* **17** (2016). https://doi.org:10.1186/s12931-016-0482-9

161 Tyler, S. R. & Bunyavanich, S. Leveraging -omics for asthma endotyping. *J Allergy Clin Immunol* **144**, 13-23 (2019). https://doi.org:10.1016/j.jaci.2019.05.015

162 Pinto Dos Santos, D., Dietzel, M. & Baessler, B. A decade of radiomics research: are images really data or just patterns in the noise? *European Radiology* **31**, 1-4 (2021). https://doi.org:10.1007/s00330-020-07108-w

163 Bannier, E. *et al.* Hyperpolarized 3He MR for sensitive imaging of ventilation function and treatment efficiency in young cystic fibrosis patients with normal lung function. *Radiology* **255**, 225-232 (2010).

164 Kaushik, S. S. *et al.* Diffusion-weighted hyperpolarized 129Xe MRI in healthy volunteers and subjects with chronic obstructive pulmonary disease. *Magnetic Resonance in Medicine* **65**, 1154-1165 (2011).

165 Trivedi, A. P. *et al.* Quantitative CT Characteristics of Cluster Phenotypes in the Severe Asthma Research Program Cohorts. *Radiology* **304**, 450-459 (2022). https://doi.org:10.1148/radiol.210363

166 Choi, S. *et al.* Quantitative computed tomographic imaging-based clustering differentiates asthmatic subgroups with distinctive clinical phenotypes. *J Allergy Clin Immunol* **140**, 690-700.e698 (2017). https://doi.org:10.1016/j.jaci.2016.11.053

167 Gupta, S. *et al.* Quantitative computed tomography–derived clusters: Redefining airway remodeling in asthmatic patients. *Journal of Allergy and Clinical Immunology* **133**, 729-738.e718 (2014). https://doi.org:10.1016/j.jaci.2013.09.039

168 Kim, S. *et al.* Phenotypic clusters on computed tomography reflects asthma heterogeneity and severity. *World Allergy Organ J* **15**, 100628 (2022). https://doi.org:10.1016/j.waojou.2022.100628

169 Eddy, R. L. *et al.* Pulmonary MRI and Cluster Analysis Help Identify Novel Asthma Phenotypes. *J Magn Reson Imaging* **56**, 1475-1486 (2022). https://doi.org:10.1002/jmri.28152

170 Svenningsen, S. *et al.* Reproducibility of Hyperpolarized ¹²⁹Xe MRI Ventilation Defect Percent in Severe Asthma to Evaluate Clinical Trial Feasibility. *Academic Radiology* **28**, 817-826 (2021). https://doi.org:10.1016/j.acra.2020.04.025

171 He, M. *et al.* Dose and pulse sequence considerations for hyperpolarized 129Xe ventilation MRI. *Magnetic resonance imaging* **33**, 877-885 (2015).

172 Capaldi, D. *et al.* in *ISMRM.* 3969-3992 (2015).

173 Kaiser, H. F. An index of factorial simplicity. *Psychometrika* **39**, 31-36 (1974). https://doi.org:10.1007/BF02291575

174 Bartlett, M. S. A Note on the Multiplying Factors for Various χ² Approximations. *Journal of the Royal Statistical Society. Series B (Methodological)* **16**, 296-298 (1954).

175 Jolliffe, I. T. & Cadima, J. Principal component analysis: a review and recent developments. *Philosophical Transactions of the Royal Society A: Mathematical, Physical and Engineering Sciences* **374**, 20150202 (2016). https://doi.org:10.1098/rsta.2015.0202

176 Banerjee, A. & Dave, R. N. in *2004 IEEE International Conference on Fuzzy Systems (IEEE Cat. No.04CH37542).* 149-153 vol.141.

177 Dinno, A. Implementing Horn's Parallel Analysis for Principal Component Analysis and Factor Analysis. *The Stata Journal: Promoting communications on statistics and Stata* **9**, 291-298 (2009). https://doi.org:10.1177/1536867x0900900207

178 Brock, G., Pihur, V., Datta, S. & Datta, S. clValid: An R Package for Cluster Validation. *Journal of Statistical Software* **25**, 1 - 22 (2008). https://doi.org:10.18637/jss.v025.i04

179 Charrad, M., Ghazzali, N., Boiteau, V. & Niknafs, A. NbClust: An R Package for Determining the Relevant Number of Clusters in a Data Set. *Journal of Statistical Software* **61**, 1 - 36 (2014). https://doi.org:10.18637/jss.v061.i06

180 Nair, P. & Hargreave, F. E. Measuring bronchitis in airways diseases: clinical implementation and application: Airway hyperresponsiveness in asthma: its measurement and clinical significance. *Chest* **138**, 38s-43s (2010). https://doi.org:10.1378/chest.10-0094

181 D'Silva, L. *et al.* Heterogeneity of Bronchitis in Airways diseases in Tertiary Care Clinical Practice. *Canadian Respiratory Journal* **18**, 144-148 (2011). https://doi.org:10.1155/2011/430317

182 Sieren, J. P. *et al.* SPIROMICS Protocol for Multicenter Quantitative Computed Tomography to Phenotype the Lungs. *American Journal of Respiratory and Critical Care Medicine* **194**, 794-806 (2016). https://doi.org:10.1164/rccm.201506-1208pp

183 Galbán, C. J. *et al.* Computed tomography–based biomarker provides unique signature for diagnosis of COPD phenotypes and disease progression. *Nature medicine* **18**, 1711-1715 (2012).

184 Hair, J. F., Black, W. C., Babin, B. J., Anderson, R. E. & Tatham, R. Multivariate data analysis: Global edition. *7th Edition: Pearson Education* (2009).

185 Hennig, C. Cluster-wise assessment of cluster stability. *Computational Statistics & Data Analysis* **52**, 258-271 (2007). https://doi.org:https://doi.org/10.1016/j.csda.2006.11.025

186 McIntosh, M. J. *et al.* (129)Xe MRI Ventilation Defects in Asthma: What is the Upper Limit of Normal and Minimal Clinically Important Difference? *Acad Radiol* (2023). https://doi.org:10.1016/j.acra.2023.03.010

187 Belda, J. *et al.* Induced Sputum Cell Counts in Healthy Adults. *American Journal of Respiratory and Critical Care Medicine* **161**, 475-478 (2000). https://doi.org:10.1164/ajrccm.161.2.9903097

188 Li, M. *et al.* Identification of the molecular subgroups in asthma by gene expression profiles: airway inflammation implications. *BMC Pulmonary Medicine* **22** (2022). https://doi.org:10.1186/s12890-022-01824-3

189 Kuo, C.-H. S. *et al.* T-helper cell type 2 (Th2) and non-Th2 molecular phenotypes of asthma using sputum transcriptomics in U-BIOPRED. *European Respiratory Journal* **49**, 1602135 (2017). https://doi.org:10.1183/13993003.02135-2016

190 Skloot, G., Permutt, S. & Togias, A. Airway hyperresponsiveness in asthma: a problem of limited smooth muscle relaxation with inspiration. *Journal of Clinical Investigation* **96**, 2393-2403 (1995). https://doi.org:10.1172/jci118296

191 Elliot, J. G. *et al.* Fatty airways: implications for obstructive disease. *Eur Respir J* **54** (2019). https://doi.org:10.1183/13993003.00857-2019

192 Peters, U. *et al.* BMI but not central obesity predisposes to airway closure during bronchoconstriction. *Respirology* **24**, 543-550 (2019). https://doi.org:10.1111/resp.13478

193 Maes, T., Joos, G. F. & Brusselle, G. G. Targeting Interleukin-4 in Asthma: Lost in Translation? *American Journal of Respiratory Cell and Molecular Biology* **47**, 261-270 (2012). https://doi.org:10.1165/rcmb.2012-0080TR

194 McLeod, J. J. A., Baker, B. & Ryan, J. J. Mast cell production and response to IL-4 and IL-13. *Cytokine* **75**, 57-61 (2015). https://doi.org:10.1016/j.cyto.2015.05.019

195 Scott, H. A. *et al.* Effect of obesity on airway and systemic inflammation in adults with asthma: a systematic review and meta-analysis. *Thorax* **78**, 957-965 (2023). https://doi.org:10.1136/thorax-2022-219268
196 Peters, M. C. *et al.* Plasma interleukin-6 concentrations, metabolic dysfunction, and asthma severity: a cross-sectional analysis of two cohorts. *The Lancet Respiratory Medicine* **4**, 574-584 (2016). https://doi.org:10.1016/s2213-2600(16)30048-0
197 Schütze, N. *et al.* Allergen-Induced IL-6 Regulates IL-9/IL-17A Balance in CD4+ T Cells in Allergic Airway Inflammation. *The Journal of Immunology* **197**, 2653-2664 (2016). https://doi.org:10.4049/jimmunol.1501599
198 Doganci, A. *et al.* The IL-6R α chain controls lung CD4+CD25+ Treg development and function during allergic airway inflammation in vivo. **115**, 313-325 (2005). https://doi.org:10.1172/jci22433
199 Morjaria, J. B. *et al.* Sputum IL-6 concentrations in severe asthma and its relationship with FEV1. *Thorax* **66**, 537 (2011). https://doi.org:10.1136/thx.2010.136523
200 Dixon, A. E., Raymond, D. M., Suratt, B. T., Bourassa, L. M. & Irvin, C. G. Lower airways disease in asthmatics with and without rhinitis. *Lung* **186**, 361-368 (2008). https://doi.org:10.1007/s00408-008-9119-1
201 SHI, H.-Z. *et al.* Effect of Inhaled Interleukin-5 on Airway Hyperreactivity and Eosinophilia in Asthmatics. *American Journal of Respiratory and Critical Care Medicine* **157**, 204-209 (1998). https://doi.org:10.1164/ajrccm.157.1.9703027
202 Tanaka, H. *et al.* Role of Interleukin-5 and Eosinophils in Allergen-Induced Airway Remodeling in Mice. *American Journal of Respiratory Cell and Molecular Biology* **31**, 62-68 (2004). https://doi.org:10.1165/rcmb.2003-0305OC
203 Kuperman, D. A. *et al.* Direct effects of interleukin-13 on epithelial cells cause airway hyperreactivity and mucus overproduction in asthma. *Nat Med* **8**, 885-889 (2002). https://doi.org:10.1038/nm734
204 Duong-Quy, S. <p>Clinical Utility Of The Exhaled Nitric Oxide (NO) Measurement With Portable Devices In The Management Of Allergic Airway Inflammation And Asthma</p>. *Journal of Asthma and Allergy* **Volume 12**, 331-341 (2019). https://doi.org:10.2147/jaa.s190489
205 Charles Kuhn, I. *et al.* Airway Hyperresponsiveness and Airway Obstruction in Transgenic Mice. *American Journal of Respiratory Cell and Molecular Biology* **22**, 289-295 (2000). https://doi.org:10.1165/ajrcmb.22.3.3690
206 Peters, M. C. *et al.* Evidence for Exacerbation-Prone Asthma and Predictive Biomarkers of Exacerbation Frequency. *Am J Respir Crit Care Med* **202**, 973-982 (2020). https://doi.org:10.1164/rccm.201909-1813OC
207 Busacker, A. *et al.* A Multivariate Analysis of Risk Factors for the Air-Trapping Asthmatic Phenotype as Measured by Quantitative CT Analysis. *Chest* **135**, 48-56 (2009). https://doi.org:10.1378/chest.08-0049
208 Moore, W. C. *et al.* Sputum neutrophil counts are associated with more severe asthma phenotypes using cluster analysis. *Journal of Allergy and Clinical Immunology* **133**, 1557-1563.e1555 (2014). https://doi.org:10.1016/j.jaci.2013.10.011
209 Coxson, H. O. & Rogers, R. M. Quantitative computed tomography of chronic obstructive pulmonary disease1. *Academic radiology* **12**, 1457-1463 (2005).

210 Cox, G. Glucocorticoid treatment inhibits apoptosis in human neutrophils. Separation of survival and activation outcomes. *Journal of Immunology (Baltimore, Md.: 1950)* **154**, 4719-4725 (1995).

211 Kim, R. Y. *et al.* Role for NLRP3 Inflammasome–mediated, IL-1β–Dependent Responses in Severe, Steroid-Resistant Asthma. *American Journal of Respiratory and Critical Care Medicine* **196**, 283-297 (2017). https://doi.org:10.1164/rccm.201609-1830OC

212 Simpson, J. L. *et al.* Elevated expression of the NLRP3 inflammasome in neutrophilic asthma. *Eur Respir J* **43**, 1067-1076 (2014). https://doi.org:10.1183/09031936.00105013

213 Lorenz, A. *et al.* Investigating the role of BAFF in murine models of allergic asthma. *European Respiratory Journal* **44**, P4213 (2014).

214 Jee, H. *et al.* Increased B-cell Activating Factor (BAFF) Level in Sputum of the Children with Asthma. *Journal of Allergy and Clinical Immunology* **123**, S73-S73 (2009). https://doi.org:10.1016/j.jaci.2008.12.251

215 Allard-Chamard, H. *et al.* Interleukin-15 in autoimmunity. *Cytokine* **136**, 155258 (2020). https://doi.org:10.1016/j.cyto.2020.155258

216 Mukherjee, M. *et al.* Sputum autoantibodies in patients with severe eosinophilic asthma. *J Allergy Clin Immunol* **141**, 1269-1279 (2018). https://doi.org:10.1016/j.jaci.2017.06.033

217 Linssen, R. S. *et al.* Neutrophil Extracellular Traps Increase Airway Mucus Viscoelasticity and Slow Mucus Particle Transit. *Am J Respir Cell Mol Biol* **64**, 69-78 (2021). https://doi.org:10.1165/rcmb.2020-0168OC

218 Wenzel, S. E. *et al.* Bronchoscopic evaluation of severe asthma. Persistent inflammation associated with high dose glucocorticoids. *Am J Respir Crit Care Med* **156**, 737-743 (1997). https://doi.org:10.1164/ajrccm.156.3.9610046

219 WENZEL, S. E. *et al.* Evidence That Severe Asthma Can Be Divided Pathologically into Two Inflammatory Subtypes with Distinct Physiologic and Clinical Characteristics. *American Journal of Respiratory and Critical Care Medicine* **160**, 1001-1008 (1999). https://doi.org:10.1164/ajrccm.160.3.9812110

220 Hastie, A. T. *et al.* Baseline sputum eosinophil+ neutrophil subgroups' clinical characteristics and longitudinal trajectories for NHLBI Severe Asthma Research Program (SARP 3) cohort. *Journal of Allergy and Clinical Immunology* **146**, 222-226 (2020).

221 Dunican, E. M., Watchorn, D. C. & Fahy, J. V. Autopsy and imaging studies of mucus in asthma. Lessons learned about disease mechanisms and the role of mucus in airflow obstruction. *Annals of the American Thoracic Society* **15**, S184-S191 (2018).

222 Mukherjee, M. & Nair, P. Autoimmune Responses in Severe Asthma. *Allergy, Asthma & Immunology Research* **10**, 428 (2018). https://doi.org:10.4168/aair.2018.10.5.428

223 Gherasim, A., Dao, A. & Bernstein, J. A. Confounders of severe asthma: diagnoses to consider when asthma symptoms persist despite optimal therapy. *World Allergy Organization Journal* **11**, 29 (2018). https://doi.org:10.1186/s40413-018-0207-2

224 Mussell, G. T. *et al.* Xenon ventilation MRI in difficult asthma: initial experience in a clinical setting. *ERJ Open Research* **7**, 00785-02020 (2021). https://doi.org:10.1183/23120541.00785-2020

225 Dunican, E. M. *et al.* Mucus Plugs and Emphysema in the Pathophysiology of Airflow Obstruction and Hypoxemia in Smokers. *American Journal of Respiratory and Critical Care Medicine* **203**, 957-968 (2021). https://doi.org:10.1164/rccm.202006-2248OC

226 van Griethuysen, J. J. M. *et al.* Computational Radiomics System to Decode the Radiographic Phenotype. *Cancer Research* **77**, e104-e107 (2017). https://doi.org:10.1158/0008-5472.Can-17-0339

227 Marrissa J McIntosh, M. S., Harkiran K Kooner, Hana Serajeddini, Anurag Bhalla, Cory Yamashita, and Grace Parraga. Hyperpolarized 129Xe MRI ventilation textures predict short- and long-term response to Anti-IL-5Rα Biologic Therapy in Eosinophilic Asthma. (2023).

228 O'Byrne, P. *et al.* Asthma progression and mortality: the role of inhaled corticosteroids. *Eur Respir J* **54** (2019). https://doi.org:10.1183/13993003.00491-2019

229 Kooner, H. K. *et al.* Pulmonary functional MRI: Detecting the structure-function pathologies that drive asthma symptoms and quality of life. *Respirology* **27**, 114-133 (2022). https://doi.org:10.1111/resp.14197

230 Wilding, J. P. H. *et al.* Once-Weekly Semaglutide in Adults with Overweight or Obesity. *New England Journal of Medicine* **384**, 989-1002 (2021). https://doi.org:10.1056/nejmoa2032183

231 Svenningsen, S. *et al.* Effects of Dupilumab on Mucus Plugging and Ventilation Defects in Patients with Moderate-to-Severe Asthma: A Randomized, Double-Blind, Placebo-controlled Trial. *Am J Respir Crit Care Med* (2023). https://doi.org:10.1164/rccm.202306-1102LE

232 Simpson, J. L., Powell, H., Boyle, M. J., Scott, R. J. & Gibson, P. G. Clarithromycin targets neutrophilic airway inflammation in refractory asthma. *American journal of respiratory and critical care medicine* **177**, 148-155 (2008).

233 Osei, E. T., Brandsma, C.-A., Timens, W., Heijink, I. H. & Hackett, T.-L. Current perspectives on the role of interleukin-1 signalling in the pathogenesis of asthma and COPD. *European Respiratory Journal* **55**, 1900563 (2020). https://doi.org:10.1183/13993003.00563-2019

234 Dinarello, C. A., Simon, A. & Van Der Meer, J. W. M. Treating inflammation by blocking interleukin-1 in a broad spectrum of diseases. *Nature Reviews Drug Discovery* **11**, 633-652 (2012). https://doi.org:10.1038/nrd3800

235 Serajeddini, H., Eddy, R. L., Licskai, C., McCormack, D. G. & Parraga, G. FEV₁and MRI ventilation defect reversibility in asthma and COPD. *European Respiratory Journal* **55**, 1901947 (2020). https://doi.org:10.1183/13993003.01947-2019

236 Rutting, S., Tonga, K. O. & King, G. G. Toward explaining fixed airflow obstruction in asthma. *Journal of Allergy and Clinical Immunology* **149**, 890-892 (2022). https://doi.org:10.1016/j.jaci.2021.12.784

237 Ash, S. Y. *et al.* Pruning of the Pulmonary Vasculature in Asthma. The Severe Asthma Research Program (SARP) Cohort. *American Journal of Respiratory and Critical Care Medicine* **198**, 39-50 (2018). https://doi.org:10.1164/rccm.201712-2426oc

238 McIntosh, M. J. *et al.* Pulmonary Vascular Differences in Eosinophilic Asthma after 2.5-Years Anti-IL-5Rα Treatment. *American Journal of Respiratory and Critical Care Medicine* (2023).